Modeling of Alford Force and Tip Clearance Flow for Turbine Blades

by

Soomyung Yoo

Submitted to the Department of Aeronautics and Astronautics
in partial fulfillment of the requirements for the degree of

Master of Science in Aeronautics and Astronautics

at the

MASSACHUSETTS INSTITUTE OF TECHNOLOGY

Feb 1993

Author .....
Department of Aeronautics and Astronautics
Feb, 1993

Certified by .....
Manuel Martinez-Sanchez
Associate Professor
Thesis Supervisor

Accepted by .....
Professor Harold Y. Wachman
Chairman, Departmental Committee on Graduate Students

Modeling of Alford Force and Tip Clearance Flow for Turbine Blades

by

Soomyung Yoo

Submitted to the Department of Aeronautics and Astronautics
on Feb, 1993, in partial fulfillment of the
requirements for the degree of
Master of Science in Aeronautics and Astronautics

Abstract

A model that calculates the flow through a turbine stage has been developed in order to predict Alford forces. This model is an extension of a series of works that have been based on actuator disk theory. Unsteadiness due to whirling of rotor shaft has been introduced.

At the same time, the effects of relative motion of endwall on tip clearance flow have been investigated. Qualitative understanding of the characteristics of the flow have been obtained and a simple two-dimensional model that is based on the integrated boundary layer method has been developed. Although this model makes integration possible without an initial condition by taking advantage of a singularity in the governing equation, mathematical difficulties that arise from approximations make it difficul to connect the singularity with a clear physical phenomenon.

Thesis Supervisor: Manuel Martinez-Sanchez
Title: Associate Professor

Contents

List of Figures

List of Tables

Chapter 1

Introduction

Turbines that are designed for aerospace applications have been required very high power. As an example of the most advanced turbines so far are the turbines in turbopumps for Space Shuttle Main Engine(SSME). With a size of only 28 cm in diameter, the turbines for LH2 and LOX pumps of this engine generate as much as 77,000 HP and 75,000 HP respectively.

In the regime on the power level and with the size of the turbines of SSME, problems that have not been very important for those with lower power levels have been encountered. One of these is the phenomenon called vibrational instability. When a rotor shaft is displaced somehow from the center of its casing and the displacement is not dampened but amplified in time, the turbine is said to suffer from a vibrational instability. Many mechanisms that are considered to cause an instability have been found and classified. There is a good summary of these instabilities by Qiu[24]. Some of the instabilities are well understood, and some are practically even solved. However instabilities are, in general, unpredictable and are found during test stages.

One of these instabilities is the one that was encountered during the test stage of the development of the SSME. This instability delayed the project six months with extra cost of as much as $ 500,000 a day.

One important mechanism for this instability was first investigated and suggested by Alford[2] in 1965 and Thomas[31] in 1958. According to their conclusion, which they reached independently, a non-uniform tip clearance distribution due to a dis-

placement of rotor shaft during vibration produces a force that causes the instability(figure B-1). They assumed that the blades with a smaller tip clearance are more efficient than those with a large clearance, and also assume that effects of redistribution of flow field due to the presence of the non-uniform tip clearance distribution are negligible. These assumptions lead to their conclusion that more work is extracted by the blades with smaller tip clearance, therefore with the second assumption, larger force acts on the blades with a smaller tip clearance. The resultant side force, which is called Alford force, drives the rotor disk in the direction of rotation. Unless a shaft has sufficient damping, this force amplifies the displacement of the shaft and, if not controlled, will lead to a catastrophic failure.

The simple model of Alford and Thomas predicts a linear dependence of the Alford force on turbine loading. This dependence was verified experimentally by Urlicks and Wohlrab with a discrepancy of 20 - 30 %. This is the reason why this Alford force is one of the most important destabilizing forces for modern high power turbines.

Despite the apparent importance of this force to the development of modern high power turbines, not much research has been conducted on this force. One of the reasons is that the Alford force, which is very small compared to the force that drives a rotor disc, is difficult to measure. Typically the Alford force is of the order of 1 % of the main force. The measurement of this small force is very delicate and costy. For a theoretical approach, this small force requires delicate considerations of many parameters that have been considered to be negligible for investigations involving larger forces. One of a few systematic researches on this Alford force is the work done at Gas Turbine Laboratory(GTL) of M.I.T([16]). This work includes measurements of the Alford force and flow field for both shrouded and unshrouded turbine rotors. Also a series of models to predict the alford force have been developed ([24],[8], and [13]).

A half of this thesis is devoted to an extension of the above series of theoretical works. The other part of this thesis treats tip clearance flow for a turbine blade, a topic that has more generality than Alford force. As mentioned before, the Alford force is a result of non-uniform distribution of tip clearance due to a displacement of

a rotor shaft. Therefore it is quite natural to investigate the flow within the tip gap region because the model by Alford and Thomas ignored the structure of the flow by replacing it by an empirical efficiency, which should be a result of a model rather than an input.

Tip clearance flow has been investigated both for compressor blades and turbine blades by many researchers for several decades. However due to its highly complicated nature, most of works are either experimental or computational as will be reviewed in more detail in Section 5.1. One of the main motivations of researchers have been the fact that a vortex rolling up in a cascade due to tip clearance flow is considered to be one of the main sources of loss in total pressure, uniformity and, therefore efficiencies. In an industry, where 10^{-1} to 1 % increase of efficiency counts much, the investigation of tip clearance flow has a practical importance.

In this thesis, an attempt has been made to make clear the viscous effects due to relative motion of the endwall on the tip clearance flow for turbine blades.

Chapter 2

Background of Actuator Disk modeling

The first theoretical model was suggested by Alford and Thomas. The main results of the model is that the Alford force is proportional to the displacement of a rotor shaft.

This dependence was verified experimentally by Urlicks and Wohlrab. The assumptions on which Alford and Thomas' model is based on are:

1. Upstream flow is not affected by the presence of non-uniform tip clearance distribution.

2. Each cascade performs as efficiently as one with the same "uniform" tip clearance.

As mentioned in Chapter 1, a series of models that have tried to improve this simple model have been developed by using a method called actuator disk theory. Although there are many variations from this method, let us choose a simple version in figure B-2 to show the basic ideas of this method.

The flow in a cascade is hopelessly complicated. However, in order to obtain upstream and downstream flows of a cascade, that complicated flow has to be treated somehow because it connects the two flows. The main idea of actuator disk theory is to look for a connecting condition between upstream and downstream flows at the

cascade. By replacing a cascade flow by a mathematical condition, one can avoid to deal with the complicated structure of a cascade directly and can consider it as a simple connecting surface, which is often called an "actuator disk." As shown in figure B-2, one can choose either x-y plane or x-z plane according to his or her purpose. The following characteristics are obvious:

1. This approach is very suitable to capture the effects of redistribution of upstream and downstream flow of a cascade.

2. The flow within a cascade can not be obtained without some modifications.

3. Results depends very much on the connecting condition.

Other than these, this approximation introduces the errors due to assumption of infinite number of blades, absence of centrifugal force and so on.

As far as modifications are concerned, there are, for examples, "double actuator disk", which has two disks, and "actuator duct", which treats a cascade as a duct with a finite length.

With these ideas in mind, the followings are the summary of the series of models with actuator disk theory:

1. x-y two-dimensional both for steady and unsteady conditions [24]

2. x-z two-dimensional for steady condition with a special treatment for a partial work done by underturned flow due to tip clearance [8]

3. x-y-z three-dimensional for steady condition [13]

The basic idea of these developments can be easily understood with figure B-3. The entire flow, although it is very complicated, can be characterized by length scales over which flow variables change. Currently three length scales have been adopted. The length scale for far upstream and downstream flows is characterized by the radius of the rotor disk R, which will be called as "R-scale" from now on. For the region near the cascade, the scale is the blade height H, called "H-scale." Similarly the

region within and very near tip gap is characterized by the tip gap t, called "t-scale." The first model of above list deals with R-scale, the second with H-scale. The last model treats both R- and H-scale, and constructs a three-dimensional solution for the entire flow region by mathematically "patching" the two with the two length scales. Although there has not been a successful treatment for the t-scale, the second model accounts for a part of the effects in t-scale, that is the partial work done by underturned flow through and near the tip gap region. That model calculates the partial work based on an inviscid collision of tip leakage flow and main flow in a cascade[8].

Following this series of developments, this thesis presents another extension to the above three-dimensional model with partial work, that is, inclusion of unsteady effects due to whirling of a rotor disk.

Chapter 3

Analysis of Actuator Disk modeling

3.1 Basic Idea

As mentioned in Chapter 2 and illustrated in figure B-4, the whole flow has been constructed by patching two flows that correspond to H-, and R-scale. More concretely this implies that we connect the flow solution in the x-z two-dimensional model with that of the x-y two-dimensional model with the treatment of the partial work. In other words,

$$\lim_{x\ (H-scale)\to\pm\infty} \Upsilon = \lim_{x\ (R-scale)\to\pm 0} \Upsilon \tag{3.1}$$

where Υ stands for a flow variable in general.

3.2 R-scale Flow

The same notations have been used as those of [13] and [8] basically. Since the detailed derivations have been reported in them, only key formulas and new modifications have been provided in this section.

3.2.1 Upstream R-scale flow

The upstream flow, with uniform far upstream condition, is expressed by a Laplace equation for velocity potential

$$\nabla^2\phi = 0 \tag{3.2}$$

The solution for this equation with an exponential decay in the x-direction is obtained as

$$\{c_x - c_x(x=-\infty)\} = \hat{c_{x_0}} e^{\frac{x}{R}+i(\frac{y}{R}-\Omega t)} \tag{3.3}$$

$$\{c_y - c_y(x=-\infty)\} = i\hat{c_{x_0}} e^{\frac{x}{R}+i(\frac{y}{R}-\Omega t)} \tag{3.4}$$

3.2.2 Downstream R-scale flow

The solutions of downstream flow are obtained by using a small perturbation method. The downstream of the rotor is divided into a main (denoted by$^-$) and a jet region of thickness Δ (denoted by$^+$). The governing equations are

$$\frac{\partial \Delta}{\partial t} + \frac{\partial (c_x^+ \Delta)}{\partial x} + \frac{\partial (c_y^+ \Delta)}{\partial y} = 0 \tag{3.5}$$

$$\frac{\partial (H-\Delta)}{\partial t} + \frac{\partial \{c_x^- (H-\Delta)\}}{\partial x} + \frac{\partial \{c_y^- (H-\Delta)\}}{\partial y} = 0 \tag{3.6}$$

and

$$\frac{\partial c_x^+}{\partial t} + c_x^+ \frac{\partial c_x^+}{\partial x} + c_y^+ \frac{\partial c_x^+}{\partial y} + \frac{1}{\rho}\frac{\partial p}{\partial x} = 0 \tag{3.7}$$

$$\frac{\partial c_y^+}{\partial t} + c_x^+ \frac{\partial c_y^+}{\partial x} + c_y^+ \frac{\partial c_y^+}{\partial y} + \frac{1}{\rho}\frac{\partial p}{\partial y} = 0 \tag{3.8}$$

$$\frac{\partial c_x^-}{\partial t} + c_x^- \frac{\partial c_x^-}{\partial x} + c_y^- \frac{\partial c_x^-}{\partial y} + \frac{1}{\rho}\frac{\partial p}{\partial x} = 0 \tag{3.9}$$

$$\frac{\partial c_y^-}{\partial t} + c_x^- \frac{\partial c_y^-}{\partial x} + c_y^- \frac{\partial c_y^-}{\partial y} + \frac{1}{\rho}\frac{\partial p}{\partial y} = 0 \tag{3.10}$$

Each of these flow variables are split into two parts. The main part $\bar{\Upsilon}$ corresponds to the values with an average gap, and the part Υ' is the perturbation part.

$$\Upsilon = \bar{\Upsilon} + \Upsilon' \tag{3.11}$$

with Υ as a flow variable in general.

Unsteadiness is expressed as $\frac{\partial}{\partial t}$ terms. This unsteadiness can be rewritten in terms of $\frac{\partial}{\partial y}$ by observing from the whirling frame. The flow from this frame is stationary, and with the following geometrical relationship between fixed and whirling frames in figure B-5,

$$y' = y - R\Omega t \tag{3.12}$$

we obtain

$$(\frac{\partial}{\partial t})_{fixed\ frame} = -R\Omega\frac{\partial}{\partial y}. \tag{3.13}$$

With consideration of the x and y directional variations as upstream, the perturbation part of a flow variable is assumed to be of the form

$$\Upsilon' = \hat{\Upsilon} exp\{\alpha x + i(\frac{y}{R} - \Omega t)\} \tag{3.14}$$

With this relation substituted into the mass and momentum equations with 3.13, the following set of equations for the eigenvalue α has been obtained.

$$\begin{bmatrix} \alpha\bar{\Delta} & \frac{i}{R}\bar{\Delta} & 0 & 0 & A_{15} & 0 \\ 0 & 0 & \alpha(H-\bar{\Delta}) & \frac{i}{R}(H-\hat{\Delta}) & A_{25} & 0 \\ A_{31} & 0 & 0 & 0 & 0 & \alpha \\ 0 & A_{42} & 0 & 0 & 0 & \frac{i}{R} \\ 0 & 0 & A_{53} & 0 & 0 & \alpha \\ 0 & 0 & 0 & A_{64} & 0 & \frac{i}{R} \end{bmatrix} \begin{bmatrix} \hat{c_x^+} \\ \hat{c_y^+} \\ \hat{c_x^-} \\ \hat{c_y^-} \\ \hat{\Delta} \\ \frac{\hat{p}}{\rho} \end{bmatrix} = 0 \tag{3.15}$$

where

$$A_{15} = A_{31} = A_{42} = \alpha\bar{c_x^+} + i(\frac{\bar{c_y^+}}{R} - \Omega)$$

$$A_{53} = A_{64} = \alpha\bar{c_x^-} + i(\frac{\bar{c_y^-}}{R} - \Omega)$$

$$A_{25} = -\alpha\bar{c_x^-} + i(\frac{\bar{c_y^-}}{R} - \Omega)$$

For this system to have a non-trivial solution, the determinant of this matrix has to vanish. The resulting sixth order algebraic equation for eigenvalue α yields six eigenvalues, out of which five have been adopted as physically meaningful(the sixth grow exponentially downstream). Therefore, the solution of the system of equations 3.15 is expressed as a linear combination of eigenfunctions that correspond to the chosen five eigenvalues.

$$\hat{\Upsilon} = \sum_{i=1}^{5} K_i \hat{v_i} \tag{3.16}$$

where $\hat{\Upsilon}$ stands for solution vector, and $\hat{v_i}$'s and K_i's, eigenfuctions and their coefficients respectively.

3.3 H-scale Flow

The details of solutions and their derivations are given in [15], and [8]. Here the key result is the functional dependence of the flow variables. In general, for a non-dimensionalized flow variable, we found from the xz (H-scale) model that

$$\Upsilon = \Upsilon(\frac{\delta}{H}, \phi, \frac{c_{y0}}{U}) \;\; ; \;\; \phi \equiv \frac{c_{x_0}}{U} \tag{3.17}$$

where Υ here stands for a non-dimensional flow parameter, and c_{x_0} is a function of y to be determined from the matching (c_{y_0} is invariant upstream).

From this dependence, the following relation is derived

$$\begin{bmatrix} \hat{c}_x^+ \\ \hat{c}_y^+ \\ \hat{c}_x^- \\ \hat{c}_y^- \\ \hat{\Delta} \\ \frac{\hat{p}}{\rho} \end{bmatrix} = [\frac{\hat{c}_x(x=0^-)}{U}\frac{\partial}{\partial\phi} + \frac{\hat{c}_y(x=0^-)}{U}\frac{\partial}{\partial\frac{c_{y_0}}{U}} + (\frac{e}{H})\frac{\partial}{\partial\frac{\delta}{H}}] \begin{bmatrix} c_{x_\infty}^+ \\ c_y^+ \\ c_{x_\infty}^- \\ c_y^- \\ \Delta \\ -\frac{p_0-p_\infty}{\rho} \end{bmatrix} \tag{3.18}$$

3.4 Matching

The coefficients of 3.16 are determined by matching the two solutions of 3.16 and 3.18 with the concept of equation 3.1.

Solving the resulting system of equations for the K_i's, and c_{x_0} we can uniquely determine the flow solution that connects two regions without a discontinuity.

3.5 Expressions for Variables of Interest

The variables of main concern are cross-force and direct-force Alford coefficients. They are defined as

$$\alpha_i = \frac{F_{i'}}{\pi R \bar{f}_y \frac{e}{H}} \ , \ i \ = \ X, \ Y \tag{3.19}$$

Here $F_{i'}$'s stand for the net projected forces to i''s axis in a rotating coordinate defined in figure B-5.

Perturbing the Euler turbine equation gives the perturbation tangent force $\hat{f}_y$ as

$$\frac{\hat{f}_y}{\bar{f}_y} = \frac{\hat{c_{x_0}}}{\bar{c}_{x_0}} + \frac{\hat{\lambda}\{(c_{y_2}^+ - c_{y_3}^+) - (c_{y_2}^- - c_{y_3}^-)\} + \bar{\lambda}(\hat{c_{y_2}^+} - \hat{c_{y_3}^+}) + (1-\bar{\lambda})(\hat{c_{y_2}^-} - \hat{c_{y_3}^-})}{\bar{\lambda}(c_{y_2}^+ - c_{y_3}^+) + (1-\bar{\lambda})(c_{y_2}^- - c_{y_3}^-)} \tag{3.20}$$

where λ is the leakage fraction.

Integrating the x and y projections of these forces gives

$$\alpha_y + i\alpha_x = -\frac{\hat{f}_y}{\bar{f}_y \frac{e}{H}}. \tag{3.21}$$

Chapter 4

Results and Discussion

In Figure B-6 to Figure B-13, some of calculated results are shown. These calculations have been based on the conditions of the experiment that was conducted at the GTL of M.I.T[16].

For design condition,

$$\begin{aligned} \alpha_2 &= 70^\circ,\ \beta_3 = 60^\circ,\ solidity = 0.756 \\ \frac{\delta}{H} &= 0.03,\ \phi = \frac{c_{x_0}}{U} = 0.58 \end{aligned}$$

Figure B-6 and figure B-7 are the results from the three-dimensional and unsteady model with partial work with respect to the parameters $\frac{\Omega}{\omega}$ and ϕ. Here $\frac{\Omega}{\omega}$ means the ratio of whirl and spin speed. For comparison, figure B-8 shows corresponding results for the steady case.

Given an experimental fact that

$$\alpha_y \ 1.2 \ - \ 1.4$$

for corresponding steady conditions (not counting the pressure contribution), the current model underpredicts α_y.

The comparison between figure B-6 and figure B-8 implies that introduction of

unsteadiness decreases α_y. In figure B-9 and figure B-10, values of corresponding upstream perturbations have been plotted. These two plots clearly show the enhancement of redistribution due to unsteadiness that results in the decrease of α_y.

Although redistribution has been introduced with a hope of improving the prediction of α_y, our results have shown increasing discrepancy from experimental data. In figure B-11, upstream flow perturbation for a steady case has been plotted. Figure B-12 and figure B-13 show perturbations at the rotor both for the underturned flow due to tip gap and for the rest of the flow that is guided by blade.

The above observations have shown that both, redistribution of xy flow, and unsteadiness due to rotor disk whirling, decrease α_y, with the result that theory underestimate data. There are a few candidates for the explanation of this trend.

1. There are other factors that offset the effects of redistribution.

2. The treatment of xy redistribution with incompressible assumption induces too strong redistribution.

3. Flow variation within a stage is not negligible.

In order to clarify the problem, more modifications seem to be necessary.

Although there have been no experimental unsteady data to which the results of theory can be compared, from the comparison at steady conditions, it seems reasonable to expect that predictions in whole range of $\frac{\Omega}{\omega}$ will be underestimated.

Chapter 5

Background for Tip Clearance Flow for Turbine Blades

5.1 General Background for Tip Clearance Flow

As briefly mentioned in Chapter 1, a main motivation of many investigations on tip clearance flow has been to estimate the loss in a cascade and improve efficiencies. There have been a great number of works on this topic both for compressor and for turbine blades. Although for both cases, most of these works are either experimental or computational, there has been a sharp contrast in the degree of success of theoretical approaches.

For compressor blades, there have been some theoretical approaches for simulating the growth of a vortex rolling up in a cascade. Some of them have shown reasonable success.

To the contrary, for turbine blades, there has been no theoretical approach that shows even minimum success.

In order to see the reason why this sharp contrast occurs, one needs to see the differences between compressor and turbine blades. Figure B-14 illustrates typical geometries of compressor and turbine rotor blades. This figure also shows the directions of tip clearance flow driven by a pressure difference across a blade and that of end wall motion in a relative frame fixed to the rotor blade. The following distinctions

are clear:

1. Blade thickness
    - Compressor blade — Thin
    - Turbine blade — Thick
2. Blade shape
    - Compressor blade — Not very cambered
    - Turbine blade — Very cambered
3. Relative direction of pressure gradient due to the pressure difference across the blade and viscous shear on the fluid due to the relative motion of end wall
    - Compressor blade — Opposite
    - Turbine blade — Same

Direct consequences that result from this differences will be discussed in the following sections. Here an important point has to be made clear. That is the distinction between a stationary cascade and a rotating cascade. The effects due to 1 and 2 of the above list can be simulated with a stationary cascade since these are the differences in geometries. However, the effects of 3 can only be simulated with either a rotating cascade or under equivalently dynamic environment. Therefore whether the results obtained from a stationary cascade are useful for practical cases or not depends on how much the effects of type 3 affect them. Now in the following two sections, the characteristics of these effects will be briefly summarized. One of them deals with the effects with a stationary endwall and another with a moving endwall.

5.2 Cascade without Endwall Motion

In order to illustrate the differences in treatment of a tip clearance flow between a compressor blade and a turbine blade, let us take a brief look at Rains' work on compressor blades.

Taking advantages of 1 and 2 in Section 5.1, he modeled a compressor blade as a thin flat plate with a pressure difference across it by the amount that is sustained by the blade at its midspan. Tip clearance flow is treated as a jet that has a component perpendicular to the plate accelerated by the pressure difference(figure B-15) and an un-modified component parallel to the plate. Although there have been some other successful models ([15],[4]), they are all based on this Rains' simplification. Historically, there have been also works by Lashminarayana ([12], [11]), which need empirical inputs that are not easy to obtain.

However in the case of a turbine blade, things are not so simple. This time, points 1 and 2 do not allow simplifications like Rains'. Adding to a difficulty in guessing the direction of tip jet that arises from its much more complicated geometry, point no.1 does not allow one to ignore the flow in the gap region as a matter of course, which Rains did by introducing his thin compressor blade.

This is the main reason why there have been no successful models for turbine blades even without a relative motion of the endwall. Therefore most works on tip clearance flow for turbine blades are either experimental or computational. In either case, these works can be classified into two groups. One includes the works that are focused on the growth of a vortex rolling up in a cascade. Another group includes works that are concerned with flow filed in the tip gap region. The number of works in the second group is much smaller than that in the first. Among the first group are [3], [33] and [28]. [19], [34], and [21] belong to the second group. Many computational works in the second group seem to be concerned with simulating a separation bubble at the leading edge of the blade tip.

5.3 Cascade with Endwall Motion

In cases of compressor blades, the effects of wall motion do not seem to alter the nature of flow in a cascade drastically. This was shown by Dean [7], who conducted a systematic measurement of flow field in a cascade with gap height and speed of endwall motion as main parameters. This work is also concentrated on physical interpretation

of the effects of these parameters. His results confirm that, for a compressor blade, there is not extraordinary changes in the nature of the flow, although there are changes like a shift of the location of the rolling vortex and a slight change in mass flow of the jet. However, these are expected changes from a simple consideration of the flow in a stationary cascade. Especially the thinness of its blade easily allows one to guess that viscous effects will not play a big role, which is in many cases a typical factor that changes a flow drastically.

In the cases of turbine blades, however, the introduction of relative endwall motion seems to affect the whole flow much more significantly. Especially the effets of wall motion, the facts that the tip gap flow is accelerated in one direction and at the same time dragged in the opposite direction by the shear due to the relative endwall motion, are quite unknown. The larger thickness of a blade, amplifies these unknown effects. Actually a flow visualization in the tip gap region with relative endwall motion by Graham[9] indicates the existence of a non-negligible region of reversed flow due to the relative motion. Figure B-16 from his work clearly shows complicated behavior of streamlines that can be only explained with a non-negligible reverse region. Figure B-17 gives a simple schematic structure of this reversed flow in a two-dimensional cross section.

Another important measurement has been conducted by Yaras and Sjolander [34]. They investigated the flow filed within a tip gap with a quite good resolution. Figure B-18 is a figure from their work, which shows velocity distribution in a tip gap region at different spanwise locations. This figure shows a fine structure such as a separation bubble at the leading edge at the tip. Despite the importance of this rare measurement, one of their conclusions seems to be wrong. They concluded, from this velocity measurement that one of a significant results caused by the relative endwall motion is the decrease of the speed in a potential core flow. However a quick look at the figure shows that the seemingly-reduced component of the velocity is mainly the one that opposes to the endwall motion. A more natural interpretation should be, it seems to this author, that the boundary layer is thicker than expected and the velocity defect comes from the existence of the boundary layer, which can be easily

understood with figure B-17. Therefore their measurement is interpreted as a direct experimental support of the non-negligible effects of endwall motion on tip clearance flow.

5.4 Aims of This Research

In the preceding sections, for turbine blades, the following facts have been made clear.

1. Even for a stationary case, there have been no successful theoretical attempts.
2. For a stationary case, the difficulties lie mainly in dealing with complicated geometry and the nature of pressure-driven flow remains essentially the same as that for a compressor blade.
3. The effects of relative endwall motion are of quite unknown nature and even a clear physical understanding has not yet been obtained. .

Under these circumstances, it seems too optimistic to expect to solve the whole problem all at once; that is to develop a model in a stationary cascade, understand the physics of the relative motion and integrate the effects on a stationary model. Since this research has started from the Alford force, which is a result of the tip gap flow, a primary interest has been the effects of the relative motion on the growth of a boundary layer through the gap. The blockage of the tip gap due to a boundary layer with a non-negligible reversed region directly affects the mass flow through the gap and, therefore, the Alford force.

In this thesis, the emphasis has been placed on the understanding of the physics of the gap flow due to the effects of the relative motion, and an attempt to make a rough estimate of the growth of the boundary layer through the tip gap. Although the physics of the flow have been understood well, the method used here has suffered from unclear connection between the physical picture and its results because of mathematical difficulties that will be discussed in Chapter 8.

Chapter 6

Modeling and Analysis of Tip Clearance Flow

6.1 Simplification of Tip Gap Flow

As the simplest model for the tip gap flow, a two-dimensional plane flow in the frame fixed to a rotor blade in Figure B-19 has been chosen. Although a turbine blade is highly cambered and its thickness varies along its camberline, this simplification can deal with at least part of the effects due to viscosity of the fluid and relative endwall motion.

For calculations a further simplification has been made, which will appear in 6.3.

6.2 Assumptions

6.2.1 Boundary Layer Approximation

Although experimental results show a separation bubble at the leading edge of the tip, they also seem to indicate that other parts of the flow have the basic structure of a boundary layer as seen from Figure B-18, that is, a steep velocity change from a solid surface to a potential flow (in this case, a core jet). Therefore the flow has been assumed to have a simple structure that consists of a potential core jet and a

boundary layer.

6.2.2 Prandtl's Boundary Layer Equation

As a governing equation, Prandtl's boundary equation has been adopted. In Section 8.3, this assumption has been examined in more detail.

6.2.3 Incompressibility

As the Mach number in many turbines is small, incompressibility has been assumed. This assumption will be also examined in Chapter 8.

6.2.4 Laminar flow

From typical Reynolds numbers for Figure B-19's simplified two-dimensional flow, the flow is considered to be turbulent.

For an example, for a very rough estimate for the turbine rotor used in [16],

$$t\ (\ tip\ gap\ )\ =\ 0.5\ mm,\ \ \bar{L}\ (\ blade\ width\ )\ \approx\ 0.5\ cm$$
$$\bar{\Delta p}\ \approx\ (\ pressure\ difference\ )\ =\ 0.1\ atm,\ \ V_{wall}\ \approx\ 54\ m/sec$$
$$\bar{\rho}\ \approx\ 10\ kg/m^3,\ \ \mu\ =\ 1.25\times 10^{-5}\ kg/m/sec,$$

Re$\approx 10^4$, which is near the critical value.

Experimental and computational works also have suggested that the flow should be turbulent. One of the discussions is based on the size of a separation bubble, which can be predicted well numerically with turbulence [19].

Despite these facts, an assumption of laminar flow has been made because of the following reasons:

1. Except for the region near the separation bubble, this unknown flow should be understood in an easier case to extract its physics.

2. Mathematically easier to be handled.

Most of the calculations have been done for endwall boundary layer, therefore the separation bubble has not been treated directly. However its effect in modifying the pressure field through blockage has been considered in choosing the potential flow imposed for calculations in this thesis. In Chapter 8, this assumption will be also examined.

6.2.5 Method of Integrated Boundary Layer Equation

Prandtl's boundary layer equation, which is a significantly reduced form of Navier-Stokes equation, is still very difficult to solve. As an approximation method, the integral method has been adopted. This method requires a velocity profile or a family of profiles with shape parameters as an input. There have been many variations of the method, typically classified by the number of parameters, therefore the number of equations, to be solved. In this thesis, so-called one-parameter profile have been chosen. The reasons why one-parameter profile has been selected over two-parameter profiles, which are supposed to be more accurate, are the following:

1. Even though not as accurate as two-parameter profiles, one-parameter profiles have been considered to produce results that are reasonable.

2. Mathematically easier to be handled.

If the flow that is under investigation is of well known nature, it is obviously better to use a more accurate method even at the cost of more manipulation and computation. However for the case of an unknown flow, the governing equations have to be explored to reveal the essence of the flow. Without a whole picture of the flow, accurate solutions can not be obtained. From these points, the simpler the governing equations are, the better. Of course not too simple. Another point is that, after all, they are all approximate methods whose errors from "real" solution can not be estimated other than by an experiment [22].

From the above considerations, a fixed parabolic profile has been tried first as the simplest case. After that, two one-parameter profiles have been adopted in this thesis. One is Pohlhausen's method[25], which expresses a velocity profile with a fourth order polynomial, and Timman's method, which uses an asymptotic form of a velocity profile that is connected to the potential flow ([32], [25]). All these assumptions will be examined and discussed in Chapter 8.

6.3 Simplified Flow Structure

6.3.1 Further Simplifications

In the assumed domain in Figure B-19, we expect two boundary layers, one on the endwall and another on the blade tip. However here, further simplification has been made. Instead of treating the two boundary layers, we deal with only one on the endwall with an imposed potential flow. This treatment has been made to isolate the phenomena of primary interest; that is, the interaction between pressure force and shear force due to the endwall. This reduces much of mathematical complications without losing the interaction. Of course, we have to pay a price for this convenience; the interaction between growth of boundary layer and the potential flow due to the blockage effect of boundary layer. Absence of this effect, however, is still tolerable as long as the thickness of the layer is small compared to the tip gap size for the first order solution.

Actually for a parabolic profile, a calculation has been made for two boundary layers and a potential flow that interact consistently. The results of this calculation will be discussed in Chapter 8.

6.3.2 Potential Flow

The potential flow that will be imposed for the calculation of boundary layer has to be realistic. Even for work that is not aimed at very accurate calculations, the results with an unrealistic potential flow have little practical meaning.

The presence of a separation bubble at the leading edge of tip changes the effective surface , therefore adding one uncertainty in choosing potential the flow.

However, to introduce a very complicated form for a solution is not feasible. Already many assumptions have been made and the model domain has been drastically simplified to isolate the effect that is of primary importance and of current interest. The potential flow has to be realistic and at the same time it should be as simple as possible for the current purposes.

Under the above circumstances, the following argument has been made. In Figure B-20, two flow domains are shown. Figure B-20-*a* corresponds to the geometry in Figure B-19. As mentioned before, the actual flows have a separation and reattachment in this region.

The geometry of the tip in Figure B-20-*b* is a streamline of a potential free jet. We never expect a separation for this constant-pressure shape, therefore the flow in this geometry serves as an example of realistic flows. Of course this flow is not exactly the same as the flow for Figure B-20-*a*.

Figure B-21 shows a comparison of the pressure distributions of the two flows. From this figure, it can be seen that these two pressure fields are qualitatively very similar. This means that the use of potential flow for Figure B-20-*a* is a reasonable approximation to Figure B-20-*b*'s flow, which does not suffer from separation and is still realistic.

With the above argument, the flow solution for Figure B-20-*a* has been adopted in this work.

6.3.3 Dimensional Analysis

For the simplified flow domain, there are seven variables that are needed to express the system. For the boundary layer thickness δ, which is of primary interest,

$$\delta = f(\Delta p, V_w, L, t, \rho, \mu) \tag{6.1}$$

where $\Delta p, V_w, L, t, \rho, \mu$ stand for pressure difference across blade at its midspan,

wall speed, tip width, tip gap height, average density of the fluid in the tip gap, and kinematic viscosity of the fluid respectively. The PI theorem, through the rank of the dimensional matrix, tells us that there are four non-dimensional variables. Here choosing t, ρ, V_w as repeating variables, the following relation is obtained:

$$\frac{\delta}{t} = g(\frac{\Delta p}{\rho {V_w}^2}, \frac{L}{t}, \frac{\mu}{\rho t V_w}) \tag{6.2}$$

The third non-dimensional variable is an inverse of Reynolds number. By defining the velocity

$$U_{ex} = \sqrt{\frac{2\Delta p}{\rho}}, \tag{6.3}$$

the first non-dimensional variable of a function g in equation 6.2 can be rewritten as $(\frac{U_{ex}}{V_w})^2$. In the calculations in the following chapter, $\frac{V_w}{U_{ex}}$ will be used instead of $\frac{\Delta p}{\rho {V_w}^2}$. From now on subscript w will be omitted.

6.4 Formulations

6.4.1 Potential Flow

As explained before, the potential flow for the domain in figure B-20 - a has been imposed for calculations of boundary layer. The potential solution is obtained by using a conformal mapping. The details of the mapping and its solutions are provided in Appendix B. For the flow domain in figure B-20 - b, Milne-Thompson[17] gives detailed formulations.

6.4.2 Integrated Boundary Layer Equation

Prandtl's boundary layer approximation in Rectangular coordinates is

$$\frac{\partial u}{\partial x} + \frac{\partial v}{\partial y} = 0 \tag{6.4}$$

$$u\frac{\partial u}{\partial x} + v\frac{\partial u}{\partial y} = -\frac{1}{\rho}\frac{dp}{dx} + \nu\frac{\partial^2 u}{\partial y^2} \tag{6.5}$$

with boundary conditions

$$u(0,x) = -V,\ u(\infty,x) = U(x)$$

By integrating the second equation with the aid of the first equation and boundary conditions, we obtain so-called "integrated boundary layer equation."

$$U^2\frac{d\delta_2}{dx} + (2\delta_2 + \delta_1)U\frac{dU}{dx} = \frac{\tau_0}{\rho} \tag{6.6}$$

where U is the potential velocity, τ_0 is the shear stress acting on the solid surface, and δ_1 and δ_2 are displacement and momentum thickness defined, for incompressible flow, as

$$\delta_1 = \int_0^\infty (1 - \frac{u}{U})dy \tag{6.7}$$

$$\delta_2 = \int_0^\infty \frac{u}{U}(1 - \frac{u}{U})dy. \tag{6.8}$$

For a one-parameter profile family,

$$\frac{\delta_1}{\delta} = f(\Lambda,\Psi) \tag{6.9}$$

$$\frac{\delta_2}{\delta} = g(\Lambda,\Psi) \tag{6.10}$$

$$\frac{\tau_0}{\rho U^2} = h1(\Lambda,\Psi)\frac{U'}{U}\delta \tag{6.11}$$

where Λ and Ψ are defined by

$$\Lambda = \frac{\delta^2}{\nu}\frac{dU}{dx} \tag{6.12}$$

$$\Psi = 1 + \frac{V_w}{U} \tag{6.13}$$

Here δ implies the boundary layer thickness for Pohlhausen's method. For Timman's method, this means a scale factor of the order of boundary layer thickness. This distinction comes from the fact that boundary layer thickness is not mathematically well defined, while displacement and momentum thickness are well defined.

Substituting equation 6.9, 6.10 and 6.11 with the definitions 6.12 and 6.13 into the integrated boundary layer equation 6.6, gives the following relation:

$$H1\frac{d\delta}{dx} = \delta\frac{U'}{U}H2 \tag{6.14}$$

where

$$H1 = g + 2\Lambda\frac{\partial g}{\partial \Lambda} \tag{6.15}$$

$$H2 = h1 - (f + 2g) - \Lambda\frac{\partial g}{\partial \Lambda}\frac{UU''}{U'^2} - (1 - \Psi)\frac{\partial g}{\partial \Psi} \tag{6.16}$$

This is an explicit form with respect to δ. If H1 ever vanishes, then, for $\frac{d\delta}{dx}$ to be finite, which has to be the case if this equation has a physical meaning, the following relation has to hold:

$$H1 = H2 = 0 \tag{6.17}$$

In usual cases with no wall motion, both H1 and H2 are positive, since δ, δ_1 and δ_2 are all positive. However in the current case, with a reversed flow region, this does not always hold. And as will be shown soon, the singular condition 6.17 does happen for all the profiles that have been tried in this thesis.

6.4.3 Timman's velocity profile

Although both a fixed parabolic profile and Pohlhausen's profile have been used, only the formulations for Timman's method are shown in this section. Those for the above two methods will be provided in the Appendix.

Timman's velocity profile is selected to have the asymptotic form of the solution of Prandtl's boundary layer equation at large y, which means at the so-called "edge" of the boundary layer.

$$\frac{u+V}{U+V} = 1 - \int_{\eta}^{\infty} e^{-\eta^2}(a + c\eta^2)d\eta - be^{-\eta^2} \equiv F(\eta) \tag{6.18}$$

where

$$\eta = \frac{y}{\delta(x)} \tag{6.19}$$

Three boundary conditions are

1. $u = -V$ at $\eta = 0 (y = 0)$

2. $\nu \frac{\partial^2 u}{\partial y^2} = -UU'$ at $\eta = 0$

3. $\frac{\partial^3 u}{\partial y^3} = 0$ at $\eta = 0$.

These are equivalent to

1. $F(0) = 1 - b - \frac{\sqrt{\pi}}{2}(a + \frac{c}{2}) = 0$

2. $F''(0) = 2b + -\frac{\Lambda}{\Psi}$

3. $F''''(0) = 2(c - a) = 0$.

Therefore

$$\begin{cases} a = c = \frac{4}{3\sqrt{\pi}}(1 - b) \\ b = -\frac{\Lambda}{2\Psi} \end{cases}$$

With these coefficients, we can obtain the expressions for boundary layer thickness.

$$\frac{\delta_1}{\delta} = \frac{4}{3}\frac{1-b}{\sqrt{\pi}} + \frac{b}{2}\sqrt{\pi} \tag{6.20}$$

$$\frac{\delta_2}{\delta} = (1-b)^2\frac{47-24\sqrt{\pi}}{18\pi}\sqrt{\frac{\pi}{2}} + \frac{b(1-b)}{\sqrt{\pi}} + b^2\frac{\sqrt{2}-1}{2}\sqrt{\frac{\pi}{2}} \tag{6.21}$$

6.4.4 Range of Shape Parameter

The parameter that decides the shape of the current velocity profile is $\frac{\Lambda}{\Psi}$. There is a constraint in the velocity profile for a steady flow, that is,

$$\forall y, \quad u \leq U$$

Also solutions from integral methods have been known to be valid up to a separation profile. The resulting range due to these limits is

$$-1 \leq \frac{\Lambda}{\Psi} \leq 4.53. \tag{6.22}$$

h he physical meaning of this parameter can be seen from the following form

$$\frac{\Lambda}{\Psi} = \frac{U\frac{dU}{dx}}{\frac{\nu(U+V)}{\delta^2}}. \tag{6.23}$$

Although δ is not a boundary layer thickness, it is a scale of the size of the boundary layer structure. Therefore $\frac{\Lambda}{\Psi}$ can be considered as a parameter that shows the order of the ratio between pressure force and shear force.

6.4.5 Singularity Condition

The singularity condition has been derived as equation 6.17 with $H1$ and $H2$ defined by equations 6.15 and 6.16.

For current the Timman's profile, these equations are written explicitly as

$$a_1\Lambda^2 + (a_2 + a_3\Psi)\Lambda + a_4\Psi^2 + a_5\Psi = 0 \tag{6.24}$$

$$b_1 + b_2\frac{\Psi}{\Lambda} + b_3\Psi + b_4\Lambda + b_5\Lambda^2 + b_6\Lambda\Psi + (b_7\Lambda + b_8\Lambda\Psi + b_9\Lambda^2)\frac{UU''}{U'^2} = 0 \qquad (6.25)$$

where

$$\begin{aligned} a_i &= 0.752253,\ -0.462823,\ -0.200961,\ 0.222966,\ -0.0189875 \\ b_i &= -0.3761265,\ 0.752253,\ -0.57886,\ 0.126639,\ 0.007595, \\ &\quad -0.074322,\ 0.066987,\ -0.74322,\ 0.007595 \end{aligned}$$

Therefore, for an imposed potential flow field, the values of $\Lambda(x)$ and $\Psi(x)$ are decided. Further specification of the value of $\frac{V}{U_{ex}}$ decides the location, and Re decides δ and other variables of the boundary layer.

6.4.6 Local Velocity

As will be seen in the next chapter, for the coming discussion we need vertical velocity distribution. Vertical velocity is obtained by integrating the mass conservation equation.

For the notations already defined in this section,

$$\frac{v}{U} = \delta\{(-\frac{U'}{U} - \Psi\frac{\delta'}{\delta} - \frac{\Psi}{2+r}\frac{dr}{dx})\int_0^\eta F dy + \Psi\frac{\delta'}{\delta}\eta F + \frac{\Psi}{2+r}\frac{dr}{dx}\eta - \frac{\sqrt{\pi}}{2}\frac{\Psi}{2+r}\frac{dr}{dx}\Phi\} \qquad (6.26)$$

where

$$r = \frac{\Lambda}{\Psi} \qquad (6.27)$$

and Φ is Fresnel function defined as

$$\Phi(\eta) = \frac{2}{\sqrt{\pi}}\int_0^\eta e^{-t^2} dt. \qquad (6.28)$$

For practical purposes, Fresnel's function has been approximated as

$$\Phi(\eta) = 1 - (\sum_{i=1}^{5} a_i t^i) e^{-\eta^2} \tag{6.29}$$

where

$$t = \frac{1}{1 + p\eta}.$$

p, and a_i's are provided in [1].

With this approximation, the integral in 6.26 can be calculated with

$$\int_0^\eta F dy = -\frac{r}{2} + (1 + \frac{r}{2}) \int_0^\eta \Phi(\eta) + \frac{1}{6}(\Phi'(\eta) - \Phi'(0)) + \frac{\sqrt{\pi}}{4}\Phi\eta. \tag{6.30}$$

6.4.7 l'Hospital's Rule Applied to a Stagnation Point

If a singularity exists somewhere in the range of x considered, then in order to the integrate equation 6.14, we have to start from the singular point. Otherwise integration explodes as it approaches the singularity. Given the fact that the current singularity is a saddle point, we can calculate the direction of integration at the singular point by applying l'Hospital's rule.

By defining a new non-dimensional parameter

$$\Delta_x = \frac{\delta U}{\nu} \frac{d\delta}{dx}, \tag{6.31}$$

we can rewrite equation 6.14, just for convenience, as

$$H1(\Lambda, \Phi)\Delta_x = H3(\Lambda, \Phi, \varphi) \tag{6.32}$$

where

$$H3 = \Lambda H2$$

$$\varphi = \frac{UU''}{U'^2}.$$

Applying l'Hospital's rule, we get

$$A\Delta_x{}^2 + B\Delta_x + C = 0 \tag{6.33}$$

where

$$A = 2\frac{U'}{U}\frac{\partial H1}{\partial \Lambda}$$

$$B = \Lambda\frac{U''}{U'}\frac{\partial H1}{\partial \Lambda} + \frac{1-\Phi}{U}U'\frac{\partial H1}{\partial \Phi} - 2\frac{U'}{U}\frac{U'}{U}\frac{\partial H3}{\partial \Lambda}$$

$$C = -\Lambda\frac{U''}{U'}\frac{\partial H3}{\partial \Lambda} + \frac{1-\Phi}{U}U'\frac{\partial H3}{\partial \Phi} - \frac{\partial H3}{\partial \varphi}\frac{d\varphi}{dx}$$

Chapter 7

Results from Tip Clearance Model

7.1 Behavior of Singular Point

Singularity has been found to exist for $\forall \frac{V}{U_{ex}}$. Some of its features have been plotted in figure B-27, figure B-28 and figure B-29. Figure B-27 shows the locations of the singular point with $\frac{V}{U_{ex}}$ as parameter. Figure B-28 shows the shape factor at the singularity $\frac{\Lambda}{\Psi}$. Figure B-29 shows the two possible derivatives at a singular point. Since the current singularity is a saddle point, there are two derivatives for a singular point.

As the existence of the singular point does not depend on Re (see equation 6.24 and equation 6.25), these results do not change for other values of Re. Re's effect appears as a scale factor of the boundary layer thickness by $\frac{1}{\sqrt{Re}}$, through Λ.

The first observation is that, for a large value of $\frac{V}{U_{ex}}$, both the location and the shape factor at the point approach certain limits. For small values of $\frac{V}{U_{ex}}$ ($\sim 10^{-1}$), they are very sensitive. The second outstanding feature is that the singular point, as $\frac{V}{U_{ex}}$ increases, moves from far upstream into the duct and at certain value of $\frac{V}{U_{ex}}$, returns back and it approaches a point that is located a little bit outside the duct ($x \approx -0.33h$). Then it stays at this location for any larger values of $\frac{V}{U_{ex}}$.

7.2 Local Velocity Distribution

Given the fact that there is no way to estimate the error due to the usage of integrated boundary layer method[22], a very rough parameter has been calculated to obtain qualitative a measure of the error.

$$P \equiv u\frac{\partial u}{\partial x} + v\frac{\partial u}{\partial y} + \frac{1}{\rho}\frac{dp}{dx} - \nu\frac{\partial^2 u}{\partial y^2} \tag{7.1}$$

P defined here has a dimension of acceleration. Non-dimensional P is defined as

$$P \equiv \frac{P}{\frac{U^2}{h}}. \tag{7.2}$$

In the tables attached (Table B-1 - Table B-7), for seven values of $\frac{V}{U_{ex}}$, the locations of singular point, local velocity distributions and P's values have been calculated and provided. The reason why there are two sets of velocities is that there are two derivatives at a singular point as shown in figure B-29 and vertical velocity depends on the derivative.

7.3 Integration from Singular Point

In figure B-22 and figure B-23, the integrations from the singular point have been shown. Each of the two plots corresponds to one of two derivatives at a singular point.

As can be seen, although integration starts smoothly from the singular point, it eventually explodes. This makes a sharp contrast to the case with a fixed parabolic profile case, where integration from a singular point always gives smooth results as shown in figure B-24.

This distinction occurs from the difference of the nature of phase planes. In case of parabolic profile, there is an isolated saddle point. However, for Timman's profile case, there exists an unexpected "crevasse", which divides the whole phase plane into two. This corresponds to a singularity, due to solely vanishing denominator. In

figure B-26 and figure B-25, corresponding phase planes are shown.

Successive integration is bound to hit the "crevasse", as can be seen from the arrows in figure B-25, and explodes immediately.

7.4 Comparison to Other Profiles

The results with Pohlhausen's method are basically the same as current results with Timman's profile. Although a singular point exists for any value of $\frac{V}{U_{ex}}$, the nature of the point changes from a saddle to a spiral for a large value of $\frac{V}{U_{ex}}$. In Appendix A, more details have been provided.

As far as a fixed parabolic profile is concerned, there are some differences. Other than one mentioned in previous section, there is a range of $\frac{V}{U_{ex}}$ so that singular a point can exist:

$$\frac{V}{U_{ex}} \leq \frac{2}{3}.$$

Chapter 8

Discussion of Tip Clearance Flow

8.1 Tip Clearance Flow from Physical Considerations

Careful consideration of streamlines for the current tip clearance flow reveals some of its interesting features.

In figure B-30, the pattern of streamlines has been shown. This pattern seems to be the only one that satisfies boundary conditions and other laws of physics. There have to be two internal stagnation points.

The stagnation point near P in this figure is due to a collision of a jet accelerated by the pressure force across the blade and the viscous shear force due to wall motion. As the non-zero pressure gradient is limited to a small portion of the domain near the leading edge, it can be said that this stagnation point is a result of a balance between pressure force and shear force. However, the other stagnation point near S is by the balance between viscous and inertia force.

Existence of circulating flow region, a simple consequence of mass conservation, suggests the possibility of a larger blockage effect due to a reverse flow region than that of an ordinary boundary layer.

8.2 Interpretation of Calculated Results

The current model is a simplification of tip clearance flow that does not take into account the structure of the suction side of a blade. The flow near the trailing edge of the tip is, as shown in figure B-30, much more disorganized than that of other regions. The phenomenon can be understood physically as a collision between tip clearance flow and the flow dragged by the endwall all the way from a neighboring cascade. A similar problem has been studied in the field of lubrication[20]. However in the current case, due to the much larger spacing of a cascade compared with the blade width, the growth of the boundary layer on the endwall can not be estimated easily, because the boundary layer experiences the effects of other strong factors such as secondary flow. Therefore among the features in figure B-30, the current model can deal with only a part of them.

8.2.1 Implications of the Singularity

Singularity sometimes plays a critical role in physics or related fields. In fluid mechanics, a singularity in Prandtl's boundary layer equation was found to allow flow separation at the point. Even a much simpler case like a quasi-one dimensional and isentropic divergent-convergent nozzle, singularity revealed that a sonic point is realized at nozzle throat.

There are always two possibilities of interpretation of a singular point. The first possibility is that a singular point conveys some physical meaning. This is especially the case when the validity of a governing equation can be relied on. Another case is that the point is an artificial singularity without any physical meaning. This can happen when a governing equation is used beyond its validity or when the introduced approximations and assumptions degrade the generality of the equation.

In the current case, it has not yet been found which of these cases applies. In the next chapter, the approximations and assumptions will be examined to see the validity of the governing equation. In the following section, the calculated results will be investigated to see their physical implications.

8.2.2 Behavior of a Singular Point

Figure B-30 basically implies that the singular point, for reasonably large $\frac{V}{U_{ex}}$, does not go away from the region with non-zero pressure gradient. This leads to the author to suspect that the singular point might be an internal stagnation point reflecting itself through the assumptions that have been made so far. There is another hint obtained from the local velocity distribution at a singular point.

8.2.3 Local Velocity Distribution

In Tables B-1 - B-7, the velocity distributions $\frac{u}{U}$, $\frac{v}{U}$ and P defined in section 7.2 have been shown in η direction from the wall surface at a singular point. In each of the tables, there are two sets of distributions marked by 1 and 2. They correspond to two derivatives at a singular point.

There is no a priori reason to choose one of the two sets over another. However a careful investigation of the second set of velocity distributions has led to the following observation:

As drawn in figure B-31 - a), there are two relative positions between a singular and stagnation point. To see the relative position, we have only to see the sign of v at the η location where u vanishes (for $x = x_{singular}$). That is ;

$$if\ \exists\eta\ u = 0,\ v < 0 \implies x_{stagnation} > x_{singular}$$
$$if\ \exists\eta\ u = 0,\ v > 0 \implies x_{stagnation} < x_{singular}$$
$$if\ \exists\eta\ u = 0,\ v = 0 \implies x_{stagnation} = x_{singular}.$$

Following this strategy, the examination of the tables has shown an interesting behavior of the two points. A singular point first stays away from a stagnation point for a small value of $\frac{V}{U_{ex}}$. As the $\frac{V}{U_{ex}}$ increases, the singular point comes closer to the stagnation point. At a point, where $\frac{V}{U_{ex}} \approx 0.8$ and $\frac{x}{h} \approx 0.37$, these two points

become identical. Further increase of $\frac{V}{U_{ee}}$ makes the singular point pass through the stagnation point.

The examination of P, which vanishes at the locations where the Prandtl's equation is satisfied, has shown an interesting trend. As the two points get closer, the number of η location with vanishing P increases from 0 to 1, 1 to 2, and 2 to 3. This means that as the two points come closer, the errors of the calculated results tend to gather around zero. As the two points go away with a further increase of $\frac{V}{U_{ee}}$, the number of $P = 0$ locations decreases back to zero eventually, which means that errors begin to increase again.

These observations are indirect and not decisive as a support of author's suspicion stated in section 8.2.2. However it seems to indicate that there is a relation between the two points. Due to the mathematical difficulties that will appear in this chapter, the author has been unable to prove his suspicion.

8.2.4 Internal Stagnation Point

In the 60's, in the context of unsteady separation, a similar stream line pattern was investigated. Efforts were made to find a similar argument to that by Goldstein for a steady case. The existence of a stagnation point in the frame moving with the point was thought to be an unsteady separation criterion, which is so-called MRS criterion([18], [26], [27], [29] and [30]). However no one has been able to prove the criterion. Ludwig conducted an experiment with a rotating cylinder as an effort in this direction[14]. Since then little work has been done on flows with this type of stagnation point.

8.2.5 Limit of Profile

The larger $\frac{V}{U_{ee}}$ becomes, the steeper the velocity profile becomes from the wall. As mentioned in Section 7.4, for large values of $\frac{V}{U_{ee}}$, the singularity with Pohlhausen's profile turns to be a spiral. Even for the case with Timman's profile, the errors seem to be larger for large values of $\frac{V}{U_{ee}}$ according to Section 8.2.3.

It seems that a profile that allows much steeper variations might make the results clearer for calculations.

8.3 Examination of Assumptions

Before we investigate the mathematical implications of the singular point, the assumptions on which solutions are based have to be examined.

8.3.1 Prandtl's Boundary Layer Equation

The Navier-Stokes equation is closely related to the biharmonic equation. However the Prandtl's boundary layer equation, which is an approximation to the Navier-Stokes equation, is a quasi-linear parabolic equation. Von Mises' transformation rewrites Prandtl's equation as

$$\frac{\partial g}{\partial x} = \mu u \frac{\partial^2 g}{\partial \Psi^2} \tag{8.1}$$

where $g = p + \frac{\rho u^2}{2}$ and Ψ is the streamfunction.

For a parabolic equation, it is said that there is a propitious direction in which its solution converges analytically, while the opposite direction leads to singularities.

As Prandtl argued in [23], a careful selection of initial function, $\frac{\partial^2 u}{\partial y^2}$ should improve the difficulties in calculating into the deleterious direction.

Numerically, integrations of the Prandtl's boundary layer equation with reversed flow regions have been known to be unstable. One of the suggestions to obtain a stable solution is to change the direction of integration in the reverse flow region[10].

The important fact is that the Prandtl's boundary layer equation does not have clear theoretical foundations despite its considerable success for decades[22].

It has been proved that imposing the potential flow can cause a singularity that is removable. As far as the current singularity is concerned, this author does not think that this is the case. Although only for a fixed parabolic profile, a calculation that interacts with potential flow through mass conservation has been done. The result

includes a singularity point and its behavior is very similar to that with an imposed potential flow. Of course, in this case, the singular condition becomes a vanishing determinant of a matrix.

The point here is that there are always uncertainties about the validity of the Prandtl's boundary layer equation, especially when a flow with an unknown nature is investigated, and the uncertainties can not be clarified mathematically.

8.3.2 Integral Method

The advantages of using this method comes from the reduction of a set of partial differential equation (PDE), the Prandtl's boundary layer equation, to an ordinary differential equation (ODE) or to a set of ODE's. However this reduction is a drastic change of the nature of differential equations. For an example, how the parabolic nature of the Prandtl's equation will reflect itself in an ODE does not seem to be answered.

The use of an approximate velocity profile also adds another uncertainty to the results. In general, errors by integrated methods can not be estimated [22].

As far as author knows, there is one indirect support about applying integrated boundary layer equation to the flow with reverse region. Danberg and Fansler used an integral method with a more sophisticated family of profiles to a rotating cylinder([5], [6]). Unlike the current method, they used an exact solution obtained by Rott[26] near a stagnation point of the rotating cylinder. They compared their results with experimental results by Ludwig[14]. However they did not provide any mathematical support to the use of integral method to their flow.

8.4 Unanswered Questions

There are three questions that need to be answered to construct the whole argument precisely and consistently.

1. Is the Prandtl's boundary layer equation a valid approximation for the current tip gap flow ?

2. Does the singularity of an internal stagnation point in the Prandtl's equation reflect itself as a singularity in the ODE that results from the integration of the PDE ?

3. How does the error due to the usage of an approximate profile affect the results ?

Unfortunately, each of these questions seems to be currently out of this author's scope.

Chapter 9

Recommendations

As made clear in chapter 8, it seems very difficult to interpret the singular point and clarify its connection with a stagnation point in a mathematically precise way.

Under these circumstances, one suggestion is to apply the current method to a rotating cylinder and to compare the calculated results with Ludwig's data.

Another suggestion is to solve a simple flow domain with pressure gradient and opposing wall motion numerically and compare the location of stagnation point to the predictions of our model. Boundary conditions can be treated by imposing a periodicity condition.

Appendix A

Application of Pohlhausen's Method

A.1 Pohlhausen's Velocity Profile

Pohlhausen's method is based on a fourth order polynomial velocity profile.

$$\frac{u+V}{U+V} = \sum_{i=1}^{4} a_i \left(\frac{y}{\delta}\right)^i \tag{A.1}$$

Here δ means boundary layer thickness unlike that of Timman's method. Coefficients a_i's are selected with the following boundary conditions.

1. $u = -V,\ v = 0\ ;\ at\ y = 0$
2. $\frac{\partial^2 u}{\partial y^2} = -\frac{1}{\nu} U \frac{dU}{dx}\ ;\ at\ y = 0$
3. $\frac{\partial u}{\partial y} = 0\ ;\ at\ y = \delta$
4. $\frac{\partial^2 u}{\partial y^2} = 0\ ;\ at\ y = \delta$
5. $u = U\ ;\ at\ y = \delta$

Out of these conditions, the first condition is satisfied by the form of A.1. Therefore other four conditions are enough to select the coefficients a_i's.

After defining a shape parameter

$$\Lambda = \frac{\delta^2}{\nu}\frac{dU}{dx},$$

equation A.1 is determined as

$$\frac{u}{U} = 1 - \Psi + \Psi F(y^*) + \frac{\Lambda}{6}G(y^*) \tag{A.2}$$

where

$$\begin{aligned}
\Psi &= 1 + \frac{V}{U} \\
y^* &= \frac{y}{\delta} \\
F &= 2y^* - 2y^{*3} + y^{*4} \\
G &= y^* - 3y^{*2} + 3y^{*3} - y^{*4}
\end{aligned}$$

A.2 Integrated Boundary Layer Equation

For the above velocity profile, boundary layer thicknesses are calculated as

$$\frac{\delta_1}{\delta} = \frac{3}{10}\Psi - \frac{\Lambda}{120} \tag{A.3}$$

$$\frac{\delta_2}{\delta} = -\frac{\Lambda^2}{9072} + \Lambda\frac{55\Psi - 63}{7560} + \frac{\Psi}{10}(-\frac{115}{63}\Psi + 3). \tag{A.4}$$

With these, the resulting integrated boundary layer equation is

$$H1(\Psi, \Lambda)\frac{d\delta}{dx} = \frac{\nu}{\delta U}H2(\Psi, \Lambda, U, \frac{dU}{dx}, \frac{d^2U}{dx^2}) \tag{A.5}$$

where

$$H1 = -\frac{5}{9072}(\Lambda - \frac{690}{25}\Psi + \frac{1134}{25})(\Lambda - 12\Psi) \quad \text{(A.6)}$$

$$\begin{aligned} H2 = {} & 2\Psi + \frac{\Lambda}{6} + (\frac{\Lambda}{4536} + \frac{55\Psi - 63}{7560})\Lambda^2 \frac{U}{(\frac{dU}{dx})^2}\frac{d^2U}{dx^2} \\ & + \Lambda(\Psi - 1)(\frac{11}{1512}\Lambda + \frac{189 - 230\Psi}{630}) \\ & - \Lambda\{-\frac{\Lambda^2}{4536} + \frac{55\Psi - 94.5}{3780}\Lambda + \frac{\Psi}{5}(-\frac{115}{63}\Psi + 4.5)\} \end{aligned} \quad \text{(A.7)}$$

A.3 Singularity

It has been shown that $H1$ and $H2$ can vanish simultaneously. The limit for this singularity, with the same constraint as that in Section ??, has been found to be

$$\frac{V}{U_{ex}} \leq 0.88. \quad \text{(A.8)}$$

Appendix B

Potential Flow Solution

The potential flow that has been imposed to calculate the boundary layer growth has been obtained for the following flow geometry by the method of conformal mapping:

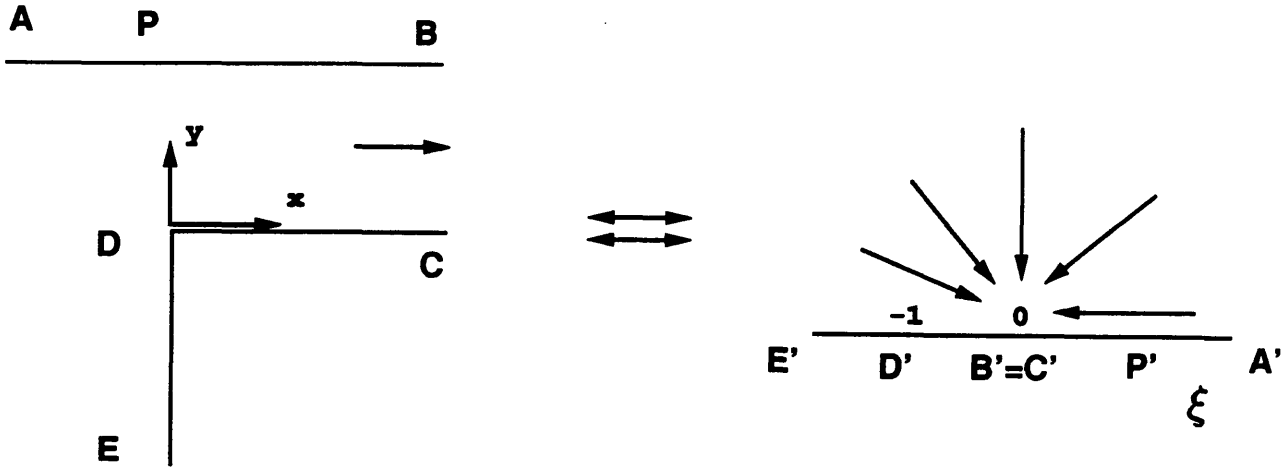

For the above coordinates, a conformal mapping, along the upper wall, is

$$\frac{x}{h} = -\frac{2}{\pi}(2\sqrt{\xi+1} + ln\frac{\sqrt{\xi+1}-1}{\sqrt{\xi+1}+1}) \qquad \text{(B.1)}$$

where h stands for a half of gap height.

Other variables of interests are

$$\frac{U}{U_{ex}} = \frac{1}{\sqrt{\xi + 1}} \tag{B.2}$$

$$\Psi = 1 + \frac{V}{U_{ex}}\sqrt{\xi + 1} \tag{B.3}$$

$$\frac{d(\frac{U}{U_{ex}})}{d\frac{x}{h}} = \frac{\pi}{4}\frac{\xi}{(\xi + 1)^2} \tag{B.4}$$

$$\frac{d^2(\frac{U}{U_{ex}})}{d(\frac{x}{h})^2} = \frac{\pi^2}{8}\frac{\xi(\xi - 1)}{(\xi + 1)^{\frac{7}{2}}}. \tag{B.5}$$

Bibliography

[1] Abramobitz and Milton. *Handbook of Mathematical Functions.* Dover, New York, 1970.

[2] J. S. Alford. "Protecting turbomachinary form self-excited rotor whirl." *Journal of Engineering for Power*, Oct 1965.

[3] J. P. Bindon and G. Morphis. "The development of axial turbine leakage loss for two profiled tip geometries using linear cascade data." *ASME Paper*, (90-GT-152), 1990.

[4] G. Chen. "Vortical structures in turbomachinary tip clearance flow." Nov 1990. Ph.D thesis, Massachusetts Institute of Technology.

[5] J. E. Danberg and K. S. Fansler. "Similarity solutions of the boundary-layer equations for flow over a moving wall." Technical Report 1741, Ballistic Research Laboratories, April 1974.

[6] J. E. Danberg and K. S. Fansler. "Separation-like similarity solutions on two-dimensional moving wall." *AIAA Journal*, 13:110–112, 1975.

[7] R. C. Dean. "The influence of tip clearance on boundary-layer flow in a rectilinear cascade." Technical Report 27-3, Gas Turbine Laboratory, M.I.T, 1954.

[8] R. P. Gauthier. "An investigation of flow field perturbation caused by constant blade-tip clearance in a turbine." Master's thesis, Massachusetts Institute of Technology, Aug 1990.

[9] J. A. H. Graham. "Investigation of a tip clearance in a water analogy rig.". *ASME Journal of Engineering for Gas Turbines and Power*, 108:38–46, 1986.

[10] J. B. Klemp and A. Acrivos. "A method for integrating the boundary-layer equations through a region of reverse flow." *Journal of Fluid Mechanics*, 53:177–191, 1972.

[11] B. Lashminarayana. "Methods of predicting the tip clearance effects in axial flow turbomachinary." *ASME Journal of Basic Engineering*, 104:467–481, 1970.

[12] B. Lashminarayana and J. H. Horlock. "Tip clearance flow and losses for an isolated compressor blade." Technical Report 3316, ARC R & M, 1962.

[13] K. Y. E. Leung. "3D Turbine tip clearance flow redistribution due to gap variation." Master's thesis, Massachusetts Institute of Technology, June 1991.

[14] G. R. Ludwig. "An experimental investigation of laminar separation from a moving wall." *AIAA Paper*, (64-6), 1964.

[15] M. Martinez-Sanchez and R. P. Gauthier. "Blade scale effects of tip leakage." Technical report, Gas Turbine Laboratory, M.I.T, Oct 1990.

[16] M. Martinez-Sanchez and B. Jaroux. "Turbine blade tip and seal clearance excitation forces." May 1992. Phase III Report on NASA Contract No. NAS8-35018.

[17] L. M. Milne-Thomson. *Theoretical Aerodynamics.* Dover Publications, New York, 1973.

[18] F. K. Moore. "On the separation of the unsteady boundary layer.". In H. Gortler, editor, *Boundary Layer Research*, pages 296–311. Springer, Berlin, 1958.

[19] J. Moore, J. G. Moore, G. S. Henry, and U. Chaudhry. "Flow and heat transfer in turbine tip gaps." *ASME Paper*, (88-GT-188), 1988.

[20] A. Mori and H. Mori. "Inlet boundary condition for submerged multi-pad bearings relative to fluid inertia forces." In D. Dowson, editor, *Fluid Film Lubrication - Osborne Reynolds Centenary.* Elsevier Science Publications, 1986.

[21] G. Morphis and J. P. Bindon. "The effects of relative motion, blade edge radius and gap size on the blade tip pressure distribution in an annular turbine cascade with clearance." *ASME Paper*, (88-GT-256), 1988.

[22] K. Nickel. "Prandtl's boundary-layer theory from the viewpoint of a mathematician." In *Annual Review of Fluid Mechanics*, pages 5:405–428. Annual Reviews, inc, 1973.

[23] L. Prandtl. "Note on the calculation of boundary layers." Technical Report TM 959, NACA, Nov 1940.

[24] Y. J. Qiu. "An investigation of destabilizing blade tip forces for shrouded and unshrouded turbines." Master's thesis, Massachusetts Institute of Technology, Aug 1983.

[25] L. (Ed.) Rosenhead. *Laminar Boundary Layers.* Oxford University Press, Oxford, 1963.

[26] N. Rott. "Unsteady viscous flow in the vicinity of a stagnation point." *Quarterly of Applied Mathematics*, 13:444–451, 1956.

[27] W. R. Sears and D. P. Telionis. "Boundary-layer separation in unsteady flow." *SIAM Journal of Applied Mathematics*, 28(1):215–235, Jan 1975.

[28] O. P. Sharma, G. F. Pickett, and R. H. Ni. "Assessment of unsteady flows in turbines." *ASME Paper*, (90-GT-150), 1990.

[29] D. P. Telionis. *Unsteady Viscous Flows.* Springer-Verlag, New York, 1981.

[30] D. P. Telionis and M. J. Werle. "boundary-layer separation from downstream-moving boundaries". *Journal of Applied Mechanics*, (95):369–374, 1973.

[31] H. J. Thomas. "Unstable oscillations of turbine rotors due to steam leakage in the clearance of the sealing glands and the buckets." *Bulletin Scientifique, A.J.M.*, 1958.

[32] R. Timman. "A one-parameter method for the calculation of laminar boundary layers." Technical Report F.35, Nationaal Luchtvaart Laboratorium, 1949.

[33] M. Yaras and S. A. Sjolander. "Development of the tip-leakage flow downstream of a planar cascade of turbine blades: Vorticity field." *ASME Paper*, (89-GT-55), 1989.

[34] M. Yaras and S. A. Sjolander. "Effects of simulated rotation on tip leakage in a planar cascade of turbine blades: Part I - Tip gap flow." *ASME Journal of Engineering for Gas Turbines and Power*, 114:652–659, 1992.

$\frac{V}{U_{ex}} = 0.79433$, $\frac{x}{h} = 0.23539$

η	$\frac{u}{U}$	$\frac{v_1}{U}$	P_1	$\frac{u}{U}$	$\frac{v_2}{U}$	P_2
.5000E-01	-.8346E+00	.4553E-05	.2152E-01	-.8346E+00	.5947E-05	-.3753E-01
.1000E+00	-.7592E+00	.1698E-04	.3625E-01	-.7592E+00	.2118E-04	-.7104E-01
.1500E+00	-.6865E+00	.3610E-04	.4507E-01	-.6865E+00	.4045E-04	-.1004E+00
.2000E+00	-.6160E+00	.6166E-04	.4892E-01	-.6160E+00	.5679E-04	-.1256E+00
.2500E+00	-.5475E+00	.9428E-04	.4872E-01	-.5475E+00	.6160E-04	-.1466E+00
.3000E+00	-.4807E+00	.1354E-03	.4535E-01	-.4807E+00	.4499E-04	-.1631E+00
.3500E+00	-.4153E+00	.1871E-03	.3962E-01	-.4153E+00	-.3915E-05	-.1752E+00
.4000E+00	-.3509E+00	.2520E-03	.3224E-01	-.3509E+00	-.9652E-04	-.1828E+00
.4500E+00	-.2875E+00	.3331E-03	.2384E-01	-.2875E+00	-.2443E-03	-.1857E+00
.5000E+00	-.2248E+00	.4334E-03	.1491E-01	-.2248E+00	-.4585E-03	-.1839E+00
.5500E+00	-.1627E+00	.5559E-03	.5862E-02	-.1627E+00	-.7492E-03	-.1775E+00
.6000E+00	-.1012E+00	.7033E-03	-.3002E-02	-.1012E+00	-.1126E-02	-.1666E+00
.6500E+00	-.4023E-01	.8779E-03	-.1146E-01	-.4023E-01	-.1595E-02	-.1515E+00
.7000E+00	.2017E-01	.1081E-02	-.1936E-01	.2017E-01	-.2162E-02	-.1325E+00
.7500E+00	.7990E-01	.1314E-02	-.2662E-01	.7990E-01	-.2831E-02	-.1102E+00
.8000E+00	.1388E+00	.1576E-02	-.3319E-01	.1388E+00	-.3602E-02	-.8504E-01
.8500E+00	.1968E+00	.1867E-02	-.3906E-01	.1968E+00	-.4473E-02	-.5784E-01
.9000E+00	.2536E+00	.2185E-02	-.4425E-01	.2536E+00	-.5441E-02	-.2927E-01
.9500E+00	.3090E+00	.2527E-02	-.4878E-01	.3090E+00	-.6498E-02	-.9084E-04
.1000E+01	.3629E+00	.2890E-02	-.5269E-01	.3629E+00	-.7638E-02	.2893E-01
.1050E+01	.4150E+00	.3270E-02	-.5602E-01	.4150E+00	-.8850E-02	.5708E-01
.1100E+01	.4652E+00	.3662E-02	-.5880E-01	.4652E+00	-.1012E-01	.8368E-01
.1150E+01	.5132E+00	.4061E-02	-.6106E-01	.5132E+00	-.1144E-01	.1081E+00
.1200E+01	.5588E+00	.4463E-02	-.6284E-01	.5588E+00	-.1280E-01	.1300E+00
.1250E+01	.6020E+00	.4862E-02	-.6415E-01	.6020E+00	-.1418E-01	.1488E+00
.1300E+01	.6427E+00	.5252E-02	-.6502E-01	.6427E+00	-.1556E-01	.1644E+00
.1350E+01	.6807E+00	.5630E-02	-.6547E-01	.6807E+00	-.1695E-01	.1765E+00
.1400E+01	.7161E+00	.5989E-02	-.6552E-01	.7161E+00	-.1832E-01	.1851E+00
.1450E+01	.7487E+00	.6327E-02	-.6519E-01	.7487E+00	-.1966E-01	.1904E+00
.1500E+01	.7787E+00	.6640E-02	-.6450E-01	.7787E+00	-.2097E-01	.1924E+00
.1550E+01	.8061E+00	.6924E-02	-.6348E-01	.8061E+00	-.2223E-01	.1914E+00
.1600E+01	.8309E+00	.7178E-02	-.6216E-01	.8309E+00	-.2344E-01	.1876E+00
.1650E+01	.8533E+00	.7399E-02	-.6057E-01	.8533E+00	-.2460E-01	.1815E+00
.1700E+01	.8734E+00	.7586E-02	-.5876E-01	.8734E+00	-.2570E-01	.1734E+00
.1750E+01	.8912E+00	.7739E-02	-.5675E-01	.8912E+00	-.2673E-01	.1636E+00
.1800E+01	.9071E+00	.7859E-02	-.5459E-01	.9071E+00	-.2770E-01	.1525E+00
.1850E+01	.9210E+00	.7944E-02	-.5233E-01	.9210E+00	-.2861E-01	.1406E+00
.1900E+01	.9332E+00	.7998E-02	-.5001E-01	.9332E+00	-.2945E-01	.1280E+00
.1950E+01	.9438E+00	.8020E-02	-.4766E-01	.9438E+00	-.3024E-01	.1153E+00
.2000E+01	.9529E+00	.8012E-02	-.4532E-01	.9529E+00	-.3097E-01	.1025E+00
.2050E+01	.9608E+00	.7977E-02	-.4303E-01	.9608E+00	-.3164E-01	.9000E-01
.2100E+01	.9675E+00	.7916E-02	-.4081E-01	.9675E+00	-.3226E-01	.7795E-01
.2150E+01	.9733E+00	.7831E-02	-.3870E-01	.9733E+00	-.3283E-01	.6650E-01
.2200E+01	.9781E+00	.7725E-02	-.3670E-01	.9781E+00	-.3336E-01	.5577E-01
.2250E+01	.9821E+00	.7599E-02	-.3484E-01	.9821E+00	-.3385E-01	.4584E-01
.2300E+01	.9855E+00	.7456E-02	-.3312E-01	.9855E+00	-.3431E-01	.3674E-01
.2350E+01	.9883E+00	.7298E-02	-.3155E-01	.9883E+00	-.3473E-01	.2851E-01
.2400E+01	.9906E+00	.7126E-02	-.3013E-01	.9906E+00	-.3513E-01	.2114E-01
.2450E+01	.9925E+00	.6942E-02	-.2887E-01	.9925E+00	-.3550E-01	.1460E-01
.2500E+01	.9940E+00	.6748E-02	-.2774E-01	.9940E+00	-.3585E-01	.8847E-02
.2550E+01	.9953E+00	.6545E-02	-.2675E-01	.9953E+00	-.3618E-01	.3837E-02
.2600E+01	.9963E+00	.6335E-02	-.2589E-01	.9963E+00	-.3650E-01	-.4887E-03
.2650E+01	.9971E+00	.6118E-02	-.2515E-01	.9971E+00	-.3680E-01	-.4193E-02
.2700E+01	.9977E+00	.5896E-02	-.2451E-01	.9977E+00	-.3710E-01	-.7338E-02
.2750E+01	.9982E+00	.5669E-02	-.2397E-01	.9982E+00	-.3738E-01	-.9989E-02
.2800E+01	.9987E+00	.5439E-02	-.2351E-01	.9987E+00	-.3766E-01	-.1220E-01
.2850E+01	.9990E+00	.5206E-02	-.2313E-01	.9990E+00	-.3793E-01	-.1404E-01
.2900E+01	.9992E+00	.4970E-02	-.2282E-01	.9992E+00	-.3819E-01	-.1556E-01
.2950E+01	.9994E+00	.4732E-02	-.2256E-01	.9994E+00	-.3845E-01	-.1679E-01
.3000E+01	.9995E+00	.4493E-02	-.2234E-01	.9995E+00	-.3871E-01	-.1780E-01
.3050E+01	.9997E+00	.4252E-02	-.2217E-01	.9997E+00	-.3897E-01	-.1861E-01

Table B.1: Velocity Distributions at a Singular Point - 1

$\frac{V}{U_{ex}} = 0.88308$, $\frac{x}{h} = 0.3674$

η	$\frac{u}{U}$	$\frac{v_1}{U}$	P_1	$\frac{u}{U}$	$\frac{v_2}{U}$	P_2
.5000E-01	-.9049E+00	.1011E-04	.3406E-01	-.9049E+00	.1685E-04	-.1689E-01
.1000E+00	-.8196E+00	.3801E-04	.5876E-01	-.8196E+00	.6365E-04	-.3277E-01
.1500E+00	-.7378E+00	.8109E-04	.7523E-01	-.7378E+00	.1338E-03	-.4740E-01
.2000E+00	-.6591E+00	.1381E-03	.8465E-01	-.6591E+00	.2196E-03	-.6059E-01
.2500E+00	-.5832E+00	.2093E-03	.8816E-01	-.5832E+00	.3119E-03	-.7209E-01
.3000E+00	-.5098E+00	.2962E-03	.8688E-01	-.5098E+00	.4011E-03	-.8166E-01
.3500E+00	-.4386E+00	.4012E-03	.8179E-01	-.4386E+00	.4766E-03	-.8906E-01
.4000E+00	-.3692E+00	.5280E-03	.7379E-01	-.3692E+00	.5277E-03	-.9402E-01
.4500E+00	-.3015E+00	.6807E-03	.6363E-01	-.3015E+00	.5436E-03	-.9631E-01
.5000E+00	-.2351E+00	.8636E-03	.5196E-01	-.2351E+00	.5140E-03	-.9575E-01
.5500E+00	-.1700E+00	.1081E-02	.3928E-01	-.1700E+00	.4294E-03	-.9224E-01
.6000E+00	-.1060E+00	.1338E-02	.2603E-01	-.1060E+00	.2813E-03	-.8575E-01
.6500E+00	-.4295E-01	.1636E-02	.1251E-01	-.4295E-01	.6249E-04	-.7636E-01
.7000E+00	.1903E-01	.1980E-02	-.9937E-03	.1903E-01	-.2324E-03	-.6427E-01
.7500E+00	.7997E-01	.2370E-02	-.1429E-01	.7997E-01	-.6070E-03	-.4976E-01
.8000E+00	.1398E+00	.2806E-02	-.2720E-01	.1398E+00	-.1063E-02	-.3324E-01
.8500E+00	.1984E+00	.3288E-02	-.3958E-01	.1984E+00	-.1601E-02	-.1516E-01
.9000E+00	.2556E+00	.3814E-02	-.5132E-01	.2556E+00	-.2217E-02	.3942E-02
.9500E+00	.3112E+00	.4379E-02	-.6231E-01	.3112E+00	-.2909E-02	.2353E-01
.1000E+01	.3652E+00	.4980E-02	-.7244E-01	.3652E+00	-.3671E-02	.4303E-01
.1050E+01	.4173E+00	.5609E-02	-.8163E-01	.4173E+00	-.4496E-02	.6192E-01
.1100E+01	.4673E+00	.6261E-02	-.8980E-01	.4673E+00	-.5375E-02	.7969E-01
.1150E+01	.5152E+00	.6928E-02	-.9688E-01	.5152E+00	-.6301E-02	.9591E-01
.1200E+01	.5606E+00	.7603E-02	-.1028E+00	.5606E+00	-.7262E-02	.1102E+00
.1250E+01	.6036E+00	.8277E-02	-.1076E+00	.6036E+00	-.8249E-02	.1224E+00
.1300E+01	.6440E+00	.8943E-02	-.1111E+00	.6440E+00	-.9253E-02	.1321E+00
.1350E+01	.6818E+00	.9593E-02	-.1135E+00	.6818E+00	-.1026E-01	.1394E+00
.1400E+01	.7170E+00	.1022E-01	-.1147E+00	.7170E+00	-.1127E-01	.1442E+00
.1450E+01	.7494E+00	.1082E-01	-.1148E+00	.7494E+00	-.1227E-01	.1466E+00
.1500E+01	.7793E+00	.1138E-01	-.1138E+00	.7793E+00	-.1325E-01	.1467E+00
.1550E+01	.8065E+00	.1190E-01	-.1119E+00	.8065E+00	-.1420E-01	.1447E+00
.1600E+01	.8312E+00	.1238E-01	-.1091E+00	.8312E+00	-.1512E-01	.1408E+00
.1650E+01	.8535E+00	.1282E-01	-.1056E+00	.8535E+00	-.1601E-01	.1353E+00
.1700E+01	.8735E+00	.1320E-01	-.1014E+00	.8735E+00	-.1686E-01	.1284E+00
.1750E+01	.8913E+00	.1354E-01	-.9668E-01	.8913E+00	-.1767E-01	.1204E+00
.1800E+01	.9071E+00	.1382E-01	-.9160E-01	.9071E+00	-.1843E-01	.1116E+00
.1850E+01	.9210E+00	.1406E-01	-.8625E-01	.9210E+00	-.1916E-01	.1023E+00
.1900E+01	.9331E+00	.1425E-01	-.8076E-01	.9331E+00	-.1984E-01	.9270E-01
.1950E+01	.9437E+00	.1439E-01	-.7522E-01	.9437E+00	-.2047E-01	.8300E-01
.2000E+01	.9529E+00	.1449E-01	-.6974E-01	.9529E+00	-.2107E-01	.7341E-01
.2050E+01	.9607E+00	.1455E-01	-.6439E-01	.9607E+00	-.2163E-01	.6409E-01
.2100E+01	.9674E+00	.1457E-01	-.5926E-01	.9674E+00	-.2216E-01	.5517E-01
.2150E+01	.9732E+00	.1456E-01	-.5439E-01	.9732E+00	-.2265E-01	.4675E-01
.2200E+01	.9780E+00	.1451E-01	-.4982E-01	.9780E+00	-.2311E-01	.3890E-01
.2250E+01	.9820E+00	.1443E-01	-.4559E-01	.9820E+00	-.2354E-01	.3166E-01
.2300E+01	.9854E+00	.1433E-01	-.4171E-01	.9854E+00	-.2395E-01	.2507E-01
.2350E+01	.9882E+00	.1421E-01	-.3819E-01	.9882E+00	-.2433E-01	.1913E-01
.2400E+01	.9905E+00	.1406E-01	-.3503E-01	.9905E+00	-.2470E-01	.1383E-01
.2450E+01	.9924E+00	.1390E-01	-.3222E-01	.9924E+00	-.2505E-01	.9138E-02
.2500E+01	.9940E+00	.1372E-01	-.2974E-01	.9940E+00	-.2538E-01	.5028E-02
.2550E+01	.9952E+00	.1352E-01	-.2758E-01	.9952E+00	-.2570E-01	.1459E-02
.2600E+01	.9963E+00	.1332E-01	-.2570E-01	.9963E+00	-.2601E-01	-.1616E-02
.2650E+01	.9971E+00	.1311E-01	-.2409E-01	.9971E+00	-.2631E-01	-.4241E-02
.2700E+01	.9977E+00	.1289E-01	-.2271E-01	.9977E+00	-.2660E-01	-.6466E-02
.2750E+01	.9982E+00	.1266E-01	-.2155E-01	.9982E+00	-.2689E-01	-.8336E-02
.2800E+01	.9986E+00	.1242E-01	-.2058E-01	.9986E+00	-.2717E-01	-.9897E-02
.2850E+01	.9990E+00	.1218E-01	-.1977E-01	.9990E+00	-.2744E-01	-.1119E-01
.2900E+01	.9992E+00	.1194E-01	-.1910E-01	.9992E+00	-.2771E-01	-.1225E-01
.2950E+01	.9994E+00	.1170E-01	-.1855E-01	.9994E+00	-.2798E-01	-.1312E-01
.3000E+01	.9995E+00	.1145E-01	-.1810E-01	.9995E+00	-.2825E-01	-.1382E-01
.3050E+01	.9997E+00	.1120E-01	-.1774E-01	.9997E+00	-.2851E-01	-.1439E-01

Table B.2: Velocity Distributions at a Singular Point - 2

$\frac{V}{U_{ex}} = 0.94624$, $\frac{x}{h} = 0.38373$

η	$\frac{u}{U}$	$\frac{v_1}{U}$	P_1	$\frac{u}{U}$	$\frac{v_2}{U}$	P_2
.5000E-01	-.9646E+00	.1242E-04	.4028E-01	-.9646E+00	.2411E-04	-.8212E-02
.1000E+00	-.8710E+00	.4645E-04	.6950E-01	-.8710E+00	.9184E-04	-.1678E-01
.1500E+00	-.7816E+00	.9839E-04	.8899E-01	-.7816E+00	.1954E-03	-.2540E-01
.2000E+00	-.6961E+00	.1662E-03	.1002E+00	-.6961E+00	.3260E-03	-.3380E-01
.2500E+00	-.6141E+00	.2496E-03	.1044E+00	-.6141E+00	.4738E-03	-.4165E-01
.3000E+00	-.5353E+00	.3499E-03	.1029E+00	-.5353E+00	.6281E-03	-.4863E-01
.3500E+00	-.4592E+00	.4696E-03	.9693E-01	-.4592E+00	.7779E-03	-.5439E-01
.4000E+00	-.3857E+00	.6128E-03	.8749E-01	-.3857E+00	.9119E-03	-.5860E-01
.4500E+00	-.3144E+00	.7840E-03	.7545E-01	-.3144E+00	.1019E-02	-.6092E-01
.5000E+00	-.2449E+00	.9884E-03	.6155E-01	-.2449E+00	.1088E-02	-.6109E-01
.5500E+00	-.1772E+00	.1231E-02	.4637E-01	-.1772E+00	.1109E-02	-.5891E-01
.6000E+00	-.1111E+00	.1518E-02	.3040E-01	-.1111E+00	.1073E-02	-.5427E-01
.6500E+00	-.4637E-01	.1852E-02	.1401E-01	-.4637E-01	.9727E-03	-.4716E-01
.7000E+00	.1699E-01	.2238E-02	-.2473E-02	.1699E-01	.8020E-03	-.3771E-01
.7500E+00	.7899E-01	.2677E-02	-.1881E-01	.7899E-01	.5564E-03	-.2612E-01
.8000E+00	.1396E+00	.3170E-02	-.3478E-01	.1396E+00	.2335E-03	-.1271E-01
.8500E+00	.1988E+00	.3717E-02	-.5020E-01	.1988E+00	-.1673E-03	.2125E-02
.9000E+00	.2564E+00	.4315E-02	-.6489E-01	.2564E+00	-.6448E-03	.1793E-01
.9500E+00	.3123E+00	.4961E-02	-.7870E-01	.3123E+00	-.1196E-02	.3420E-01
.1000E+01	.3664E+00	.5650E-02	-.9148E-01	.3664E+00	-.1816E-02	.5046E-01
.1050E+01	.4185E+00	.6374E-02	-.1031E+00	.4185E+00	-.2500E-02	.6621E-01
.1100E+01	.4685E+00	.7127E-02	-.1134E+00	.4685E+00	-.3240E-02	.8101E-01
.1150E+01	.5162E+00	.7900E-02	-.1223E+00	.5162E+00	-.4027E-02	.9446E-01
.1200E+01	.5616E+00	.8684E-02	-.1298E+00	.5616E+00	-.4854E-02	.1062E+00
.1250E+01	.6044E+00	.9470E-02	-.1357E+00	.6044E+00	-.5712E-02	.1161E+00
.1300E+01	.6447E+00	.1025E-01	-.1401E+00	.6447E+00	-.6591E-02	.1239E+00
.1350E+01	.6824E+00	.1101E-01	-.1430E+00	.6824E+00	-.7483E-02	.1295E+00
.1400E+01	.7174E+00	.1175E-01	-.1443E+00	.7174E+00	-.8378E-02	.1329E+00
.1450E+01	.7498E+00	.1246E-01	-.1442E+00	.7498E+00	-.9270E-02	.1343E+00
.1500E+01	.7795E+00	.1313E-01	-.1427E+00	.7795E+00	-.1015E-01	.1336E+00
.1550E+01	.8066E+00	.1376E-01	-.1399E+00	.8066E+00	-.1101E-01	.1311E+00
.1600E+01	.8312E+00	.1433E-01	-.1361E+00	.8312E+00	-.1185E-01	.1270E+00
.1650E+01	.8535E+00	.1486E-01	-.1313E+00	.8535E+00	-.1267E-01	.1214E+00
.1700E+01	.8734E+00	.1533E-01	-.1257E+00	.8734E+00	-.1345E-01	.1148E+00
.1750E+01	.8912E+00	.1574E-01	-.1194E+00	.8912E+00	-.1420E-01	.1072E+00
.1800E+01	.9070E+00	.1609E-01	-.1127E+00	.9070E+00	-.1491E-01	.9904E-01
.1850E+01	.9208E+00	.1639E-01	-.1057E+00	.9208E+00	-.1559E-01	.9041E-01
.1900E+01	.9330E+00	.1664E-01	-.9851E-01	.9330E+00	-.1623E-01	.8158E-01
.1950E+01	.9436E+00	.1683E-01	-.9129E-01	.9436E+00	-.1684E-01	.7273E-01
.2000E+01	.9527E+00	.1697E-01	-.8417E-01	.9527E+00	-.1741E-01	.6403E-01
.2050E+01	.9606E+00	.1706E-01	-.7724E-01	.9606E+00	-.1795E-01	.5560E-01
.2100E+01	.9673E+00	.1711E-01	-.7060E-01	.9673E+00	-.1846E-01	.4757E-01
.2150E+01	.9730E+00	.1712E-01	-.6431E-01	.9730E+00	-.1894E-01	.4002E-01
.2200E+01	.9779E+00	.1709E-01	-.5844E-01	.9779E+00	-.1940E-01	.3299E-01
.2250E+01	.9819E+00	.1703E-01	-.5300E-01	.9819E+00	-.1983E-01	.2654E-01
.2300E+01	.9853E+00	.1693E-01	-.4803E-01	.9853E+00	-.2023E-01	.2068E-01
.2350E+01	.9882E+00	.1681E-01	-.4353E-01	.9882E+00	-.2062E-01	.1541E-01
.2400E+01	.9905E+00	.1667E-01	-.3949E-01	.9905E+00	-.2099E-01	.1071E-01
.2450E+01	.9924E+00	.1650E-01	-.3590E-01	.9924E+00	-.2135E-01	.6562E-02
.2500E+01	.9939E+00	.1632E-01	-.3275E-01	.9939E+00	-.2169E-01	.2935E-02
.2550E+01	.9952E+00	.1612E-01	-.2999E-01	.9952E+00	-.2202E-01	-.2094E-03
.2600E+01	.9962E+00	.1591E-01	-.2760E-01	.9962E+00	-.2235E-01	-.2913E-02
.2650E+01	.9970E+00	.1568E-01	-.2556E-01	.9970E+00	-.2266E-01	-.5220E-02
.2700E+01	.9977E+00	.1545E-01	-.2381E-01	.9977E+00	-.2297E-01	-.7171E-02
.2750E+01	.9982E+00	.1521E-01	-.2234E-01	.9982E+00	-.2327E-01	-.8810E-02
.2800E+01	.9986E+00	.1496E-01	-.2111E-01	.9986E+00	-.2356E-01	-.1018E-01
.2850E+01	.9989E+00	.1470E-01	-.2008E-01	.9989E+00	-.2385E-01	-.1130E-01
.2900E+01	.9992E+00	.1444E-01	-.1924E-01	.9992E+00	-.2414E-01	-.1223E-01
.2950E+01	.9994E+00	.1418E-01	-.1854E-01	.9994E+00	-.2443E-01	-.1299E-01
.3000E+01	.9995E+00	.1392E-01	-.1798E-01	.9995E+00	-.2471E-01	-.1360E-01
.3050E+01	.9997E+00	.1365E-01	-.1752E-01	.9997E+00	-.2499E-01	-.1409E-01

Table B.3: Velocity Distributions at a Singular Point - 3

$\frac{V}{U_{ex}} = 0.97275$, $\frac{x}{h} = 0.38133$

η	$\frac{u}{U}$	$\frac{v_1}{U}$	P_1	$\frac{u}{U}$	$\frac{v_2}{U}$	P_2
.5000E-01	-.9908E+00	.1304E-04	.4239E-01	-.9908E+00	.2704E-04	-.5298E-02
.1000E+00	-.8937E+00	.4860E-04	.7305E-01	-.8937E+00	.1032E-03	-.1143E-01
.1500E+00	-.8010E+00	.1025E-03	.9340E-01	-.8010E+00	.2202E-03	-.1807E-01
.2000E+00	-.7125E+00	.1725E-03	.1049E+00	-.7125E+00	.3687E-03	-.2490E-01
.2500E+00	-.6279E+00	.2578E-03	.1091E+00	-.6279E+00	.5385E-03	-.3158E-01
.3000E+00	-.5466E+00	.3598E-03	.1074E+00	-.5466E+00	.7185E-03	-.3775E-01
.3500E+00	-.4685E+00	.4810E-03	.1009E+00	-.4685E+00	.8973E-03	-.4302E-01
.4000E+00	-.3932E+00	.6255E-03	.9071E-01	-.3932E+00	.1063E-02	-.4703E-01
.4500E+00	-.3203E+00	.7980E-03	.7783E-01	-.3203E+00	.1205E-02	-.4941E-01
.5000E+00	-.2495E+00	.1004E-02	.6300E-01	-.2495E+00	.1310E-02	-.4985E-01
.5500E+00	-.1807E+00	.1249E-02	.4684E-01	-.1807E+00	.1370E-02	-.4812E-01
.6000E+00	-.1136E+00	.1539E-02	.2984E-01	-.1136E+00	.1375E-02	-.4407E-01
.6500E+00	-.4812E-01	.1878E-02	.1241E-01	-.4812E-01	.1317E-02	-.3768E-01
.7000E+00	.1584E-01	.2269E-02	-.5125E-02	.1584E-01	.1189E-02	-.2903E-01
.7500E+00	.7831E-01	.2717E-02	-.2251E-01	.7831E-01	.9867E-03	-.1831E-01
.8000E+00	.1393E+00	.3221E-02	-.3951E-01	.1393E+00	.7079E-03	-.5814E-02
.8500E+00	.1987E+00	.3780E-02	-.5593E-01	.1987E+00	.3514E-03	.8086E-02
.9000E+00	.2565E+00	.4394E-02	-.7157E-01	.2565E+00	-.8196E-04	.2295E-01
.9500E+00	.3125E+00	.5058E-02	-.8628E-01	.3125E+00	-.5895E-03	.3830E-01
.1000E+01	.3667E+00	.5768E-02	-.9988E-01	.3667E+00	-.1167E-02	.5365E-01
.1050E+01	.4188E+00	.6515E-02	-.1122E+00	.4188E+00	-.1809E-02	.6854E-01
.1100E+01	.4688E+00	.7293E-02	-.1232E+00	.4688E+00	-.2508E-02	.8251E-01
.1150E+01	.5165E+00	.8093E-02	-.1327E+00	.5165E+00	-.3256E-02	.9519E-01
.1200E+01	.5619E+00	.8907E-02	-.1406E+00	.5619E+00	-.4046E-02	.1063E+00
.1250E+01	.6047E+00	.9723E-02	-.1468E+00	.6047E+00	-.4868E-02	.1155E+00
.1300E+01	.6449E+00	.1053E-01	-.1514E+00	.6449E+00	-.5714E-02	.1227E+00
.1350E+01	.6826E+00	.1133E-01	-.1543E+00	.6826E+00	-.6575E-02	.1278E+00
.1400E+01	.7175E+00	.1210E-01	-.1555E+00	.7175E+00	-.7442E-02	.1308E+00
.1450E+01	.7498E+00	.1284E-01	-.1553E+00	.7498E+00	-.8307E-02	.1318E+00
.1500E+01	.7795E+00	.1354E-01	-.1535E+00	.7795E+00	-.9164E-02	.1309E+00
.1550E+01	.8066E+00	.1419E-01	-.1504E+00	.8066E+00	-.1001E-01	.1282E+00
.1600E+01	.8312E+00	.1480E-01	-.1462E+00	.8312E+00	-.1083E-01	.1239E+00
.1650E+01	.8534E+00	.1535E-01	-.1409E+00	.8534E+00	-.1162E-01	.1184E+00
.1700E+01	.8734E+00	.1584E-01	-.1347E+00	.8734E+00	-.1239E-01	.1117E+00
.1750E+01	.8911E+00	.1628E-01	-.1279E+00	.8911E+00	-.1313E-01	.1042E+00
.1800E+01	.9069E+00	.1665E-01	-.1206E+00	.9069E+00	-.1383E-01	.9609E-01
.1850E+01	.9208E+00	.1697E-01	-.1129E+00	.9208E+00	-.1450E-01	.8759E-01
.1900E+01	.9329E+00	.1723E-01	-.1051E+00	.9329E+00	-.1514E-01	.7890E-01
.1950E+01	.9435E+00	.1743E-01	-.9729E-01	.9435E+00	-.1574E-01	.7022E-01
.2000E+01	.9526E+00	.1759E-01	-.8957E-01	.9526E+00	-.1631E-01	.6170E-01
.2050E+01	.9605E+00	.1769E-01	-.8207E-01	.9605E+00	-.1685E-01	.5346E-01
.2100E+01	.9673E+00	.1774E-01	-.7489E-01	.9673E+00	-.1736E-01	.4562E-01
.2150E+01	.9730E+00	.1776E-01	-.6810E-01	.9730E+00	-.1785E-01	.3825E-01
.2200E+01	.9778E+00	.1773E-01	-.6176E-01	.9778E+00	-.1830E-01	.3141E-01
.2250E+01	.9819E+00	.1767E-01	-.5590E-01	.9819E+00	-.1874E-01	.2514E-01
.2300E+01	.9853E+00	.1757E-01	-.5054E-01	.9853E+00	-.1915E-01	.1944E-01
.2350E+01	.9881E+00	.1745E-01	-.4569E-01	.9881E+00	-.1954E-01	.1432E-01
.2400E+01	.9905E+00	.1730E-01	-.4134E-01	.9905E+00	-.1992E-01	.9759E-02
.2450E+01	.9924E+00	.1713E-01	-.3748E-01	.9924E+00	-.2028E-01	.5738E-02
.2500E+01	.9939E+00	.1695E-01	-.3408E-01	.9939E+00	-.2063E-01	.2224E-02
.2550E+01	.9952E+00	.1674E-01	-.3112E-01	.9952E+00	-.2097E-01	-.8214E-03
.2600E+01	.9962E+00	.1652E-01	-.2855E-01	.9962E+00	-.2130E-01	-.3439E-02
.2650E+01	.9970E+00	.1629E-01	-.2635E-01	.9970E+00	-.2162E-01	-.5670E-02
.2700E+01	.9977E+00	.1605E-01	-.2448E-01	.9977E+00	-.2194E-01	-.7557E-02
.2750E+01	.9982E+00	.1580E-01	-.2290E-01	.9982E+00	-.2225E-01	-.9140E-02
.2800E+01	.9986E+00	.1555E-01	-.2157E-01	.9986E+00	-.2255E-01	-.1046E-01
.2850E+01	.9989E+00	.1528E-01	-.2047E-01	.9989E+00	-.2285E-01	-.1155E-01
.2900E+01	.9992E+00	.1502E-01	-.1956E-01	.9992E+00	-.2315E-01	-.1244E-01
.2950E+01	.9994E+00	.1475E-01	-.1882E-01	.9994E+00	-.2344E-01	-.1317E-01
.3000E+01	.9995E+00	.1447E-01	-.1821E-01	.9995E+00	-.2373E-01	-.1376E-01
.3050E+01	.9997E+00	.1420E-01	-.1772E-01	.9997E+00	-.2402E-01	-.1424E-01

Table B.4: Velocity Distributions at a Singular Point - 4

$\frac{V}{U_{ex}} = 1.0914$, $\frac{x}{h} = 0.34247$

η	$\frac{u}{U}$	$\frac{v_1}{U}$	P_1	$\frac{u}{U}$	$\frac{v_2}{U}$	P_2
.5000E-01	-.1114E+01	.1387E-04	.4943E-01	-.1114E+01	.3934E-04	.5201E-02
.1000E+00	-.1000E+01	.5057E-04	.8441E-01	-.1000E+01	.1509E-03	.7806E-02
.1500E+00	-.8925E+00	.1041E-03	.1068E+00	-.8925E+00	.3244E-03	.8232E-02
.2000E+00	-.7905E+00	.1706E-03	.1186E+00	-.7905E+00	.5483E-03	.6898E-02
.2500E+00	-.6936E+00	.2483E-03	.1215E+00	-.6936E+00	.8102E-03	.4260E-02
.3000E+00	-.6016E+00	.3379E-03	.1175E+00	-.6016E+00	.1097E-02	.8121E-03
.3500E+00	-.5139E+00	.4417E-03	.1080E+00	-.5139E+00	.1396E-02	-.2923E-02
.4000E+00	-.4301E+00	.5640E-03	.9438E-01	-.4301E+00	.1693E-02	-.6410E-02
.4500E+00	-.3500E+00	.7103E-03	.7774E-01	-.3500E+00	.1974E-02	-.9135E-02
.5000E+00	-.2731E+00	.8871E-03	.5901E-01	-.2731E+00	.2226E-02	-.1063E-01
.5500E+00	-.1990E+00	.1101E-02	.3890E-01	-.1990E+00	.2439E-02	-.1051E-01
.6000E+00	-.1276E+00	.1360E-02	.1799E-01	-.1276E+00	.2599E-02	-.8504E-02
.6500E+00	-.5853E-01	.1668E-02	-.3286E-02	-.5853E-01	.2699E-02	-.4445E-02
.7000E+00	.8310E-02	.2033E-02	-.2457E-01	.8310E-02	.2729E-02	.1688E-02
.7500E+00	.7306E-01	.2458E-02	-.4557E-01	.7306E-01	.2684E-02	.9790E-02
.8000E+00	.1358E+00	.2946E-02	-.6604E-01	.1358E+00	.2560E-02	.1964E-01
.8500E+00	.1966E+00	.3496E-02	-.8575E-01	.1966E+00	.2355E-02	.3091E-01
.9000E+00	.2553E+00	.4109E-02	-.1045E+00	.2553E+00	.2067E-02	.4321E-01
.9500E+00	.3120E+00	.4781E-02	-.1220E+00	.3120E+00	.1700E-02	.5608E-01
.1000E+01	.3666E+00	.5507E-02	-.1382E+00	.3666E+00	.1255E-02	.6906E-01
.1050E+01	.4190E+00	.6280E-02	-.1528E+00	.4190E+00	.7391E-03	.8168E-01
.1100E+01	.4691E+00	.7093E-02	-.1656E+00	.4691E+00	.1571E-03	.9352E-01
.1150E+01	.5169E+00	.7936E-02	-.1766E+00	.5169E+00	-.4834E-03	.1042E+00
.1200E+01	.5621E+00	.8800E-02	-.1856E+00	.5621E+00	-.1174E-02	.1134E+00
.1250E+01	.6049E+00	.9673E-02	-.1925E+00	.6049E+00	-.1907E-02	.1209E+00
.1300E+01	.6450E+00	.1055E-01	-.1973E+00	.6450E+00	-.2673E-02	.1265E+00
.1350E+01	.6825E+00	.1141E-01	-.2000E+00	.6825E+00	-.3463E-02	.1302E+00
.1400E+01	.7173E+00	.1225E-01	-.2008E+00	.7173E+00	-.4269E-02	.1319E+00
.1450E+01	.7495E+00	.1305E-01	-.1995E+00	.7495E+00	-.5082E-02	.1317E+00
.1500E+01	.7791E+00	.1382E-01	-.1965E+00	.7791E+00	-.5896E-02	.1298E+00
.1550E+01	.8061E+00	.1454E-01	-.1918E+00	.8061E+00	-.6703E-02	.1262E+00
.1600E+01	.8307E+00	.1521E-01	-.1857E+00	.8307E+00	-.7498E-02	.1213E+00
.1650E+01	.8529E+00	.1582E-01	-.1784E+00	.8529E+00	-.8276E-02	.1151E+00
.1700E+01	.8728E+00	.1637E-01	-.1700E+00	.8728E+00	-.9032E-02	.1080E+00
.1750E+01	.8906E+00	.1686E-01	-.1609E+00	.8906E+00	-.9764E-02	.1002E+00
.1800E+01	.9063E+00	.1728E-01	-.1512E+00	.9063E+00	-.1047E-01	.9183E-01
.1850E+01	.9202E+00	.1764E-01	-.1412E+00	.9202E+00	-.1115E-01	.8321E-01
.1900E+01	.9324E+00	.1793E-01	-.1310E+00	.9324E+00	-.1179E-01	.7449E-01
.1950E+01	.9430E+00	.1816E-01	-.1208E+00	.9430E+00	-.1241E-01	.6584E-01
.2000E+01	.9522E+00	.1833E-01	-.1108E+00	.9522E+00	-.1300E-01	.5740E-01
.2050E+01	.9601E+00	.1845E-01	-.1013E+00	.9601E+00	-.1356E-01	.4931E-01
.2100E+01	.9669E+00	.1851E-01	-.9195E-01	.9669E+00	-.1410E-01	.4163E-01
.2150E+01	.9727E+00	.1852E-01	-.8327E-01	.9727E+00	-.1461E-01	.3446E-01
.2200E+01	.9776E+00	.1849E-01	-.7518E-01	.9776E+00	-.1510E-01	.2783E-01
.2250E+01	.9817E+00	.1842E-01	-.6772E-01	.9817E+00	-.1557E-01	.2176E-01
.2300E+01	.9851E+00	.1832E-01	-.6091E-01	.9851E+00	-.1601E-01	.1628E-01
.2350E+01	.9880E+00	.1818E-01	-.5476E-01	.9880E+00	-.1644E-01	.1136E-01
.2400E+01	.9903E+00	.1801E-01	-.4926E-01	.9903E+00	-.1686E-01	.6999E-02
.2450E+01	.9922E+00	.1781E-01	-.4438E-01	.9922E+00	-.1726E-01	.3161E-02
.2500E+01	.9938E+00	.1760E-01	-.4009E-01	.9938E+00	-.1765E-01	-.1849E-03
.2550E+01	.9951E+00	.1736E-01	-.3635E-01	.9951E+00	-.1803E-01	-.3078E-02
.2600E+01	.9961E+00	.1711E-01	-.3313E-01	.9961E+00	-.1840E-01	-.5559E-02
.2650E+01	.9970E+00	.1685E-01	-.3036E-01	.9970E+00	-.1876E-01	-.7669E-02
.2700E+01	.9976E+00	.1657E-01	-.2800E-01	.9976E+00	-.1912E-01	-.9451E-02
.2750E+01	.9982E+00	.1628E-01	-.2602E-01	.9982E+00	-.1947E-01	-.1094E-01
.2800E+01	.9986E+00	.1599E-01	-.2436E-01	.9986E+00	-.1981E-01	-.1218E-01
.2850E+01	.9989E+00	.1569E-01	-.2298E-01	.9989E+00	-.2016E-01	-.1321E-01
.2900E+01	.9992E+00	.1538E-01	-.2184E-01	.9992E+00	-.2049E-01	-.1405E-01
.2950E+01	.9994E+00	.1507E-01	-.2090E-01	.9994E+00	-.2083E-01	-.1473E-01
.3000E+01	.9995E+00	.1476E-01	-.2015E-01	.9995E+00	-.2117E-01	-.1528E-01
.3050E+01	.9996E+00	.1444E-01	-.1953E-01	.9996E+00	-.2150E-01	-.1573E-01

Table B.5: Velocity Distributions at a Singular Point - 5

$\frac{V}{U_{ex}} = 1.11695$, $\frac{x}{h} = 0.30803$

η	$\frac{u}{U}$	$\frac{v_1}{U}$	P_1	$\frac{u}{U}$	$\frac{v_2}{U}$	P_2
.5000E-01	-.1197E+01	.1310E-04	.5256E-01	-.1197E+01	.4688E-04	.1102E-01
.1000E+00	-.1073E+01	.4672E-04	.8909E-01	-.1073E+01	.1802E-03	.1847E-01
.1500E+00	-.9554E+00	.9378E-04	.1118E+00	-.9554E+00	.3884E-03	.2280E-01
.2000E+00	-.8444E+00	.1495E-03	.1228E+00	-.8444E+00	.6587E-03	.2448E-01
.2500E+00	-.7395E+00	.2116E-03	.1244E+00	-.7395E+00	.9775E-03	.2404E-01
.3000E+00	-.6402E+00	.2801E-03	.1184E+00	-.6402E+00	.1330E-02	.2203E-01
.3500E+00	-.5462E+00	.3574E-03	.1067E+00	-.5462E+00	.1702E-02	.1908E-01
.4000E+00	-.4569E+00	.4478E-03	.9077E-01	-.4569E+00	.2079E-02	.1581E-01
.4500E+00	-.3719E+00	.5572E-03	.7177E-01	-.3719E+00	.2444E-02	.1283E-01
.5000E+00	-.2908E+00	.6927E-03	.5072E-01	-.2908E+00	.2785E-02	.1073E-01
.5500E+00	-.2132E+00	.8621E-03	.2839E-01	-.2132E+00	.3087E-02	.9975E-02
.6000E+00	-.1389E+00	.1073E-02	.5367E-02	-.1389E+00	.3339E-02	.1094E-01
.6500E+00	-.6737E-01	.1333E-02	-.1790E-01	-.6737E-01	.3529E-02	.1387E-01
.7000E+00	.1466E-02	.1649E-02	-.4105E-01	.1466E-02	.3648E-02	.1884E-01
.7500E+00	.6782E-01	.2025E-02	-.6381E-01	.6782E-01	.3690E-02	.2579E-01
.8000E+00	.1318E+00	.2466E-02	-.8592E-01	.1318E+00	.3649E-02	.3455E-01
.8500E+00	.1936E+00	.2973E-02	-.1071E+00	.1936E+00	.3521E-02	.4480E-01
.9000E+00	.2531E+00	.3546E-02	-.1273E+00	.2531E+00	.3307E-02	.5614E-01
.9500E+00	.3103E+00	.4182E-02	-.1461E+00	.3103E+00	.3007E-02	.6815E-01
.1000E+01	.3653E+00	.4876E-02	-.1634E+00	.3653E+00	.2625E-02	.8032E-01
.1050E+01	.4180E+00	.5624E-02	-.1789E+00	.4180E+00	.2163E-02	.9220E-01
.1100E+01	.4683E+00	.6416E-02	-.1925E+00	.4683E+00	.1630E-02	.1033E+00
.1150E+01	.5161E+00	.7244E-02	-.2040E+00	.5161E+00	.1031E-02	.1134E+00
.1200E+01	.5614E+00	.8097E-02	-.2134E+00	.5614E+00	.3756E-03	.1219E+00
.1250E+01	.6042E+00	.8965E-02	-.2204E+00	.6042E+00	-.3285E-03	.1288E+00
.1300E+01	.6443E+00	.9836E-02	-.2251E+00	.6443E+00	-.1072E-02	.1337E+00
.1350E+01	.6818E+00	.1070E-01	-.2276E+00	.6818E+00	-.1846E-02	.1368E+00
.1400E+01	.7166E+00	.1154E-01	-.2278E+00	.7166E+00	-.2641E-02	.1379E+00
.1450E+01	.7488E+00	.1236E-01	-.2258E+00	.7488E+00	-.3449E-02	.1371E+00
.1500E+01	.7784E+00	.1314E-01	-.2219E+00	.7784E+00	-.4262E-02	.1345E+00
.1550E+01	.8055E+00	.1387E-01	-.2162E+00	.8055E+00	-.5073E-02	.1304E+00
.1600E+01	.8300E+00	.1455E-01	-.2090E+00	.8300E+00	-.5876E-02	.1249E+00
.1650E+01	.8522E+00	.1517E-01	-.2004E+00	.8522E+00	-.6665E-02	.1182E+00
.1700E+01	.8722E+00	.1573E-01	-.1907E+00	.8722E+00	-.7436E-02	.1105E+00
.1750E+01	.8900E+00	.1622E-01	-.1802E+00	.8900E+00	-.8185E-02	.1022E+00
.1800E+01	.9058E+00	.1665E-01	-.1691E+00	.9058E+00	-.8909E-02	.9343E-01
.1850E+01	.9197E+00	.1701E-01	-.1576E+00	.9197E+00	-.9608E-02	.8440E-01
.1900E+01	.9319E+00	.1731E-01	-.1461E+00	.9319E+00	-.1028E-01	.7531E-01
.1950E+01	.9426E+00	.1754E-01	-.1345E+00	.9426E+00	-.1092E-01	.6634E-01
.2000E+01	.9518E+00	.1771E-01	-.1233E+00	.9518E+00	-.1154E-01	.5761E-01
.2050E+01	.9598E+00	.1782E-01	-.1124E+00	.9598E+00	-.1213E-01	.4926E-01
.2100E+01	.9666E+00	.1788E-01	-.1020E+00	.9666E+00	-.1269E-01	.4137E-01
.2150E+01	.9724E+00	.1788E-01	-.9228E-01	.9724E+00	-.1323E-01	.3401E-01
.2200E+01	.9773E+00	.1784E-01	-.8320E-01	.9773E+00	-.1374E-01	.2722E-01
.2250E+01	.9815E+00	.1776E-01	-.7484E-01	.9815E+00	-.1424E-01	.2102E-01
.2300E+01	.9849E+00	.1763E-01	-.6722E-01	.9849E+00	-.1471E-01	.1542E-01
.2350E+01	.9878E+00	.1748E-01	-.6034E-01	.9878E+00	-.1517E-01	.1041E-01
.2400E+01	.9902E+00	.1729E-01	-.5419E-01	.9902E+00	-.1562E-01	.5977E-02
.2450E+01	.9922E+00	.1708E-01	-.4874E-01	.9922E+00	-.1605E-01	.2079E-02
.2500E+01	.9938E+00	.1684E-01	-.4396E-01	.9938E+00	-.1647E-01	-.1316E-02
.2550E+01	.9950E+00	.1658E-01	-.3979E-01	.9950E+00	-.1687E-01	-.4247E-02
.2600E+01	.9961E+00	.1631E-01	-.3619E-01	.9961E+00	-.1727E-01	-.6757E-02
.2650E+01	.9969E+00	.1602E-01	-.3311E-01	.9969E+00	-.1766E-01	-.8891E-02
.2700E+01	.9976E+00	.1572E-01	-.3049E-01	.9976E+00	-.1805E-01	-.1069E-01
.2750E+01	.9981E+00	.1540E-01	-.2828E-01	.9981E+00	-.1843E-01	-.1220E-01
.2800E+01	.9986E+00	.1508E-01	-.2643E-01	.9986E+00	-.1880E-01	-.1345E-01
.2850E+01	.9989E+00	.1476E-01	-.2489E-01	.9989E+00	-.1918E-01	-.1448E-01
.2900E+01	.9992E+00	.1442E-01	-.2362E-01	.9992E+00	-.1954E-01	-.1532E-01
.2950E+01	.9994E+00	.1409E-01	-.2259E-01	.9994E+00	-.1991E-01	-.1601E-01
.3000E+01	.9995E+00	.1374E-01	-.2174E-01	.9995E+00	-.2027E-01	-.1656E-01
.3050E+01	.9996E+00	.1340E-01	-.2106E-01	.9996E+00	-.2064E-01	-.1701E-01

Table B.6: Velocity Distributions at a Singular Point - 6

$\frac{V}{U_{ex}} = 0.1.2589,\ \frac{x}{h} = 0.26818$

η	$\frac{u}{U}$	$\frac{v_1}{U}$	P_1	$\frac{u}{U}$	$\frac{v_2}{U}$	P_2
.5000E-01	-.1294E+01	.1129E-04	.5513E-01	-.1294E+01	.5508E-04	.1725E-01
.1000E+00	-.1158E+01	.3870E-04	.9261E-01	-.1158E+01	.2122E-03	.2990E-01
.1500E+00	-.1029E+01	.7408E-04	.1149E+00	-.1029E+01	.4584E-03	.3846E-01
.2000E+00	-.9081E+00	.1117E-03	.1247E+00	-.9081E+00	.7796E-03	.4342E-01
.2500E+00	-.7940E+00	.1487E-03	.1243E+00	-.7940E+00	.1161E-02	.4536E-01
.3000E+00	-.6865E+00	.1846E-03	.1159E+00	-.6865E+00	.1586E-02	.4493E-01
.3500E+00	-.5851E+00	.2218E-03	.1017E+00	-.5851E+00	.2039E-02	.4282E-01
.4000E+00	-.4894E+00	.2647E-03	.8308E-01	-.4894E+00	.2503E-02	.3978E-01
.4500E+00	-.3989E+00	.3197E-03	.6152E-01	-.3989E+00	.2961E-02	.3654E-01
.5000E+00	-.3130E+00	.3946E-03	.3805E-01	-.3130E+00	.3398E-02	.3380E-01
.5500E+00	-.2314E+00	.4982E-03	.1347E-01	-.2314E+00	.3799E-02	.3215E-01
.6000E+00	-.1536E+00	.6394E-03	-.1164E-01	-.1536E+00	.4149E-02	.3206E-01
.6500E+00	-.7923E-01	.8268E-03	-.3682E-01	-.7923E-01	.4437E-02	.3386E-01
.7000E+00	-.8036E-02	.1068E-02	-.6174E-01	-.8036E-02	.4652E-02	.3771E-01
.7500E+00	.6023E-01	.1371E-02	-.8612E-01	.6023E-01	.4786E-02	.4360E-01
.8000E+00	.1258E+00	.1738E-02	-.1097E+00	.1258E+00	.4832E-02	.5139E-01
.8500E+00	.1887E+00	.2175E-02	-.1324E+00	.1887E+00	.4786E-02	.6077E-01
.9000E+00	.2491E+00	.2680E-02	-.1538E+00	.2491E+00	.4647E-02	.7136E-01
.9500E+00	.3071E+00	.3253E-02	-.1737E+00	.3071E+00	.4415E-02	.8270E-01
.1000E+01	.3627E+00	.3890E-02	-.1920E+00	.3627E+00	.4092E-02	.9430E-01
.1050E+01	.4157E+00	.4585E-02	-.2083E+00	.4157E+00	.3684E-02	.1057E+00
.1100E+01	.4663E+00	.5332E-02	-.2226E+00	.4663E+00	.3194E-02	.1163E+00
.1150E+01	.5144E+00	.6119E-02	-.2346E+00	.5144E+00	.2632E-02	.1258E+00
.1200E+01	.5598E+00	.6938E-02	-.2442E+00	.5598E+00	.2004E-02	.1339E+00
.1250E+01	.6027E+00	.7778E-02	-.2513E+00	.6027E+00	.1321E-02	.1402E+00
.1300E+01	.6429E+00	.8626E-02	-.2558E+00	.6429E+00	.5909E-03	.1447E+00
.1350E+01	.6805E+00	.9471E-02	-.2578E+00	.6805E+00	-.1762E-03	.1471E+00
.1400E+01	.7153E+00	.1030E-01	-.2574E+00	.7153E+00	-.9710E-03	.1476E+00
.1450E+01	.7476E+00	.1111E-01	-.2546E+00	.7476E+00	-.1785E-02	.1461E+00
.1500E+01	.7772E+00	.1188E-01	-.2497E+00	.7772E+00	-.2608E-02	.1429E+00
.1550E+01	.8043E+00	.1260E-01	-.2429E+00	.8043E+00	-.3435E-02	.1380E+00
.1600E+01	.8290E+00	.1328E-01	-.2343E+00	.8290E+00	-.4257E-02	.1318E+00
.1650E+01	.8512E+00	.1390E-01	-.2244E+00	.8512E+00	-.5068E-02	.1243E+00
.1700E+01	.8712E+00	.1446E-01	-.2132E+00	.8712E+00	-.5864E-02	.1160E+00
.1750E+01	.8891E+00	.1495E-01	-.2012E+00	.8891E+00	-.6641E-02	.1070E+00
.1800E+01	.9050E+00	.1537E-01	-.1885E+00	.9050E+00	-.7395E-02	.9754E-01
.1850E+01	.9190E+00	.1573E-01	-.1756E+00	.9190E+00	-.8125E-02	.8787E-01
.1900E+01	.9313E+00	.1602E-01	-.1625E+00	.9313E+00	-.8828E-02	.7818E-01
.1950E+01	.9420E+00	.1625E-01	-.1495E+00	.9420E+00	-.9505E-02	.6865E-01
.2000E+01	.9513E+00	.1641E-01	-.1368E+00	.9513E+00	-.1015E-01	.5942E-01
.2050E+01	.9594E+00	.1651E-01	-.1246E+00	.9594E+00	-.1078E-01	.5061E-01
.2100E+01	.9662E+00	.1655E-01	-.1130E+00	.9662E+00	-.1138E-01	.4230E-01
.2150E+01	.9721E+00	.1654E-01	-.1021E+00	.9721E+00	-.1195E-01	.3457E-01
.2200E+01	.9771E+00	.1649E-01	-.9197E-01	.9771E+00	-.1250E-01	.2745E-01
.2250E+01	.9812E+00	.1638E-01	-.8264E-01	.9812E+00	-.1303E-01	.2096E-01
.2300E+01	.9847E+00	.1624E-01	-.7415E-01	.9847E+00	-.1354E-01	.1511E-01
.2350E+01	.9876E+00	.1606E-01	-.6649E-01	.9876E+00	-.1403E-01	.9891E-02
.2400E+01	.9901E+00	.1585E-01	-.5965E-01	.9901E+00	-.1451E-01	.5269E-02
.2450E+01	.9920E+00	.1561E-01	-.5359E-01	.9920E+00	-.1498E-01	.1215E-02
.2500E+01	.9937E+00	.1535E-01	-.4828E-01	.9937E+00	-.1543E-01	-.2311E-02
.2550E+01	.9950E+00	.1507E-01	-.4365E-01	.9950E+00	-.1587E-01	-.5353E-02
.2600E+01	.9960E+00	.1477E-01	-.3966E-01	.9960E+00	-.1630E-01	-.7955E-02
.2650E+01	.9969E+00	.1445E-01	-.3624E-01	.9969E+00	-.1673E-01	-.1016E-01
.2700E+01	.9976E+00	.1412E-01	-.3333E-01	.9976E+00	-.1714E-01	-.1202E-01
.2750E+01	.9981E+00	.1378E-01	-.3088E-01	.9981E+00	-.1756E-01	-.1358E-01
.2800E+01	.9985E+00	.1343E-01	-.2883E-01	.9985E+00	-.1796E-01	-.1487E-01
.2850E+01	.9989E+00	.1307E-01	-.2713E-01	.9989E+00	-.1837E-01	-.1594E-01
.2900E+01	.9991E+00	.1271E-01	-.2573E-01	.9991E+00	-.1877E-01	-.1681E-01
.2950E+01	.9994E+00	.1234E-01	-.2458E-01	.9994E+00	-.1917E-01	-.1751E-01
.3000E+01	.9995E+00	.1196E-01	-.2365E-01	.9995E+00	-.1956E-01	-.1808E-01
.3050E+01	.9996E+00	.1159E-01	-.2290E-01	.9996E+00	-.1996E-01	-.1854E-01

Table B.7: Velocity Distributions at a Singular Point - 7

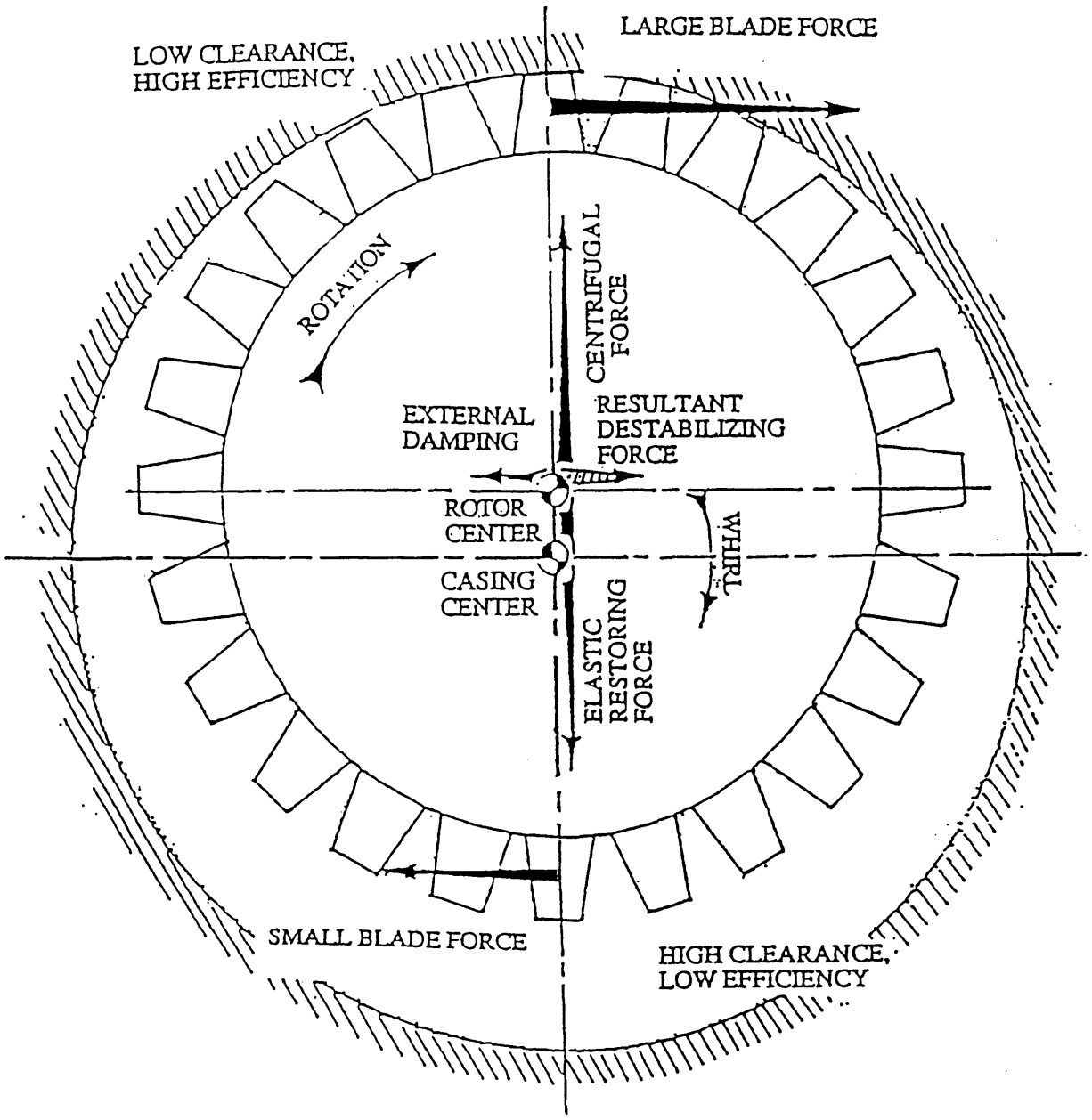

Figure B-1: Mechanism of Alford Force

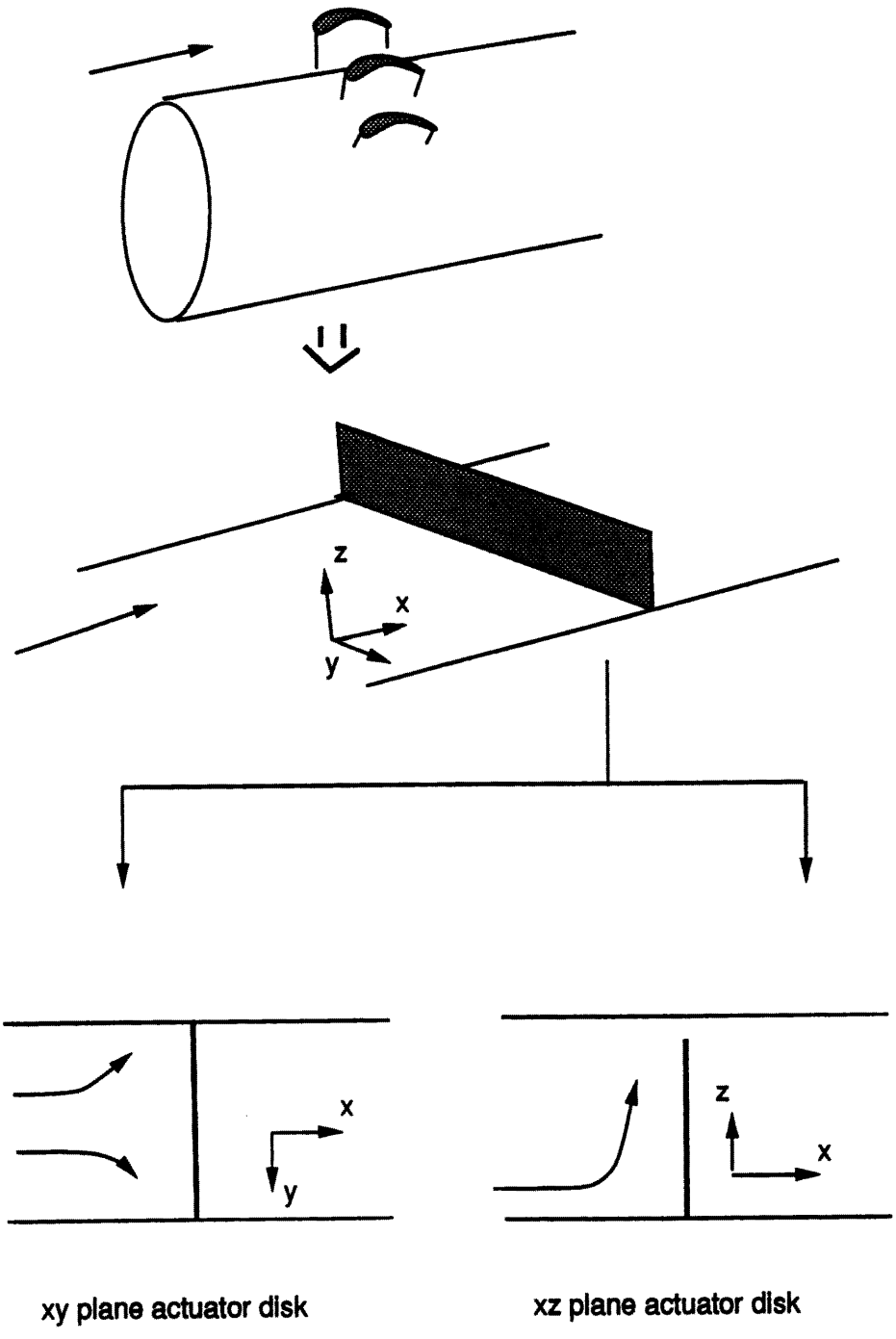

Figure B-2: Concept of Actuator Disk Theory

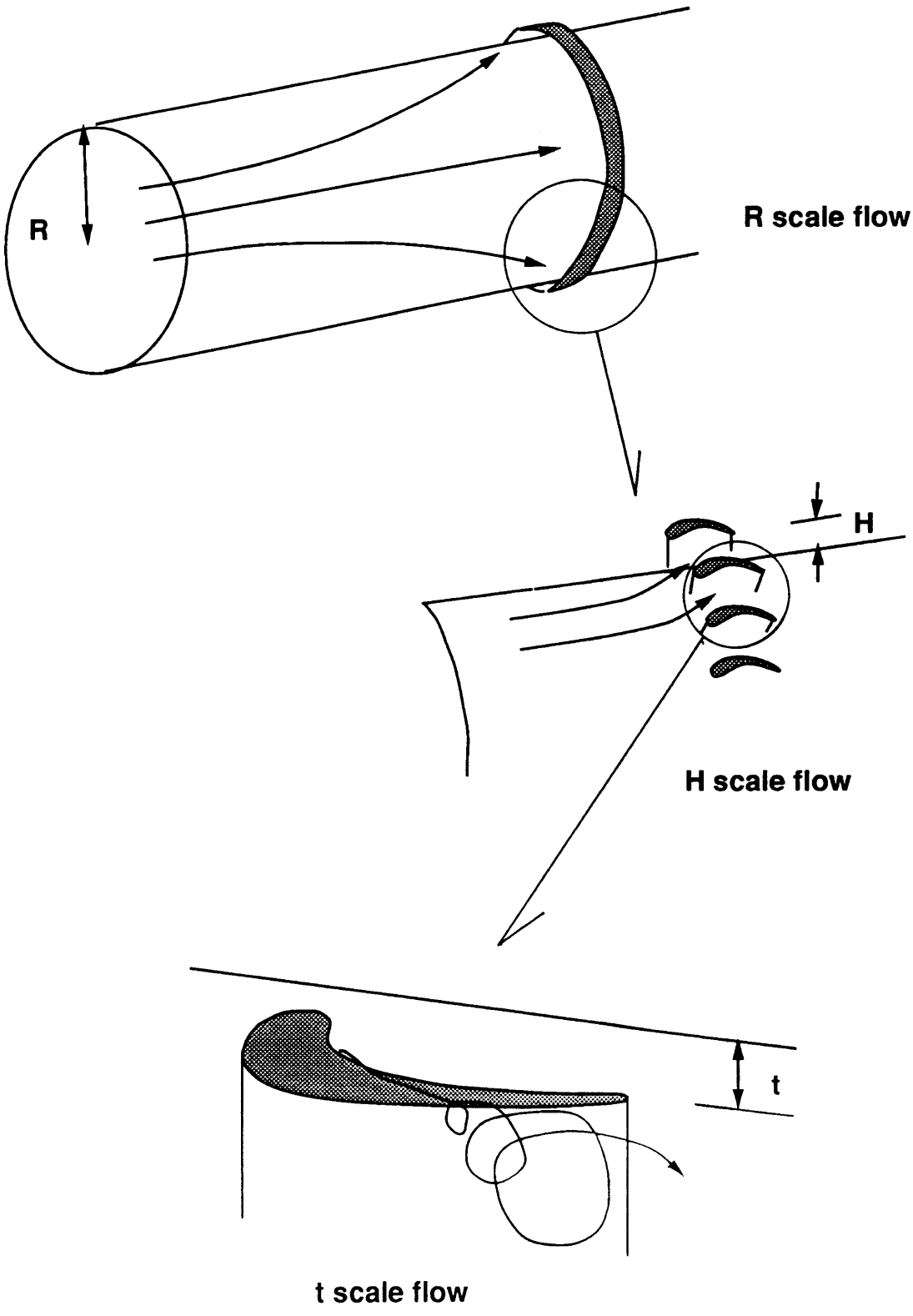

Figure B-3: Flow Characterized with Different Length Scales

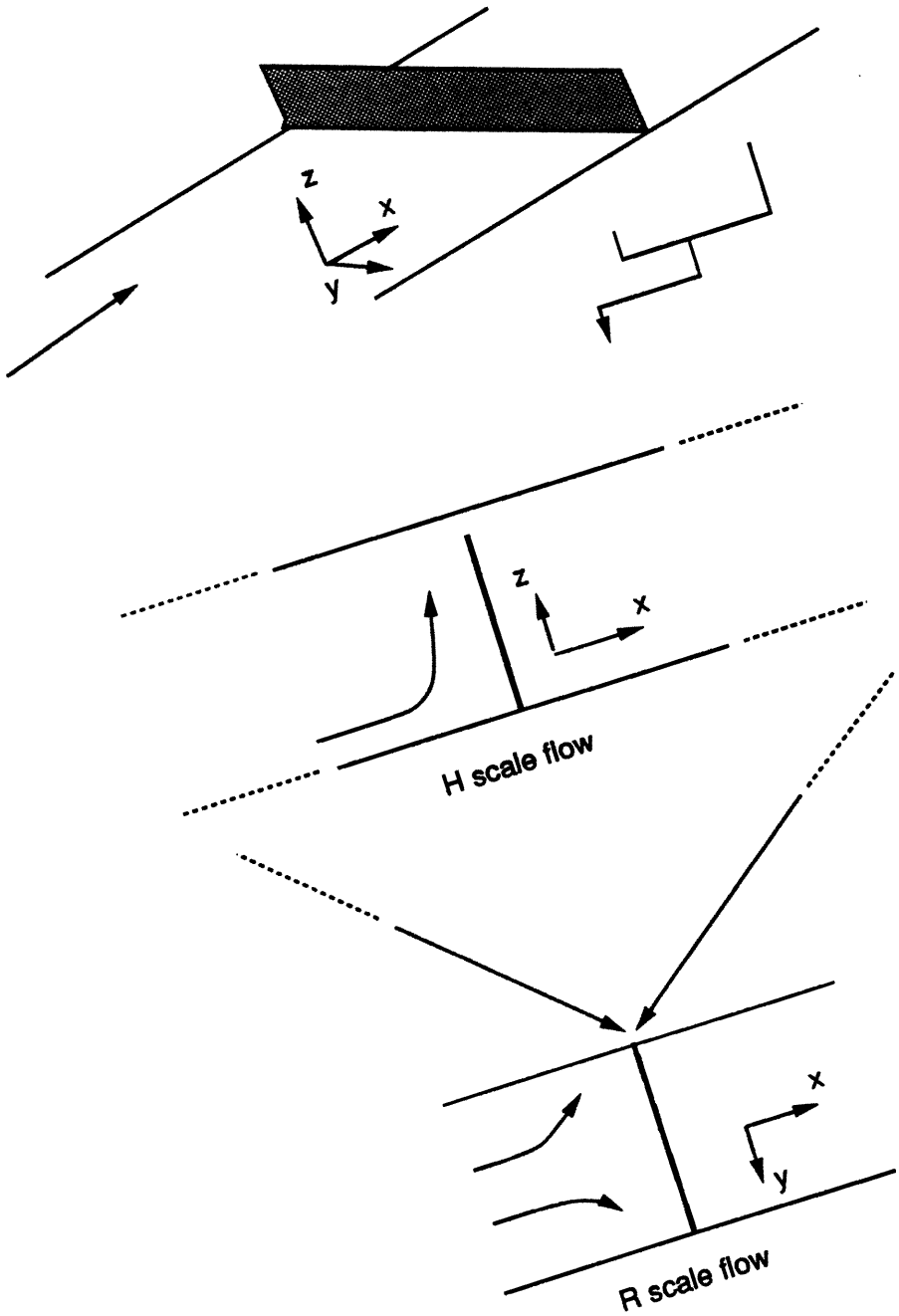

Figure B-4: Modelling of Whole Flow Field

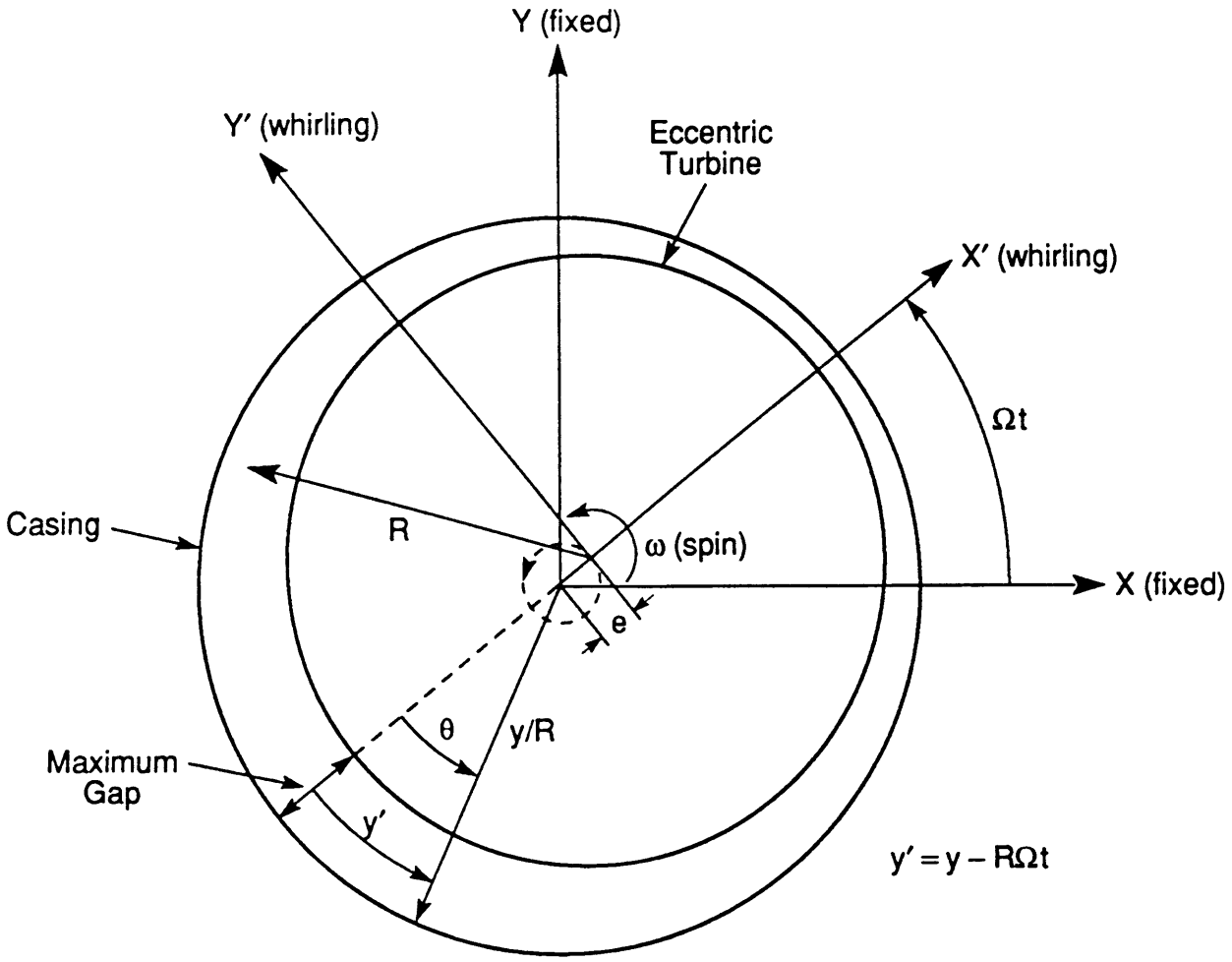

Figure B-5: Coordinates in Steady and Unsteady Frames

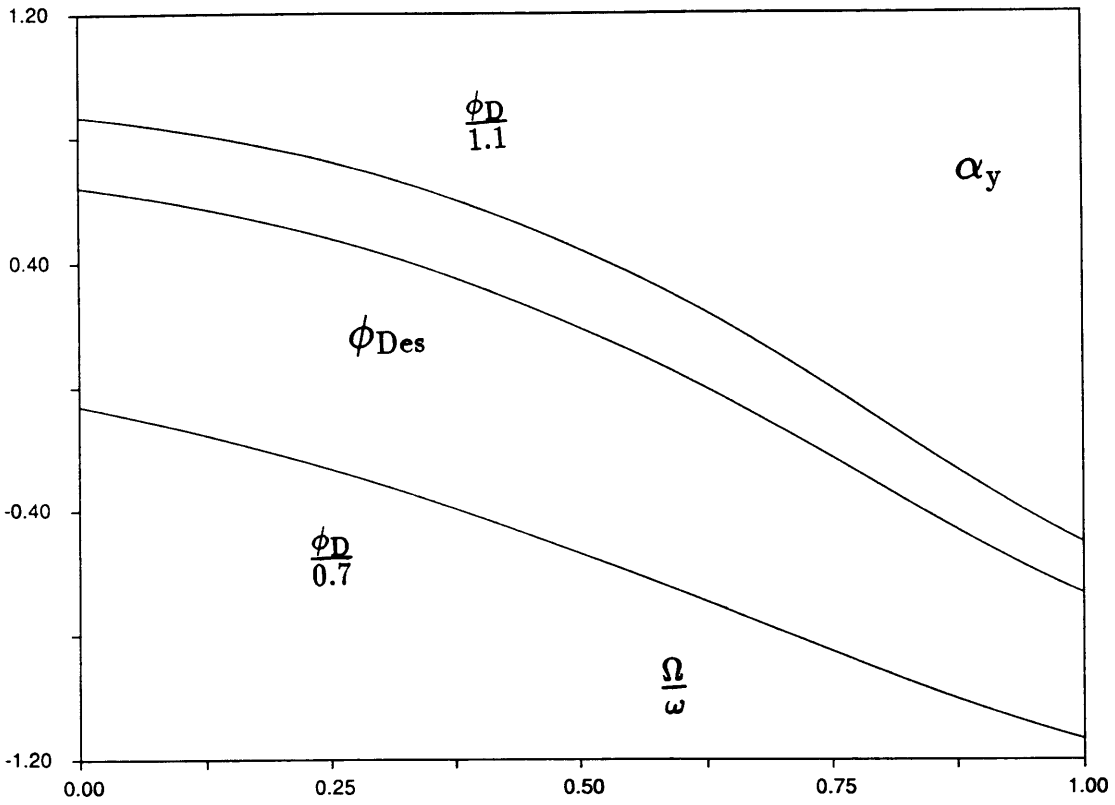

Figure B-6: α_y Variation for Unsteady Conditions

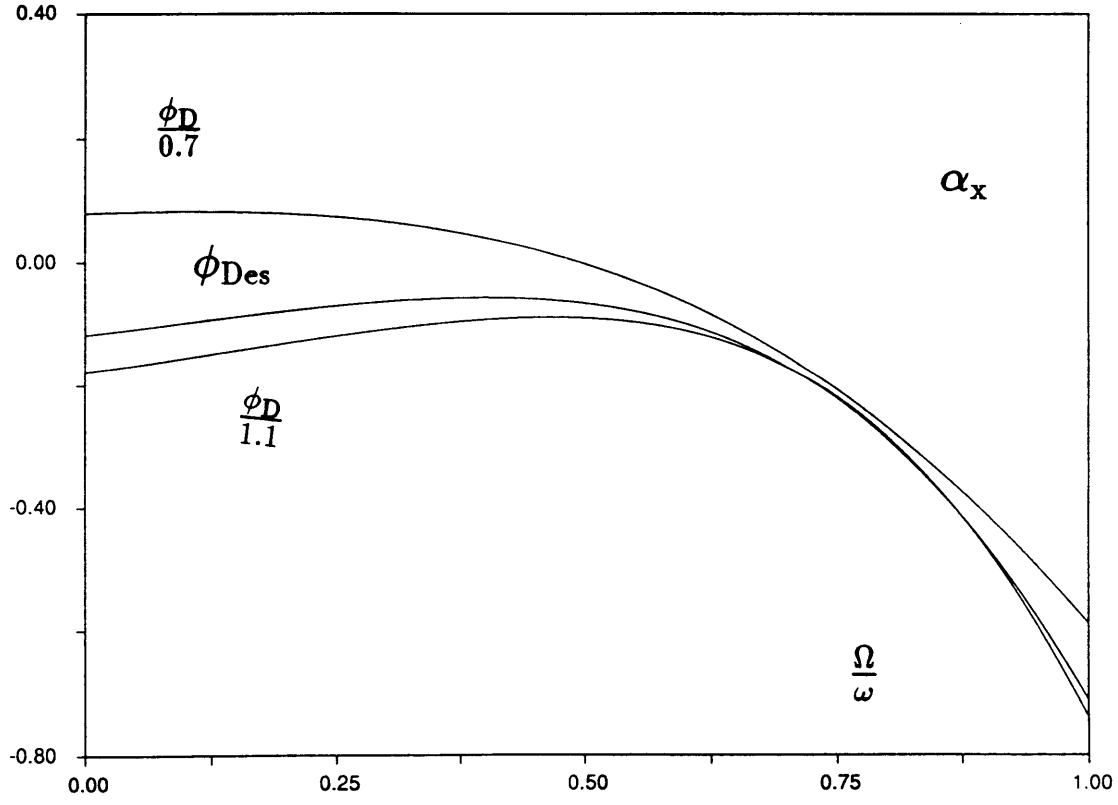

Figure B-7: α_x Variation for Unsteady Conditions

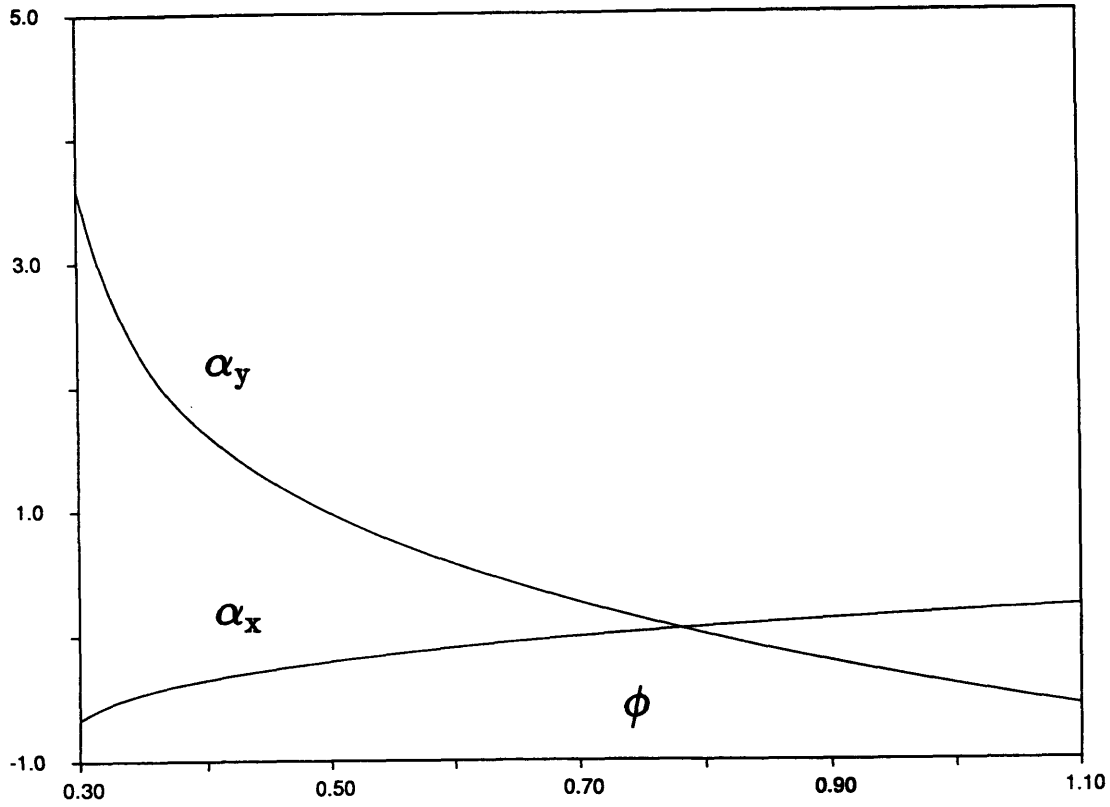

Figure B-8: α_x and α_y Variation for Steady Conditions

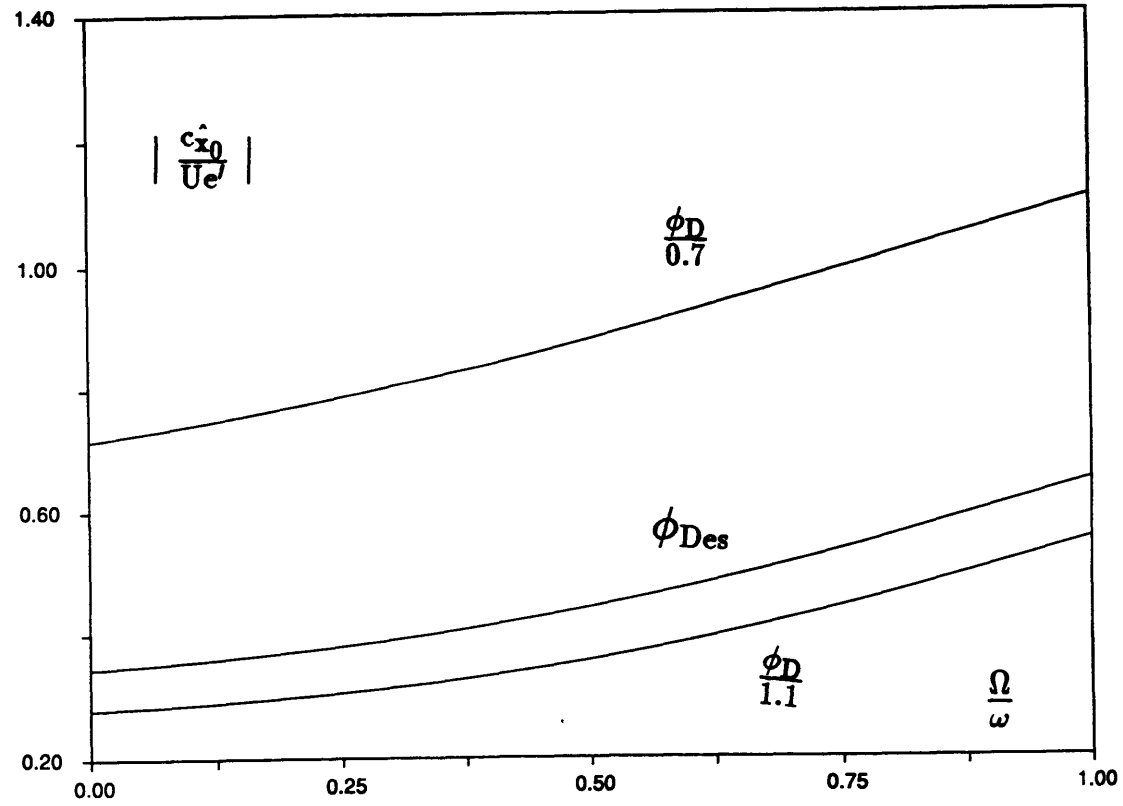

Figure B-9: Upstream Perturbation for Unsteady Cases (Magnitude)

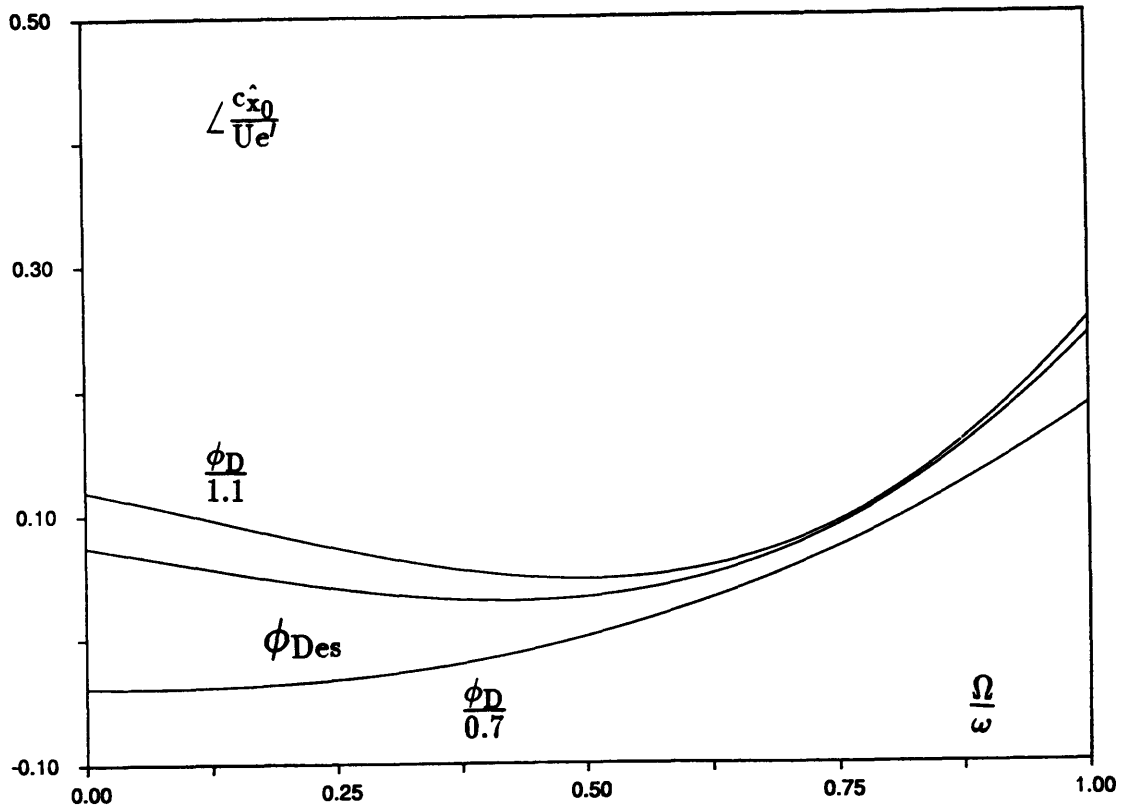

Figure B-10: Upstream Perturbation for Unsteady Cases (Phase)

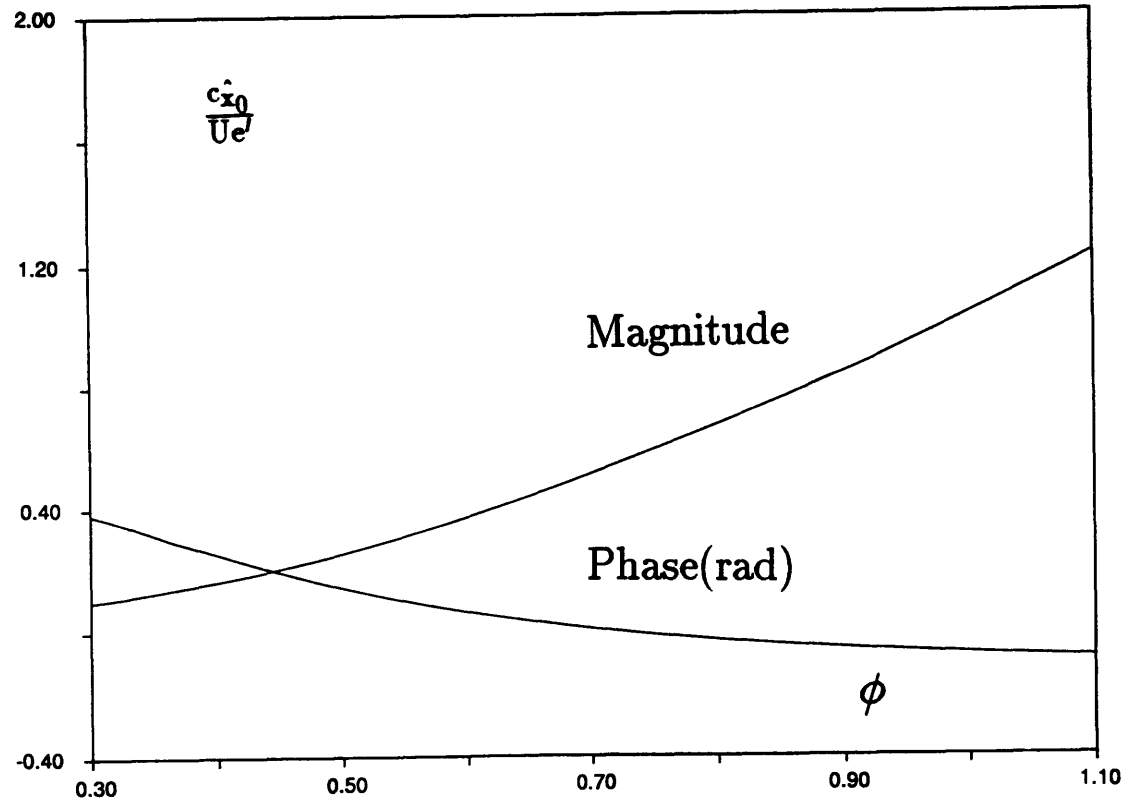

Figure B-11: Upstream Perturbation for Steady Cases

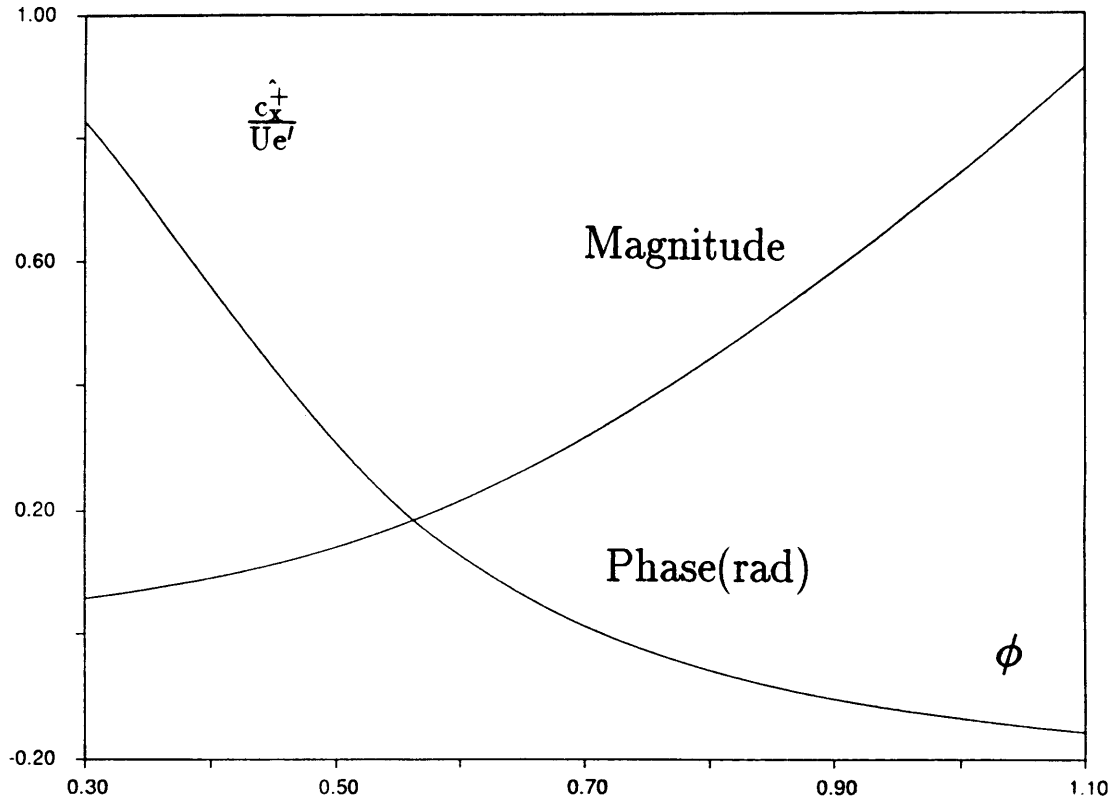

Figure B-12: Axial Velocity Perturbation at Rotor (Underturned Flow due to Gap)

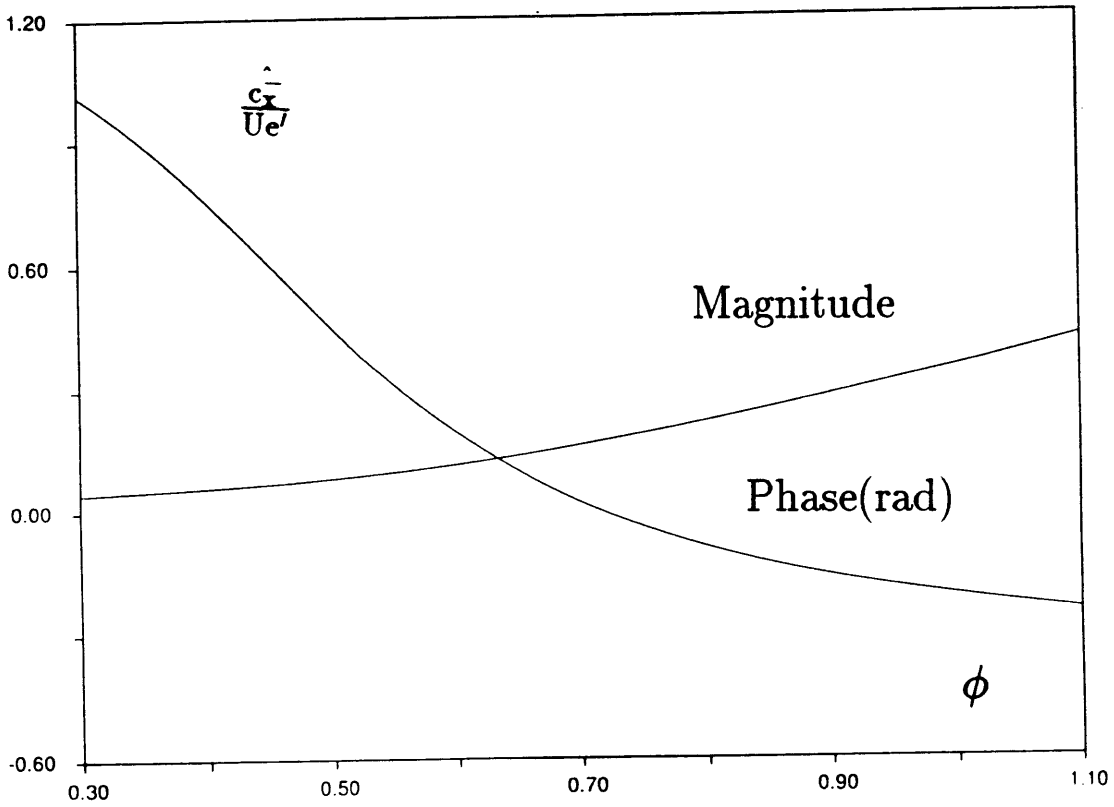

Figure B-13: Axial Velocity Perturbation at Rotor (Guided Flow through Blade)

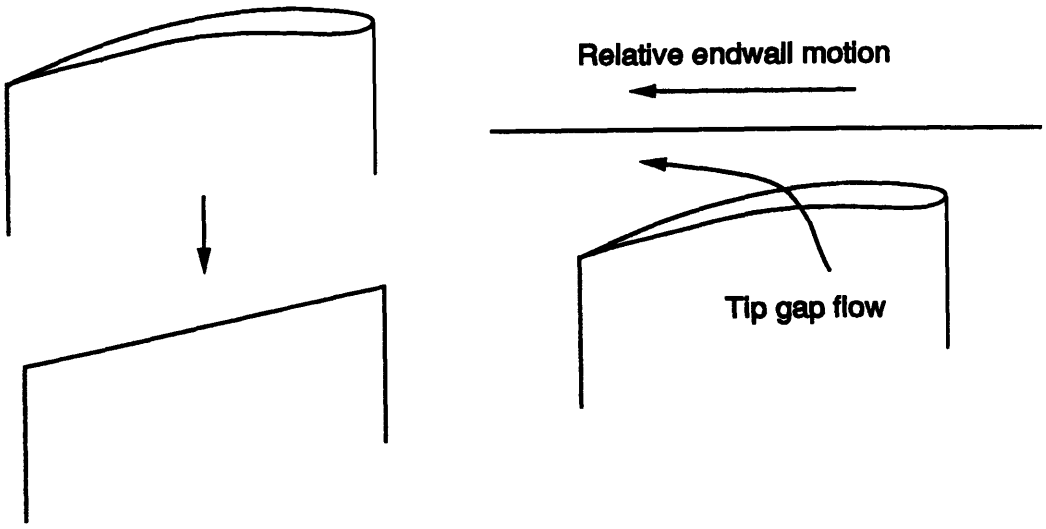

Compressor blade

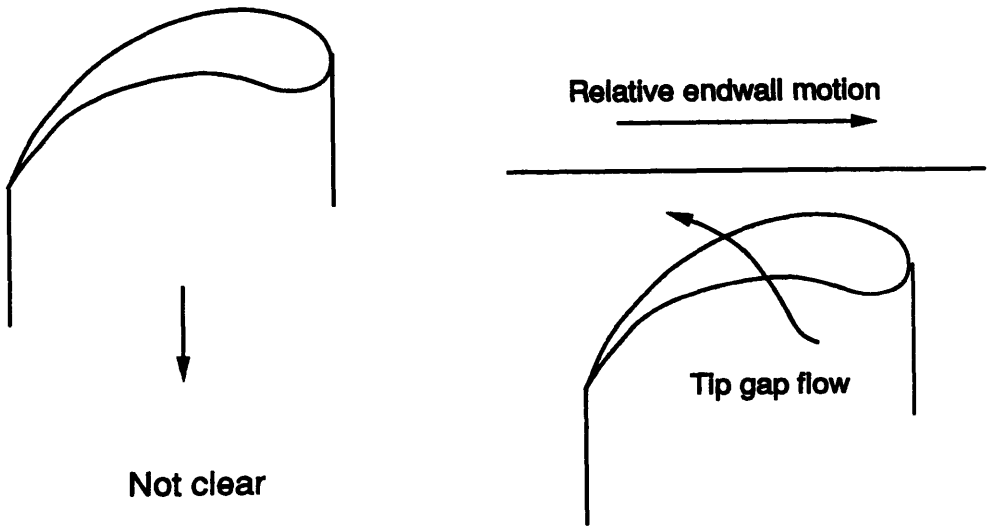

Turbine blade

Figure B-14: Comparisons between Compressor and Turbine Blade

$$Wt = \sqrt{\frac{2\Delta p}{\rho}}$$

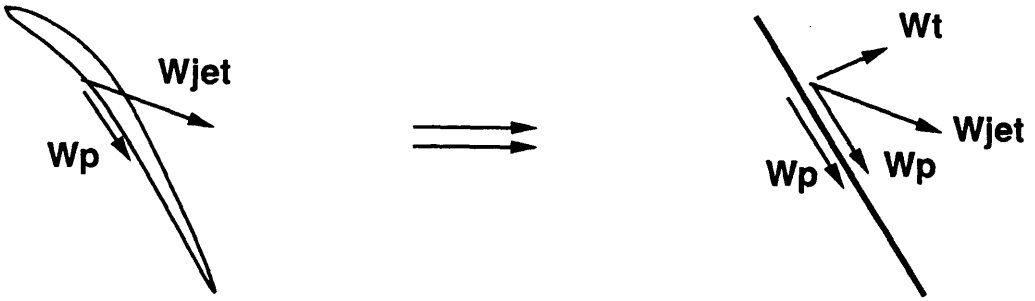

Figure B-15: Simplification of Tip Gap Flow by Rains

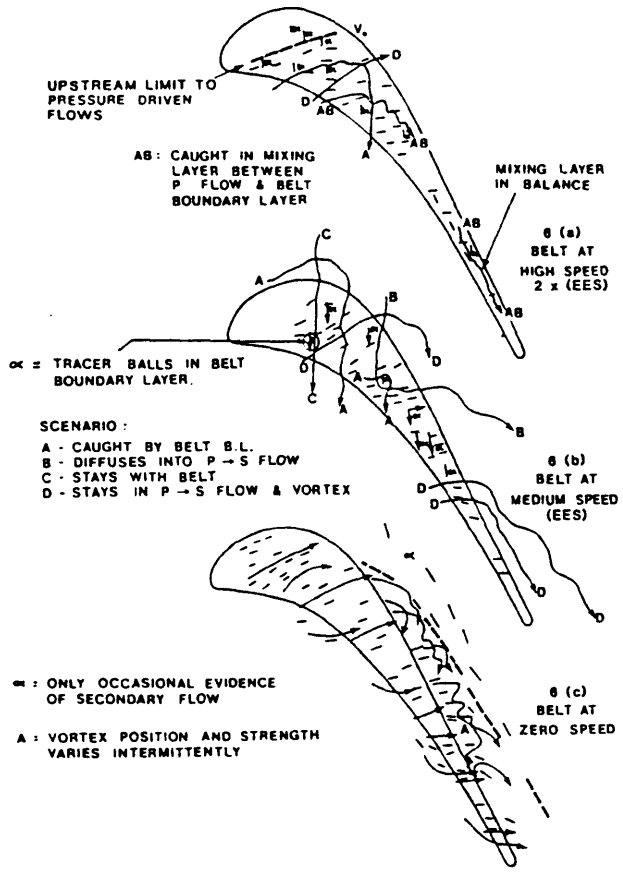

FIG. 6 : TIP CLEARANCE FLOW COMPARISON WITH MAXIMUM CLEARANCE OF 2.5% AT VARIOUS SPEEDS

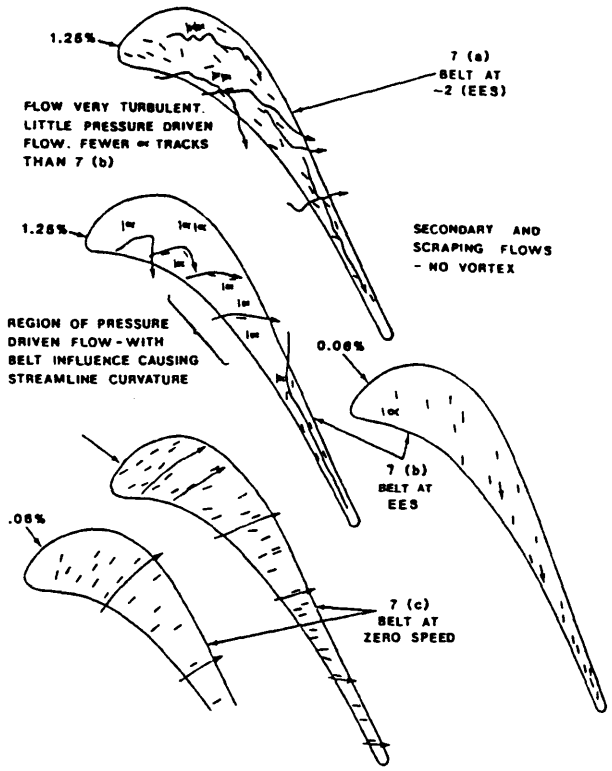

FIG. 7 : TIP CLEARANCE FLOW COMPARISON WITH CLEARANCE OF 1.25% AND 0.6% AT VARIOUS SPEEDS

Figure B-16: Visualization of Tip Gap Flow with Endwall Motion by Graham

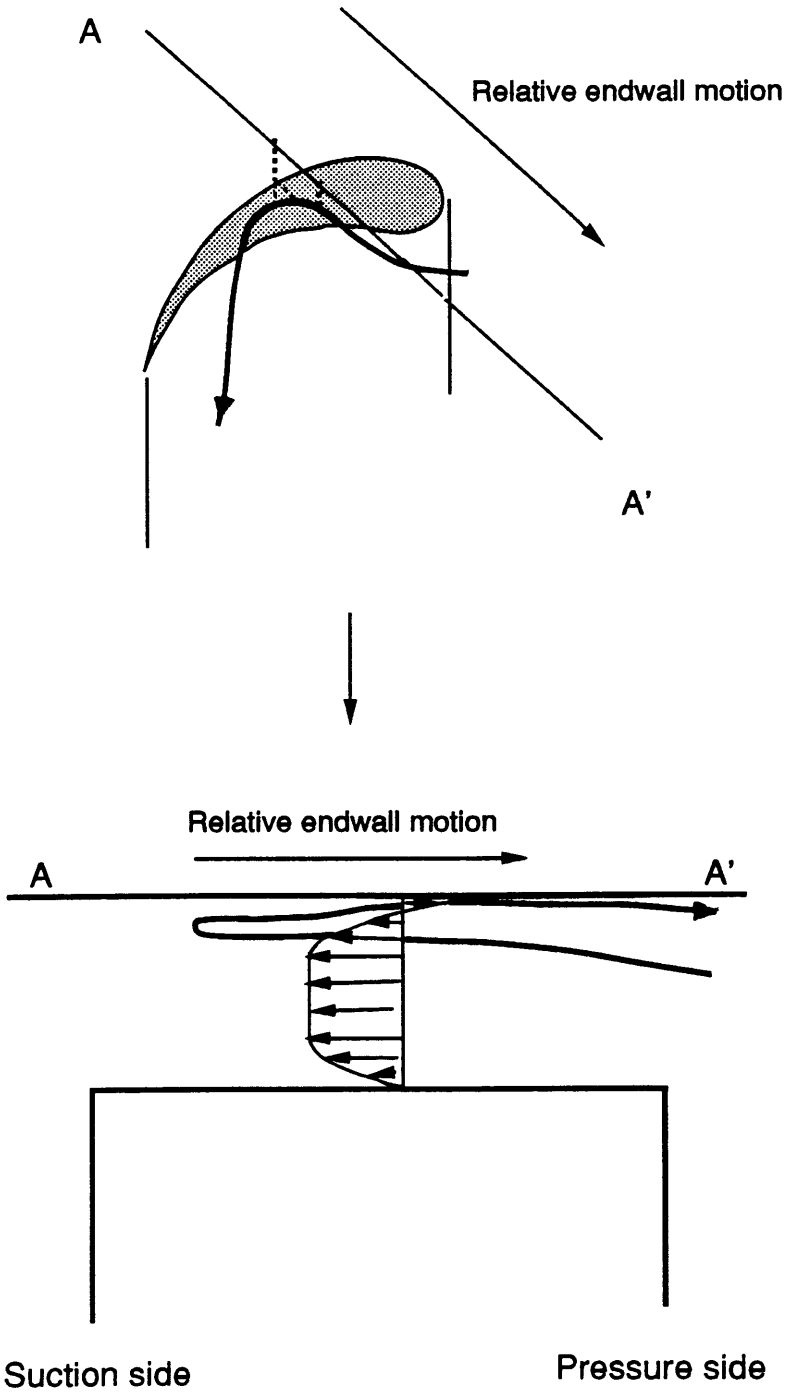

Figure B-17: Basic Structure of Tip Gap Flow

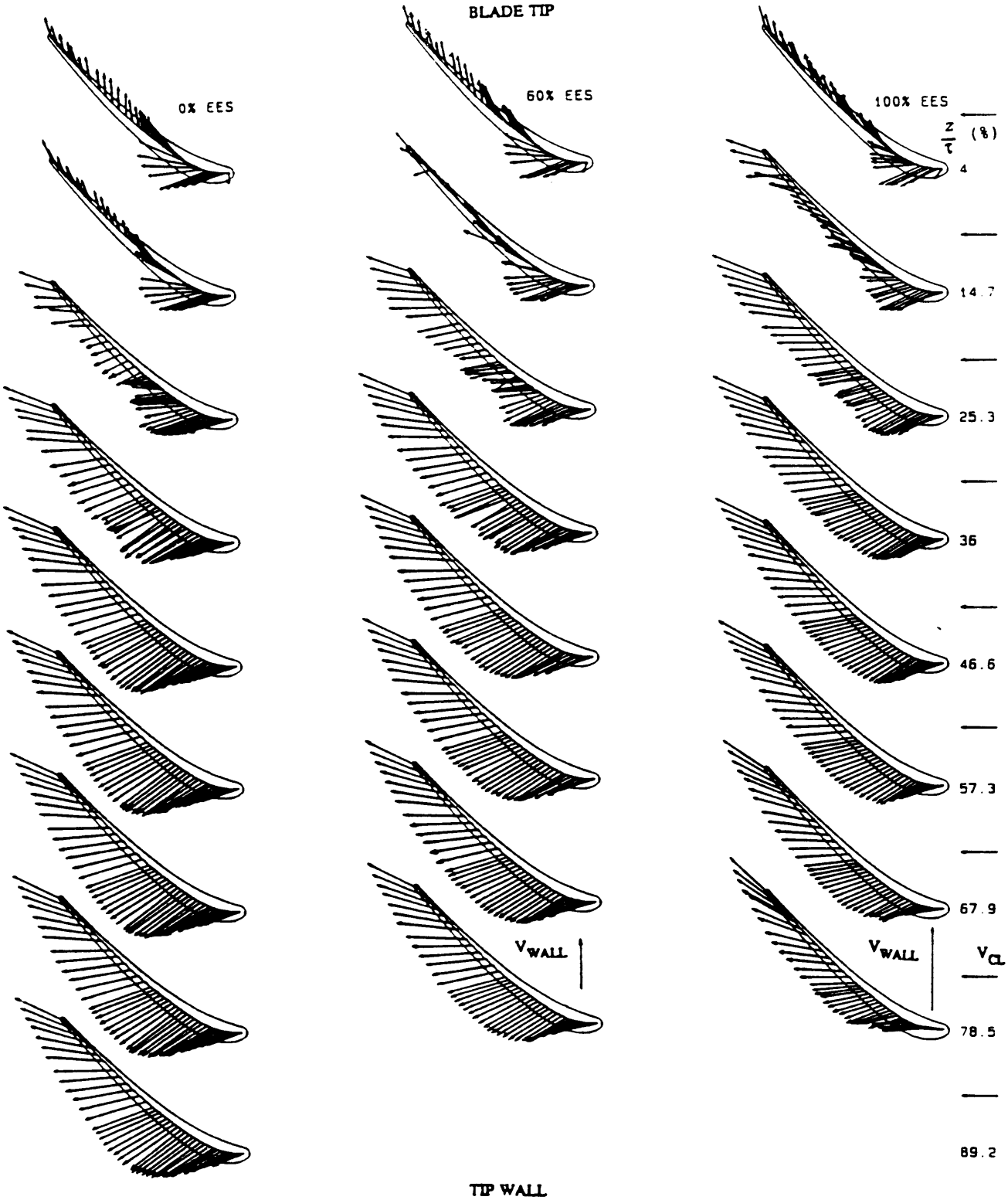

Fig. 5 Tip-gap velocity vectors (τ/c = 0.038)

Figure B-18: Velocity Measurement by Yaras and Sjolander

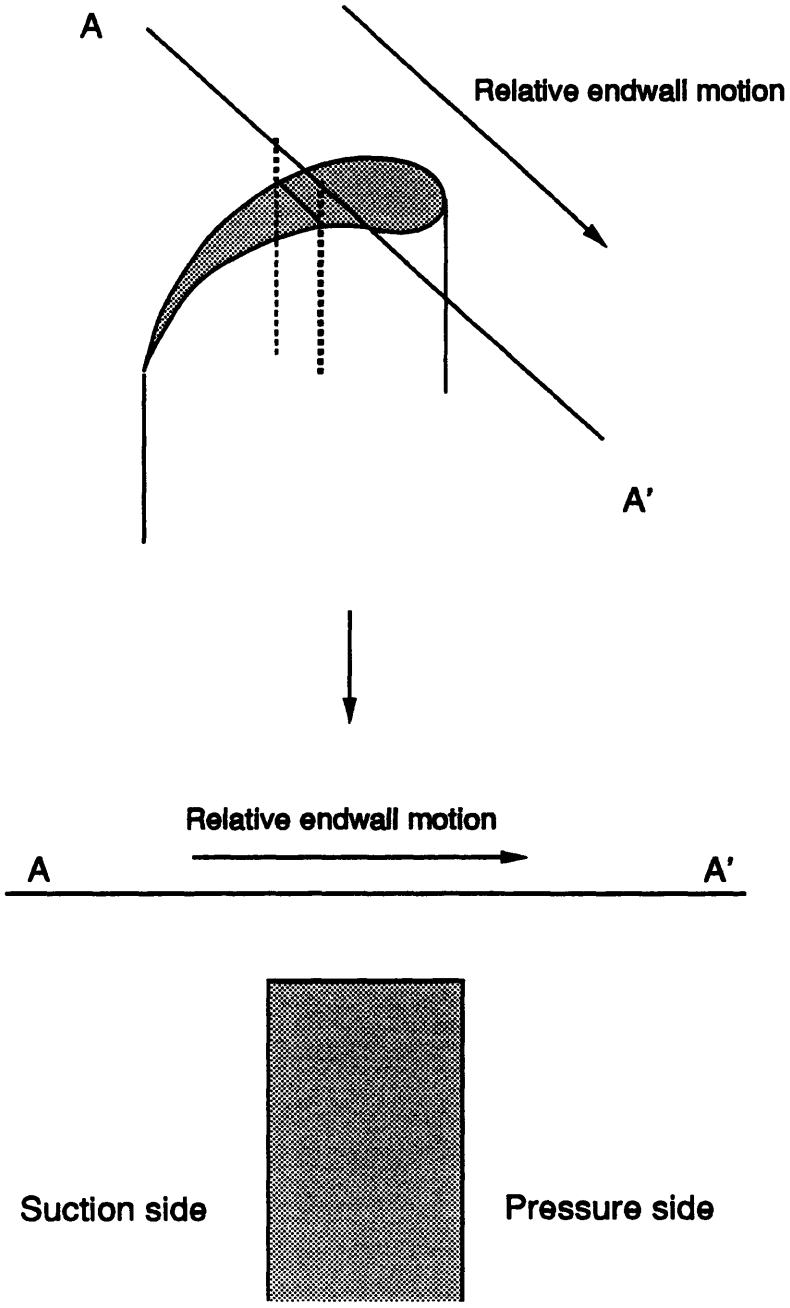

Figure B-19: Model Domain

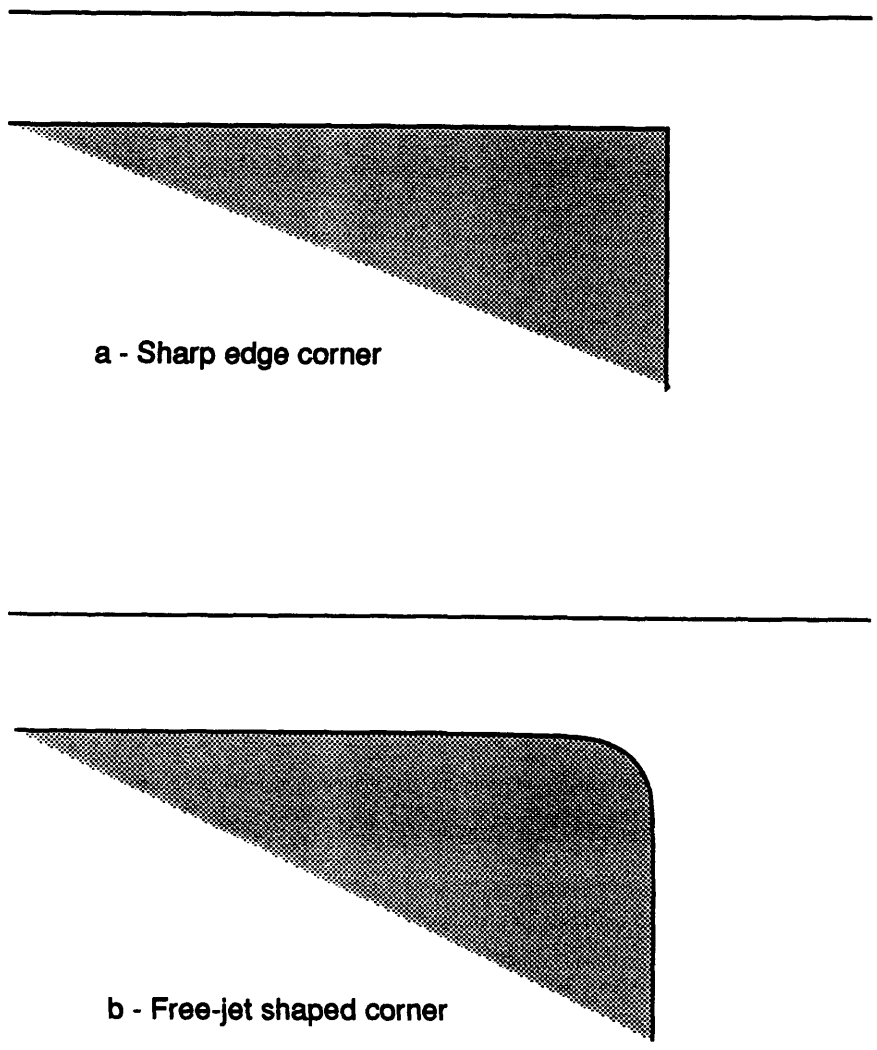

Figure B-20: Two Models of a Corner of Leading Edge of Tip

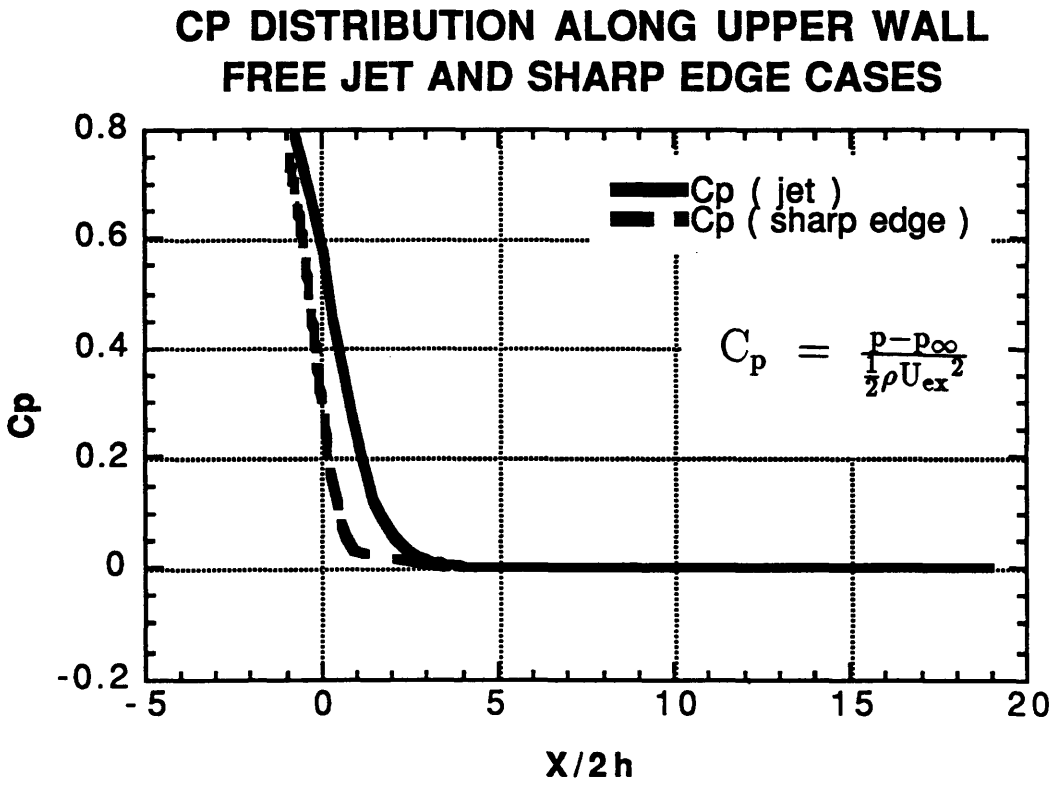

Figure B-21: Comparison of Pressure Field between Two Corners

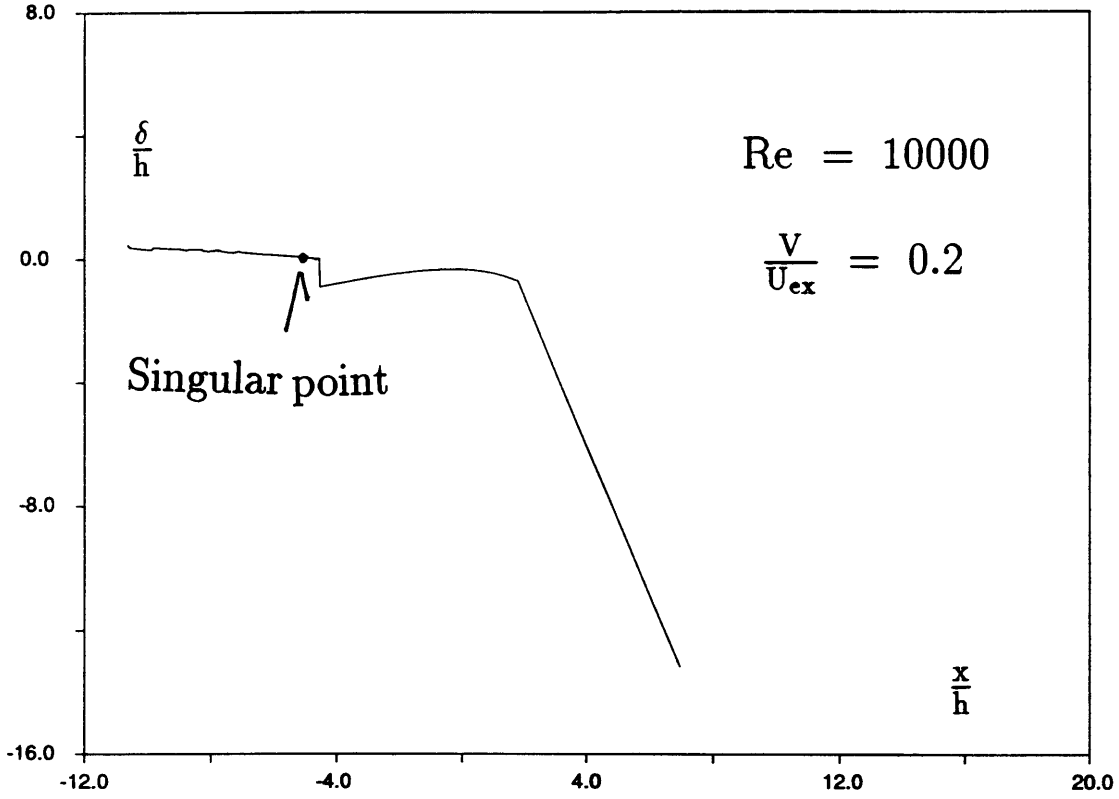

Figure B-22: Integration from a Singular Point for Timman's Profile - 1

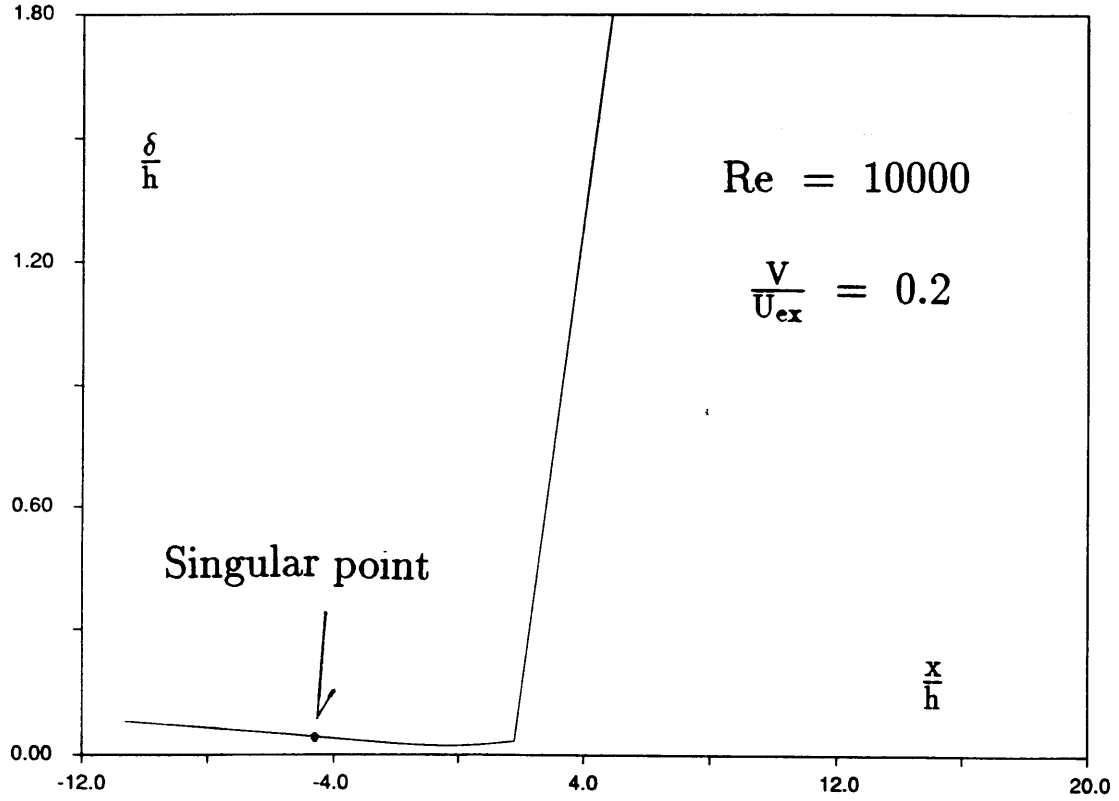

Figure B-23: Integration from a Singular Point for Timman's Profile - 2

$$\frac{V}{U_{ex}} = 0.1$$

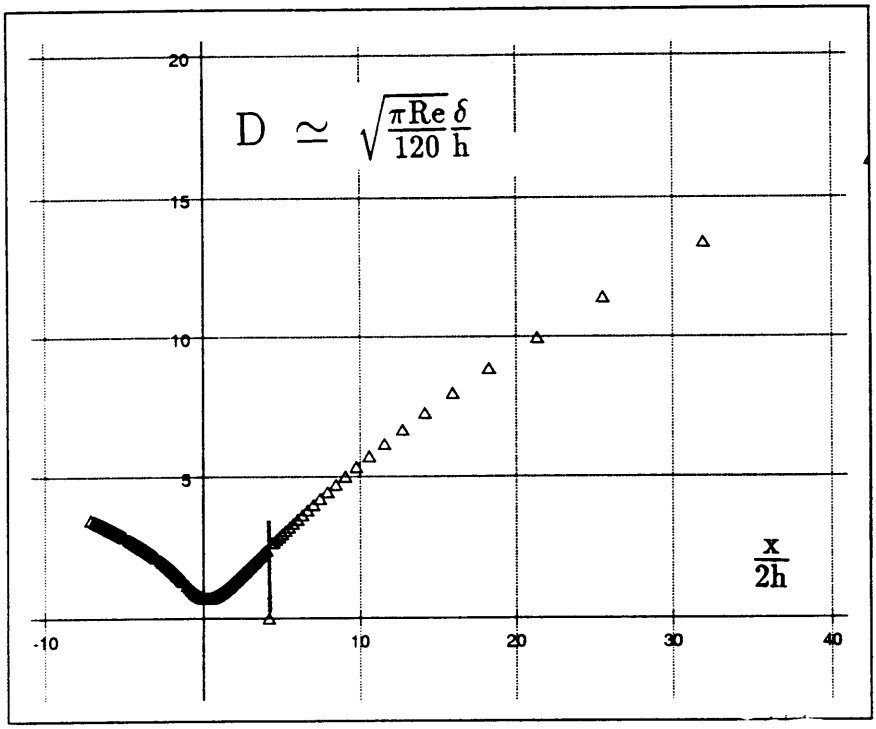

Figure B-24: Integration from a Singular Point for Parabolic Profile

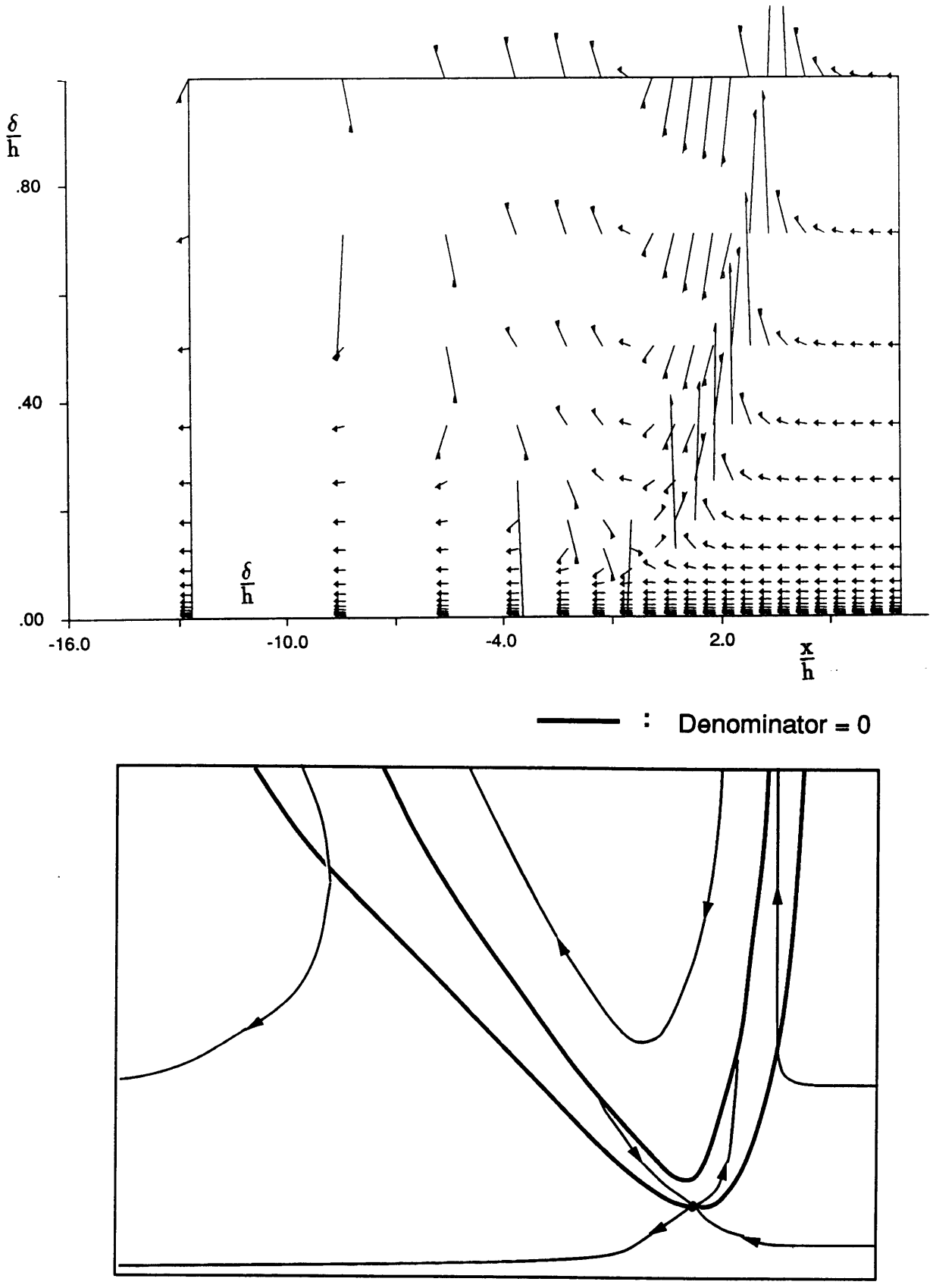

Figure B-25: Phase Space for Timman's Profile

$$\mathrm{Re} = 10000 \ \frac{V}{U_{ex}} = 5.0$$

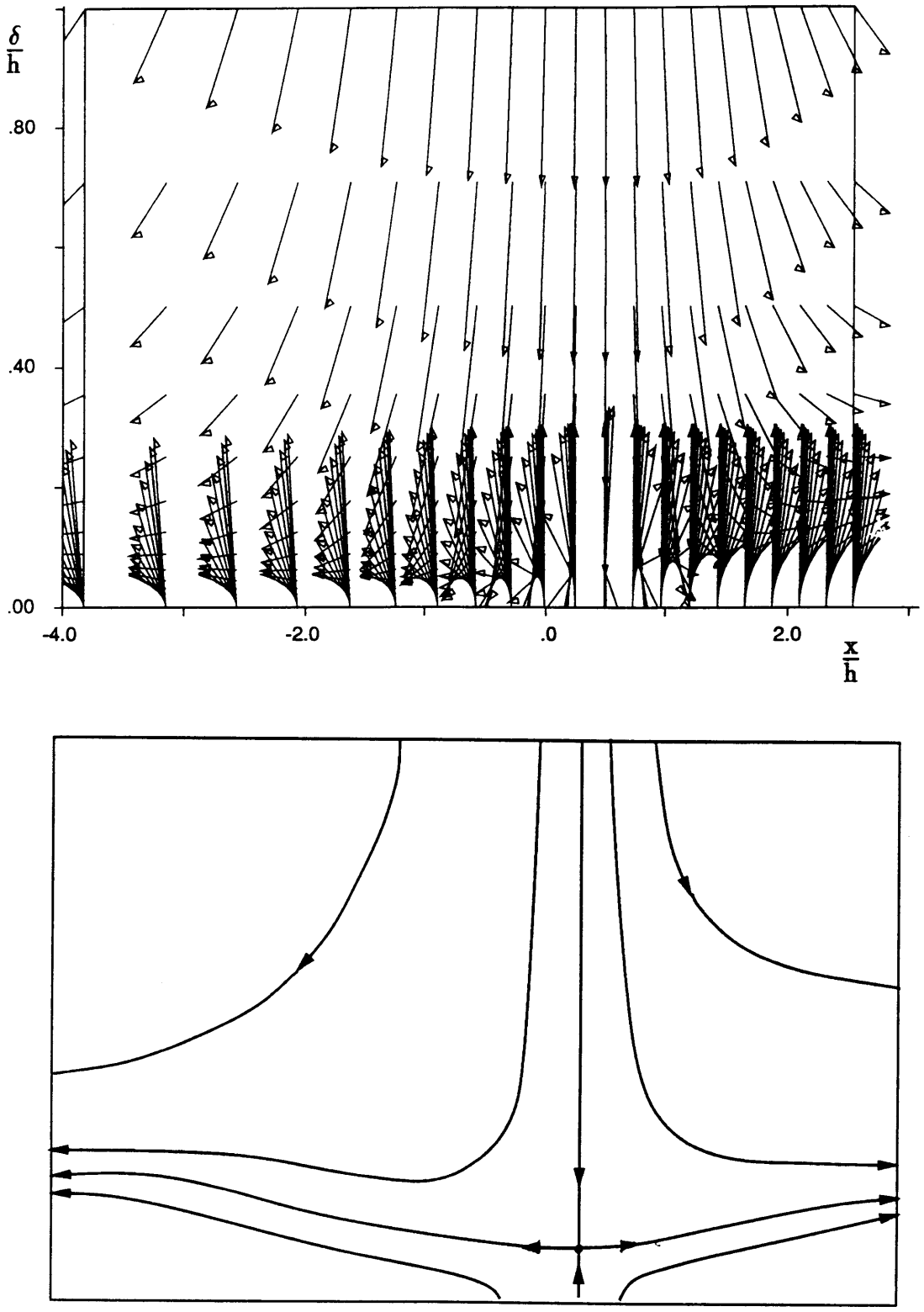

Figure B-26: Phase Space for Parabolic Profile

$$\mathrm{Re} = 10000 \quad \frac{V}{U_{ex}} = 0.6$$

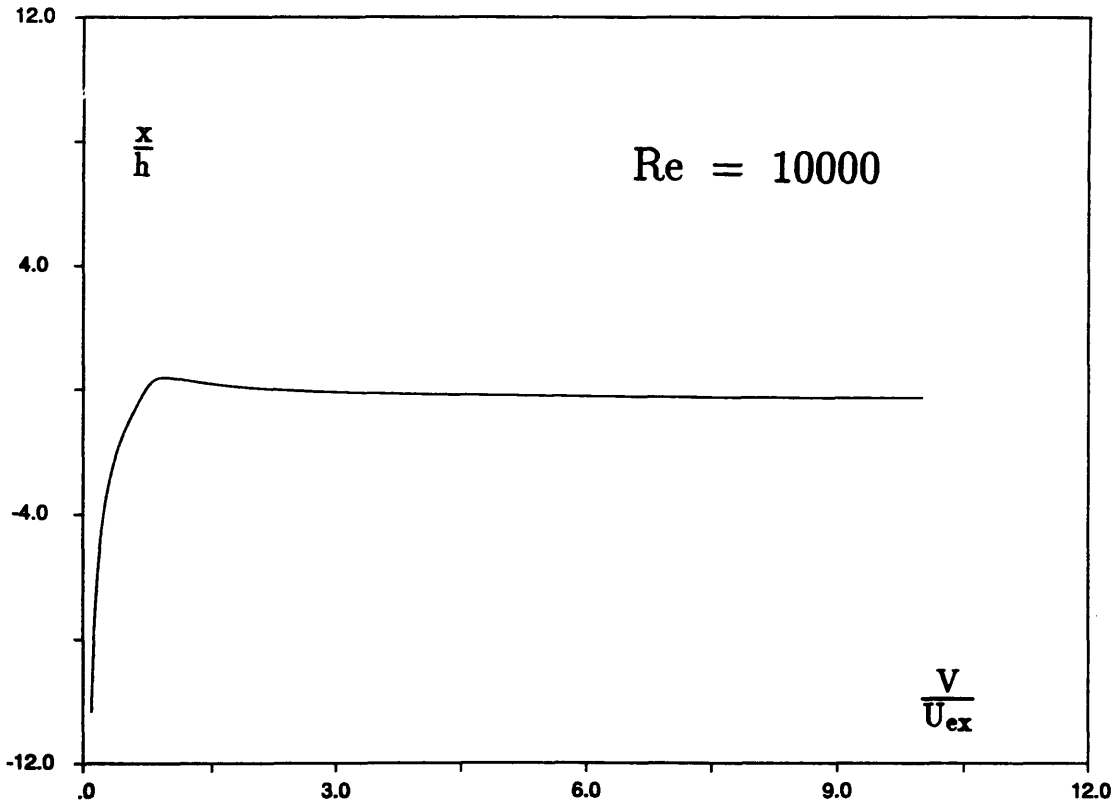

Figure B-27: Locations of Singular Points for Timman's Profile

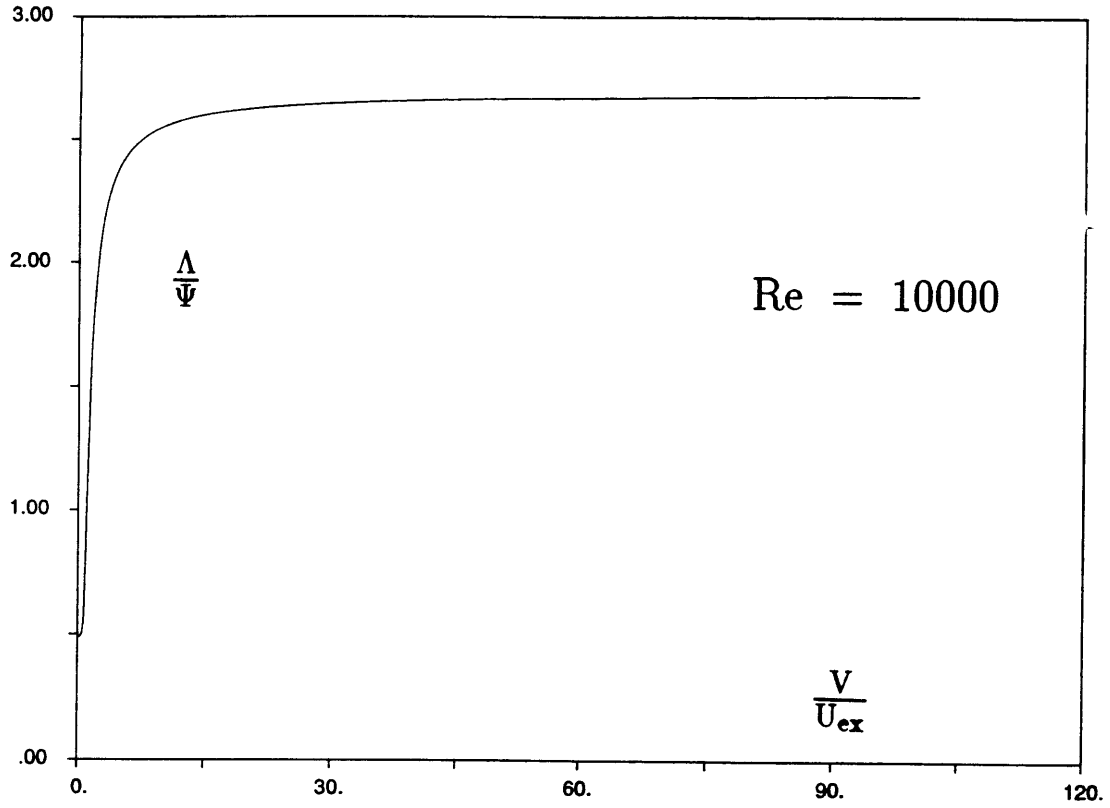

Figure B-28: Shape Factors at Singular Points for Timman's Profile

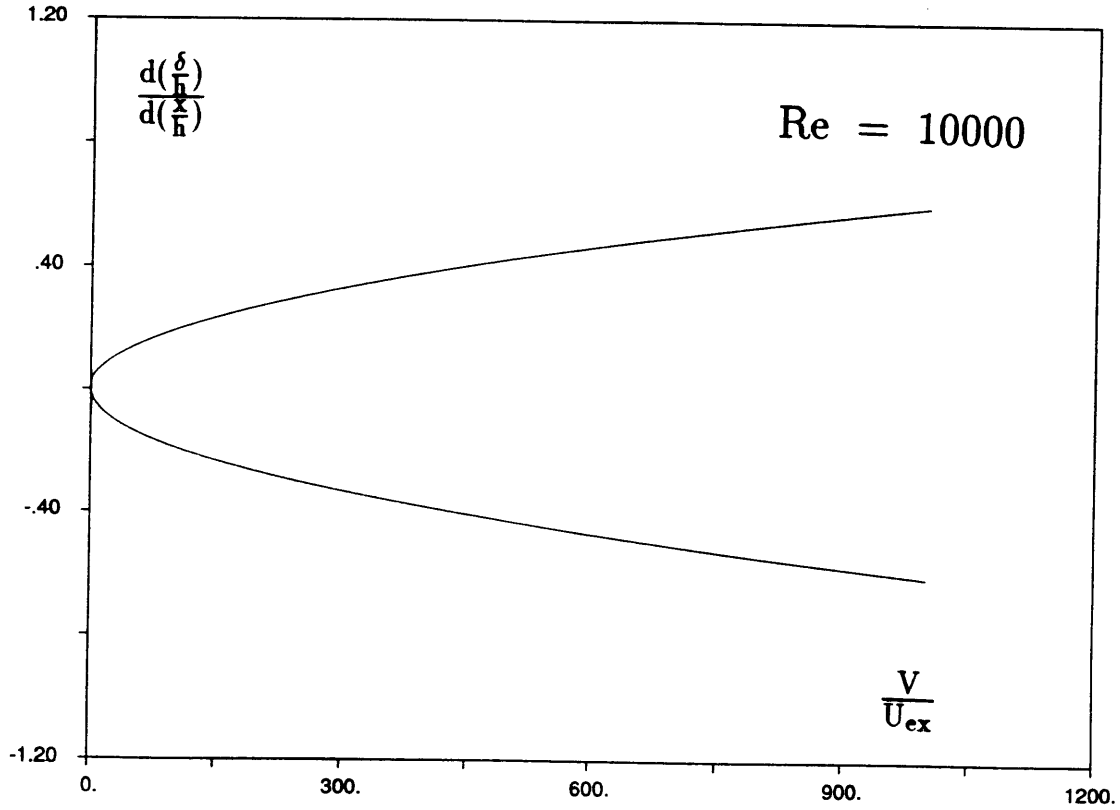

Figure B-29: Derivatives at Singular Point for Timman's Profile

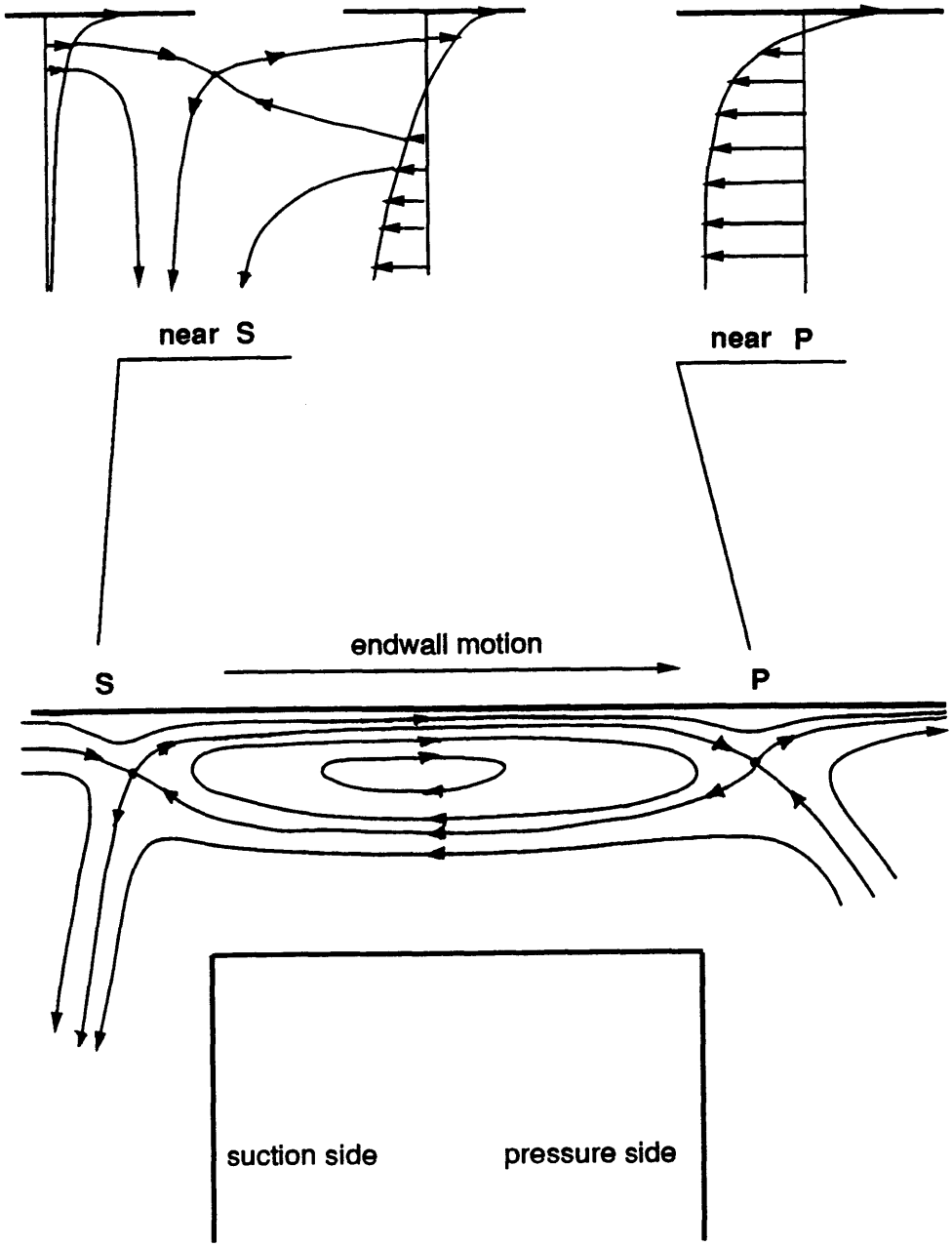

Figure B-30: Pattern of Stream Lines in Tip Gap Region

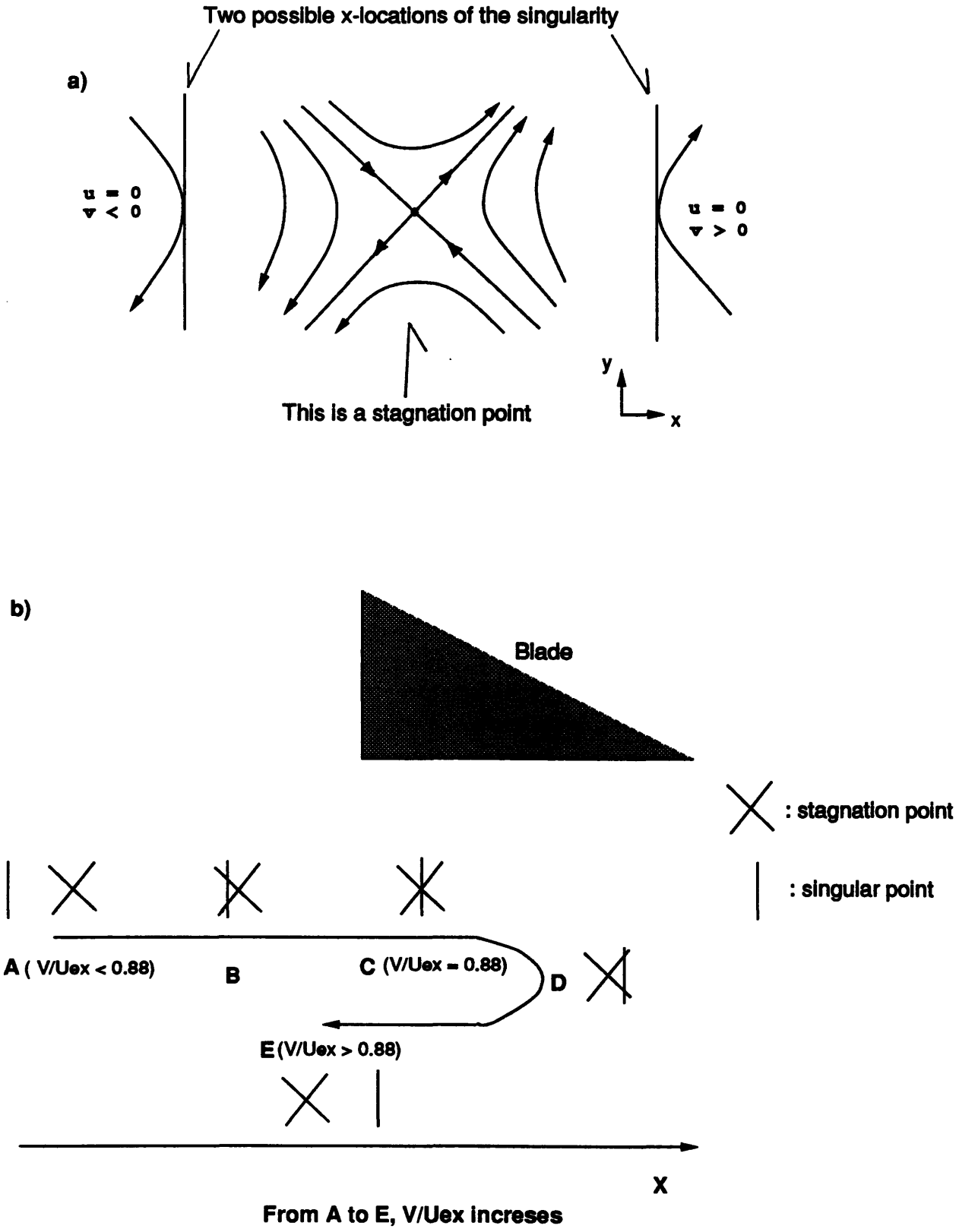

Figure B-31: Behavior of Singular Point and Stagnation Point